SYNTHESIS AND CRYSTAL STRUCTURE STUDIES OF ORGANIC SALTS, CO-CRYSTALS AND METAL-ORGANIC COMPOUNDS

SITI ARTIKAH BINTI MAHMUD SAFBRI

FACULTY OF SCIENCE
UNIVERSITY OF MALAYA
KUALA LUMPUR

2016

SYNTHESIS AND CRYSTAL STRUCTURE STUDIES OF ORGANIC SALTS, CO-CRYSTALS AND METAL-ORGANIC COMPOUNDS

SITI ARTIKAH BINTI MAHMUD SAFBRI

DESSERTATION SUBMITTED IN FULFILMENT OF THE REQUIREMENTS FOR THE DEGREE OF MASTER OF SCIENCE

DEPARTMENT OF CHEMISTRY
FACULTY OF SCIENCE
UNIVERSITY OF MALAYA
KUALA LUMPUR

2016

UNIVERSITY OF MALAYA
ORIGINAL LITERARY WORK DECLARATION

Name of Candidate: Siti Artikah Mahmud Safbri (I.C/Passport No: [redacted])

Registration/Matric No: SGR 140028

Name of Degree: Master of Science

Title of Project Paper/Research Report/Dissertation/Thesis ("this Work"):

Synthesis and Crystal Structure Studies of Organic Salts, Co-crystals and Metal-Organic Compounds

Field of Study: Inorganic Chemistry

I do solemnly and sincerely declare that:

(1) I am the sole author/writer of this Work;
(2) This Work is original;
(3) Any use of any work in which copyright exists was done by way of fair dealing and for permitted purposes and any excerpt or extract from, or reference to or reproduction of any copyright work has been disclosed expressly and sufficiently and the title of the Work and its authorship have been acknowledged in this Work;
(4) I do not have any actual knowledge nor do I ought reasonably to know that the making of this work constitutes an infringement of any copyright work;
(5) I hereby assign all and every rights in the copyright to this Work to the University of Malaya ("UM"), who henceforth shall be owner of the copyright in this Work and that any reproduction or use in any form or by any means whatsoever is prohibited without the written consent of UM having been first had and obtained;
(6) I am fully aware that if in the course of making this Work I have infringed any copyright whether intentionally or otherwise, I may be subject to legal action or any other action as may be determined by UM.

Candidate's Signature Date:

Subscribed and solemnly declared before,

Witness's Signature Date:

Name:

Designation:

ABSTRACT

All prepared compounds were fully characterized *via* FT- IR spectroscopic technique and elemental analysis; CHN including melting point, PXRD and SCXRD. The first project covers the synthesis of organic salts and co-crystals using carboxylic acid; 2-amino-4-chlorobenzoic acid (**BA**) and 1, 2, 4, 5-benzenetetracarboxylic acid (**TCA)** in combination with amines: piperazine (**PIP**), 1-methylpiperazine (**MPIP**), 1, 10-phenanthroline (**PHEN**), and 2-dipyridylketone (**DPK**) respectively in 1:1 ratios *via* mechanochemical grinding and vapor diffusion techniques. This series successfully obtained four organic salts and four co-crystals. The reaction of **BA-PIP and BA-MPIP** show deprotonation of carboxylic acid and protonation of amine in the solid state. Reaction of **TCA-DPK** results in formation of co-crystals whilst **TCA-PHEN** shows the formation of organic salts. Structural studies reveal that these organic molecules undergo molecular recognition process to obtain a range of two dimensional networks through persistent hydrogen-bonding patterns adopted by certain functional groups, which acts as template and rely on the robustness of such motifs to create new solid- state structures. The second project aims to synthesis of crystals using Zn^{2+} and Cd^{2+} to form metal complexes with $^{-}S_2CN(CH_2CH_2OH)R$ ligand where R = isopropyl, hydroxyethyl, methyl groups. A total of 4 metal-organic compounds were obtained which serves as a precursor in preparing mixed ligand complexes with 2, 2-bipyridyl (**BIPY**), **PIP**, **PHEN** and pyrazine (**PYR**). Results show that the presence of the N donor ligands increases the dimensionality in the crystal structure. Apart from that, PXRD pattern shows that the single crystals are the representative of the bulk materials obtained from the normal solution technique.

ABSTRAK

Semua sebatian yang disediakan dicirikan sepenuhnya melalui spektroskopi FT- IR dan analisis bahan; CHN termasuk takat lebur , PXRD dan SCXRD. Projek pertama meliputi sintesis garam organik dan *co-crystal* menggunakan asid karboksilik; 2-amino-4-klorobenzoik asid (**BA**) dan 1, 2, 4, 5-benzentetrakarboksilik asid (**TCA**) dikombinasikan dengan sebatian amina: piperazin (**PIP**), 1-metilpiperazin (**MPIP**), 1, 10-fenantrolin (**PHEN**) , dan 2-dipiridilketon (**DPK**) dengan nisbah 1: 1 melalui teknik melecek dan teknik penyebaran wap. Siri ini berjaya menghasilkan empat garam organik dan empat *co-crystal*. Reaksi **BA-PIP** dan **BA-MPIP** menunjukkan deprotonasi asid karboksilik dan disertai dengan protonasi sebatian amina dalam keadaan pepejal. Reaksi **TCA-DPK** menghasilkan *co-crystal* manakala **TCA-PHEN** menghasilkan garam organik. Kajian struktur menunjukkan bahawa molekul organik melalui proses penyesuaian molekul untuk mendapatkan dua rangkaian dimensi melalui corak ikatan-hidrogen berterusan yang diguna pakai oleh kumpulan berfungsi tertentu yang bertindak sebagai templat dan bergantung kepada keteguhan motif tersebut untuk membentuk struktur keadaan pepejal yang baru. Projek kedua bertujuan untuk menghasilkan hablur menggunakan Zn^{2+} dan Cd^{2+} untuk membentuk kompleks logam dengan $-S_2CN(CH_2CH_2OH)R$ ligan dimana R = isopropil, hidroksietil dan metil. Sebanyak 4 sebatian logam organik diperolehi dan berfungsi sebagai pelopor dalam menyediakan kompleks ligan dicampur dengan 2, 2-bipiridil (**BIPY**)), **PIP**, **PHEN** dan pirazin (**PYR**). Hasil kajian menunjukkan bahawa kehadiran N atom sebagai penderma ligan meningkatkan rangkaian dimensi dalam struktur hablur. Disamping itu, corak PXRD menunjukkan bahawa hablur tunggal mewakili bahan pukal diperolehi daripada teknik larutan normal.

ACKNOWLEDGEMENTS

Alhamdulillah, all praises to Allah, the Most Gracious and the Most Merciful for the strengths and His blessing in completing this thesis.

First and foremost, I would like to express my deep gratitude to Dr. Siti Nadiah binti Abdul Halim, my research supervisors, for her patient guidance, enthusiastic encouragement and useful critiques of this research work. Her invaluable help of constructive comments and suggestions throughout the experimental and thesis works have contributed to the success of this research. I would also like to extend my thanks to Professor Edward R.T. Tiekink for his contributions in idea to support my research program.

Sincere thanks to my friends (Sofia, Izzati, Jimmy, Suhaila, Farha, Subathra, Fatem, Athirah, Nadiah, Tan Tiek Aun) and seniors (Dr Shima, Dr Yee Seng, Dr Elly) for their kindness and moral support during my study. Not to forget, I would like to express my gratitude to technicians of the laboratory of the Chemistry Department for their help in offering me the resources in running the program.

Also, my deepest gratitude goes to my parents and also to my siblings for their endless love, prayers and encouragement. To those who indirectly contributed in this research, your kindness means a lot to me.

Lastly, thanks to the Ministry of Higher Education (MyBrain15) for scholarship provided and Postgraduate Research Grant (PPP) for allocation given to carry out my research at Department of Chemistry, University of Malaya.

Thank you very much.

TABLE OF CONTENTS

Abstract iv

Abstrak v

Acknowledgements vi

Table of Contents vii

List of Figures x

List of Schemes xiv

List of Tables xv

List of Symbols and Abbreviations xvi

List of Appendices xviii

CHAPTER 1: INTRODUCTION AND LITERATURE REVIEW 1

1.1 Crystal Engineering, Supramolecular Chemistry and their Terminologies 1

1.2 Co-crystal and Organic Salts 5

1.3 Metal-Organic Framework and Coordination Polymer 8

1.4 The Project and Objectives 10

CHAPTER 2: SUPRAMOLECULAR STRUCTURES OF BA AND TCA WITH SELECTED AMINES 11

2.1 Introduction and Literature Review 11

2.2 Methodology 14

  2.2.1 Materials 14

  2.2.2 Experimental 14

    2.2.2.1 Synthesis of 2-amino-4-chlorobenzoic acid series 14

    2.2.2.2 Synthesis of 1, 2, 4, 5-benzenetetracarboxylic acid series 15

  2.2.3 Instrument and Measurement Parameters 17

2.2.3.1 Spectroscopic Characterization of 2-amino-4-chlorobenzoic acid series……………………………………………………………..19

2.2.4 Spectroscopic Characterization of TCA series..20

2.2.5 Single Crystal X-Ray Crystallography (SCXRD)...................................23

2.2.6 Powder X-Ray Diffraction (PXRD)..37

2.2.6.1 PXRD for 2-amino-4-chlorobenzoic acid series.......................37

2.2.6.2 PXRD for 1, 2, 4, 5-benzenetetracarboxylic acid series...........38

2.3 Conclusion..40

CHAPTER 3: CRYSTAL ENGINEERING OF DITHIOCARBAMATE COMPLEXES: 2D TO 3D STRUCTURES..42

3.1 Introduction and Literature Review...42

3.2 Methodology...47

3.2.1 Materials...47

3.2.2 Experimental...47

3.2.2.1 Syntheses of Dithiocarbamate Ligands....................................47

3.2.2.2 Syntheses of *di* R1, R2 and R3 metal complexes......................48

3.2.2.3 Synthesis of mixed-ligand complexes.......................................50

3.2.3 Measurements..53

3.3 Results and Discussion...54

3.3.1 General spectroscopic characterization of complexes 1-7.......................54

3.3.2 Single Crystal X-Ray Diffraction Analysis...57

3.3.2.1 Crystal description of ZnR2 and ZnR3 precursor.....................57

3.3.2.2 Crystal structure description of mixed-ligand complexes.........62

3.3.3 Powder X-Ray Diffraction (PXRD)..87

3.4 Conclusion..89

CHAPTER 4: CONCLUSIONS 91

references 93

List of Publications and Papers Presented 100

Appendix 101

LIST OF FIGURES

Figure 1.1: Lock and key analogy (Source: chemistry.elmhurst.edu) 2

Figure 1.2: A few supramolecular synthons with their probability of occurrences (%) in the CSD (Vishweshwar et al., 2003).. 3

Figure 1.3: Molecular recognition of tectons to give a set of motif................................. 3

Figure 1.4: The structure Quinhydrone, the first co-crystal reported (Wood et al., 2014)6

Figure 1.5:'Crinkled tape' (a) and 'Rosette' (b) motif of barbital and 6

Figure 1.6: The intermolecular hydrogen bond synthon of 3-Aminopyridinium and 3,5-dihydroxybenzoate 7

Figure 1.7: Hydrogen-bonding environment around the piperazine cation 8

Figure 1.8: Single crystal structure of MOF-5 and MOF-101 with large yellow sphere represent the largest sphere 9

Figure 2.1: Asymmetric unit of BA-PIP 23

Figure 2.2: The hydrogen bond synthons environment of $[BA]^-$ 24

Figure 2.3: The intermolecular hydrogen bond synthons of $[PIP]^+$ 25

Figure 2.4: The intermolecular (O-H····O) hydrogen bond synthons of $[BA]^-$ and water molecules... 26

Figure 2.5: Square pores resulted from the intermolecular interactions along *a* axis..... 26

Figure 2.6: Crystal packing of BA-PIP showing two-dimensional square pores 27

Figure 2.7: Asymmetric unit crystal structure of BA-MPIP 28

Figure 2.8: The structure of two molecules of BA-MPIP related by the centre of inversion (yellow dots) along *a* axis 28

Figure 2.9: Intermolecular and intramolecular hydrogen bond synthons similar to crystal BA-PIP 29

Figure 2.10: Crystal packing view along the *a* (a) and *c* (b) axis respectively. 30

Figure 2.11: Asymmetric unit of TCA-PHEN 30

Figure 2.12: Molecular structure of TCA-PHEN with the presence of center of inversion (yellow dots) 31

Figure 2.13: Intermolecular interaction of PHEN with TCA..... 32

Figure 2.14: Intermolecular hydrogen bonding environment between TCA molecules. 32

Figure 2.15: Crystal packing of compound TCA-PHEN..... 33

Figure 2.16: The asymmetric unit of TCA-DPK 33

Figure 2.17: Molecular structure of TCA-DPK..... 34

Figure 2.18: The TCA molecules showing an intermolecular hydrogen bonding..... 34

Figure 2.19: Crystal packing of compound TCA-DPK 35

Figure 2.20: Red = bulk product from mechanochemical grinding, blue = simulated single crystal at 273 K, yellow = starting material of pure 1, 10-phenanthroline and green = starting material of pure BA 38

Figure 2.21: Red = bulk product from mechanochemical grinding, blue = simulated single crystal at 273 K, yellow = starting material of pure piperazine and green = starting material of pure TCA 39

Figure 3.1: Molecular structure of $Zn(C_5H_{10}NS_2)_2$-$(C_{12}H_8N_2)$ 44

Figure 3.2: Molecular structure of $Cd(C_6H_{11}N_2S_2)_2(C_5H_5N)_2$ 44

Figure 3.3: Asymmetric unit of ZnR2..... 57

Figure 3.4: Molecular structure of ZnR2 58

Figure 3.5: Hydrogen bond synthon between the molecules 59

Figure 3.6: Crystal packing of ZnR2..... 59

Figure 3.7: Asymmetric structure of ZnR3 60

Figure 3.8: Molecular structure of ZnR3 61

Figure 3.9: O–H····O hydrogen bond synthon environment of ZnR3 61

Figure 3.10: Crystal packing of ZnR3 62

Figure 3.11: Asymmetric crystal structure of 1 62

Figure 3.12: Molecular structure of crystal 1..... 63

Figure 3.13: Environment of hydrogen bond synthon environment 64

Figure 3.14: View of C–H····S intermolecular interactions along *c* axis 64

Figure 3.15: Crystal packing of crystal 1 along *c* axis 65

Figure 3.16: Asymmetric unit of crystal 2 65

Figure 3.17: Molecular structure of crystal 2 view along *a* axis 66

Figure 3.18: O–H····O hydrogen bond synthons environment in the molecular structure 67

Figure 3.19: A view of unit cell content showing O–H····S interactions of crystal 2 67

Figure 3.20: Asymmetric unit of crystal 3 68

Figure 3.21: Intermolecular interactions of crystal 3 along *b* axis 69

Figure 3.22: Intermolecular interactions of crystal 3 along *b* axis 69

Figure 3.23: Crystal packing of crystal 3 70

Figure 3.24: Asymmetric unit of crystal 4 70

Figure 3.25: Asymmetric unit and molecular structure of crystal 4 71

Figure 3.26: Rotation axis in molecular structure of crystal 4 71

Figure 3.27: Environment of hydrogen bond synthons crystal 4 72

Figure 3.28: C–H····S and C–H····O short contacts presence as weak intermolecular interactions 73

Figure 3.29: π-π interactions between pyridyl rings of PHEN 73

Figure 3.30: Crystal packing of crystal 4 74

Figure 3.31: Asymmetric unit of crystal 5 74

Figure 3.32: Molecular structure of crystal 5 showing the center of inversion (yellow dots) 75

Figure 3.33: O–H····S and C–H····O weak interactions in crystal 5 75

Figure 3.34: Crystal packing of crystal 5 76

Figure 3.35: Molecular structure of crystal 6 which resembles the asymmetric unit 77

Figure 3.36: Environment of O–H····O hydrogen bond synthons of crystal 6 78

Figure 3.37: C–H····S short contacts between molecules in crystal 6 79

Figure 3.38: The centroid····centroid distance between pyridyl ring of BIPY showing π-π interaction 79

Figure 3.39: Three dimensional crystal packing of crystal 6 80

Figure 3.40: Asymmetric and molecular structure of crystal 7 81

Figure 3.41: Symmetry operation (yellow dots) and rotation axis perpendicular to *c* axis in crystal 7 81

Figure 3.42: O–H····O hydrogen bond synthon of crystal 7 82

Figure 3.43: Environment of intermolecular interactions (N–H····O and O–H····N) of crystal 7 83

Figure 3.44: Stabilization provided by weak interaction of C–H····S short contacts 83

Figure 3.45: Crystal packing of crystal 7 84

Figure 3.46: PXRD patterns for mixed-ligand complexes with BIPY. Red = bulk product calculated from stirring, blue = simulated at 273 K 88

Figure 3.47: PXRD patterns of complexes 4,5 and 7. Red = bulk product calculated from stirring, blue = simulated at 273 K 88

LIST OF SCHEMES

Scheme 2.1: Synthesis diagram of BA and TCA series 13

Scheme 3.1 42

Scheme 3.2: Chemical structure of DTC series used 43

Scheme 3.3: Chemical structure of four reported precursor used 45

Scheme 3.4: Synthesis diagram of BIPY with metal precursor 46

Scheme 3.5: Synthesis diagram of PHEN, PYR and PIP organic linker with metal precursor 46

LIST OF TABLES

Table 2.1: Crystallographic and refinement details for (BA-PIP), (BA-MPIP), (TCA-PHEN) and (TCA-DPK) 36

Table 3.1: Crystallographic and refinement details for complex 1, 2, 3 and 6 85

Table 3.2: Crystallographic and refinement details for complex 4, 5 and 7 86

LIST OF SYMBOLS AND ABBREVIATIONS

% : percentage

°C : degree Celcius

mL : milliliter

mmol : millimoles

CSD : Cambridge Structural Database

FT-IR : Fourier Transform Infrared

CHN : Carbon, Hydrogen, Nitrogen

PXRD : Powder X-Ray Diffraction

SCXRD : Single Crystal X-Ray Diffraction

DTC : Dithiocarbamate

MOF : Metal Organic Framework

CP : Coordination Polymer

BA : 2-amino-4-chlorobenzoic acid

TCA : 1,2,4,5-benzenetetracarboxylic acid

PIP : Piperazine

MPIP : Methylpiperazine

PHEN : 1,10-phenonthroline

DPK : Di-2-pyridylketone

BIPY : 2,2-bipyridine

PYR : Pyrazine

R1 : *N*-hydroxyethyl-*N*-isopropyldithiocarbamate

R2 : *N*, *N'*-dihydroxyethyldithiocarbamate

R3 : *N*-hydroxyethyl-*N*-methyldithiocarbamate

SBU: Secondary building unit

CIF : Crystallographic information file

LIST OF APPENDICES

Table of bond lengths, Å for crystals BA-PIP, BA-MPIP, TCA-PHEN and TCA-DPK……………………………………………………………………………..101

Table of hydrogen bond lengths, Å for crystals BA-PIP and BA-MPIP.............102

Table of hydrogen bond lengths, Å for crystals TCA-PHEN and TCA-DPK….102

Table of bond angle for crystals BA-PIP, BA-MPIP, TCA-PHEN and TCA-DPK…………………………………………………………………..103-104

Table of bond lengths, Å for crystals 1-4………………………………….105-106

Table of bond lengths, Å for crystals 5-7………………………………….106-107

Table of bond angles for crystals 1-7……………………………………...108-111

Table of hydrogen bond lengths, Å for crystals 1-7……………………….112-113

CHAPTER 1: INTRODUCTION AND LITERATURE REVIEW

1.1 Crystal Engineering, Supramolecular Chemistry and their Terminologies

The idea of crystal engineering was developed by Schmidt and his co-worker during 1960s through the study of photochemical dimerization reaction of cinnamic acid derivatives (Schmidt, 1971; Veerakanellore et al., 2016). Later in 1988, Desiraju defined crystal engineering as "…the understanding of intermolecular interactions in the content of crystal packing and in the utilization of such understanding in the design of new solids with desired physical and chemical properties." (Anthony et al., 1998).

The ultimate goal of crystal engineering is to design crystal structures with desired properties based on the understanding of intermolecular interactions in the context of crystal packing. Thus, crystal engineering adopts the concept of building blocks to build crystals; from small to large crystals by adapting internal and external, shapes and also the symmetry of the building blocks. Small energy differences between crystal packing motifs lead to different crystal structures.

Besides that, the supramolecular aggregation can be classified into two major categories: 1) molecular recognition in solution known as supramolecular chemistry; and 2) organized self-assembly in the solid state as crystal engineering (Nangia, 2009).

The area of crystal engineering also correlates to the area of supramolecular chemistry. Both area focus on assembled molecules or building block which also referred as "tectons". Supramolecular chemistry refers to "the chemistry beyond the molecule" or "the chemistry of noncovalent bond" (Lehn, 1995). The basic concept for supramolecular chemistry can be summarized with Emil Fischer's lock and key principle (1894). In this analogy, its shows that only the correctly sized key fits into the key hole of the lock as shown in **Figure 1.1**.

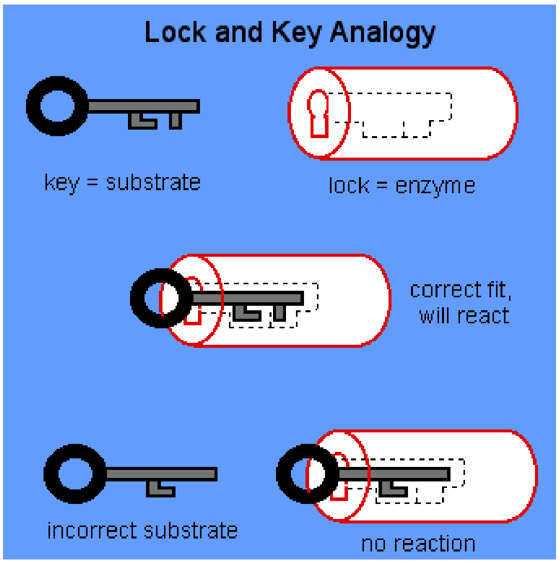

Figure 1.1: Lock and key analogy (Source: chemistry.elmhurst.edu)

In the area of crystal engineering and supramolecular chemistry, building block which also known as tectons usually are chosen based on the possible or expected interactions based on the functional groups in the molecule (Aakeröy, 1997). There are wide ranges of tectons which it can be organic, inorganic, and neutral or charged.

In addition, the presence of functional groups in the molecular structure of the tectons lead to the formation of secondary bondings; hydrogen and halogen bonding, π-π stacking and other non-covalent interactions to be named (Desiraju, 1995). These intermolecular interactions are known as supramolecular synthons usually formed based on the possible or desired periodic pattern offered by certain functional groups embedded in the tecton. Supramolecular synthons can be categorized into: 1) supramolecular homosynthons: composed of identical self-complementary functionalities; 2) supramolecular heterosynthons: composed of different but complementary functionalities (**Figure 1.2**).

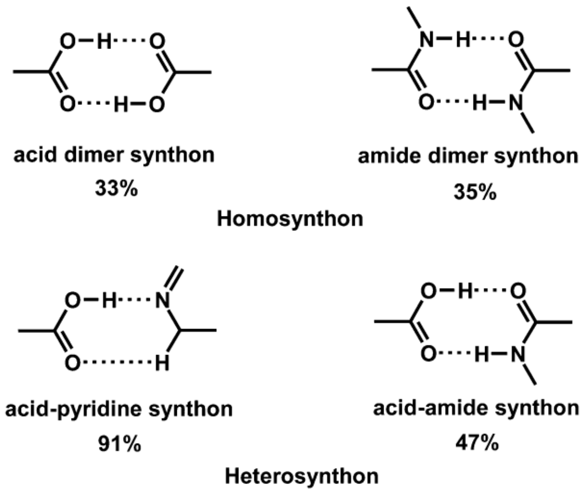

Figure 1.2: A few supramolecular synthons with their probability of occurrences (%) in the CSD (Vishweshwar et al., 2003)

Amongst all, hydrogen bonding is the most important since it is the most reliable directional interaction in supramolecular interaction and also the strongest. The O-H···O and N-H···O hydrogen bonds is ~20-40 kJ mol^{-1} and C-H···O and O-H···π interactions ~2-20kJ mol^{-1} (Desiraju, 1995). This can be seen from numerous papers published in which many crystal engineers have focused on the hydrogen bond synthons, including the charged-assisted hydrogen bonding (Brook & Koch, 1997; Morgado et al., 1997). Repetition of synthons leads to the formation of motifs. **Figure 1.3** illustrate the molecular recognition of tectons to give synthons and periodic arrangement of supermolecules (motifs) in crystal lattice.

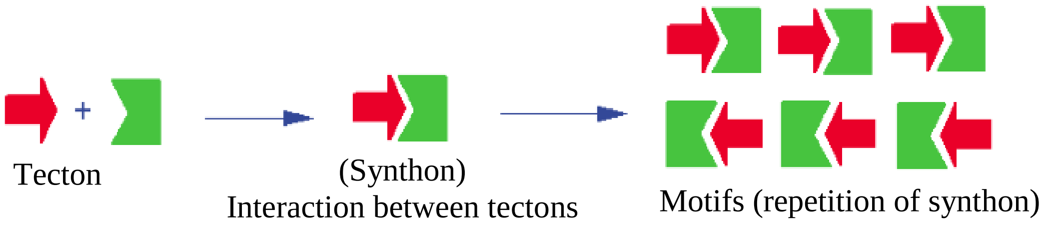

Figure 1.3: Molecular recognition of tectons to give a set of motif

According to Etter, there are three general rules of hydrogen bond: 1) all good proton donors and acceptors are used in hydrogen bonding; 2) if six-membered ring intramolecular hydrogen bonds can form, they will usually do so in preference to forming intermolecular hydrogen bonds; 3) the best proton donors and acceptors remaining after intramolecular hydrogen-bond formation form intermolecular hydrogen bonds to one another.

Moreover, the orientation of the solid can be predicted with a reasonable angle accuracy by the presence of either strong or weak interactions in combination of the acid and base properties. This is summarized by four pattern designators (G), which are C (chain), R (ring), D (dimer) and S (used for intramolecular hydrogen bonds). The number of donors (d) and acceptors (a) are assigned as subscripts and superscripts respectively of pattern designator (G), whilst the degree of motif (r) is written in a bracket as shown below (Margaret E. Etter, 1991).

$$\mathrm{G}_{d}^{a}[\mathrm{r}]$$

Kuleshova and Zorky were the first to apply graph theory to organic crystal structures where the repetition process leads to a set of molecules that are hydrogen bonded to each other (Kuleshova & Zorky, 1980). The motifs will be different if different solvents are used in the same compound and generated from intermolecular hydrogen bonds.

Repetition of motifs can result in 2D or 3D supramolecular structures which can be chains, nets and many more depending on the molecular recognition processes. Wells was the first who described the 3D nets with many kinds of building blocks in 1950s and 1960s (Ohrström & Larsson, 2004). The structures are often called (*n*, *p*), where *p* is the number of links at each node and *n* is the number of nodes in the shortest path resulting in ring closure.

The area of crystal engineering and supramolecular chemistry depend very much on Cambridge Structural Database (CSD) which contains over 600,000 collections of small molecule organic and organometallic crystal structures that have been analyzed using X-ray diffraction techniques.

1.2 Co-crystal and Organic Salts

The area of crystal engineering and supramolecular chemistry proceeds with variety components which highlight the existence of tectons which can exist as neutral or charged organic or inorganic compounds (J. T. A. Jones et al., 2011). However, the most common combinations are between neutral or charged organic-organic molecules which will result in formation of either co-crystals or organic salt.

The interest in co-crystal is not only focusing understanding from supramolecular perspective on solid-state chemistry research field but now it’s been growing into practical application in the pharmaceutical industry with the help of modern computational methods due to the improvement in solubility and chemical stability of the structure (Berge, Bighley, & Monkhouse, 1977; Taylor, Tanna, & Sahota, 2010; Shan & Zaworotko, 2010). Then, with the understanding of crystal engineering and supramolecular chemistry, a class of pharmaceutical co-crystals has been developed where crystalline API’s are being interest due to the relative ease of isolation, less impurities of product formed, and stability of the physico-chemical of the crystalline solid state (Andricopulo et al., 2009). Quinhydrone is the first reported structure showing interaction between benzoquinone and hydroquinone as shown in **Figure 1.4** reported by Wohler in 1844 (Patrick Stahly, 2009).

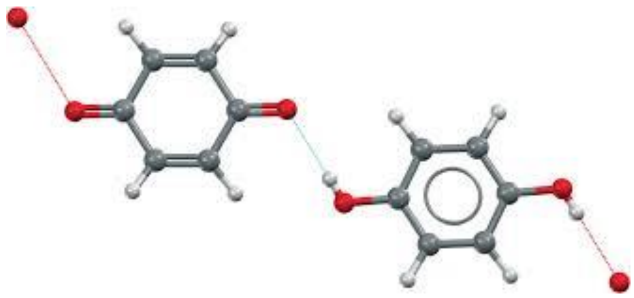

Figure 1.4: The structure Quinhydrone, the first co-crystal reported (Wood et al., 2014)

Pharmaceutical co-crystals can be defined as “a subset of a broader group of multi-component crystals that also includes salts, solvates, chlorates, inclusion crystals and hydrates” (Almarsson & Zaworotko, 2004). According to literature, it is believed that the first pharmaceutical co-crystal studies that related to crystal engineering was by Whitesides et al. on a series of substituted barbituric acid and various form of potential diversity discussed in the case studies (Taylor et al., 2010). **Figure 1.5** show the crystal packing of 5,5-diethylbarbituric acid (barbital) with melamine derivatives series.

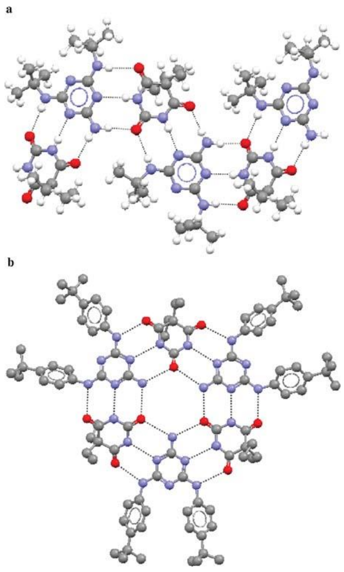

Figure 1.5:‘Crinkled tape’ (a) and ‘Rosette’ (b) motif of barbital and Melamine derivatives co-crystals

The formation of organic salts on the other hand requires molecules with ionisable groups for occurrence of proton-transfer within the molecules. In 2008, Nangia et al. reported on a series of molecular salt formation in combination of hydroxybenzoic acids with aminopyridines which resulted in 11 products which is consistent with CSD analysis (Sarma et al., 2009) (**Figure 1.6**).

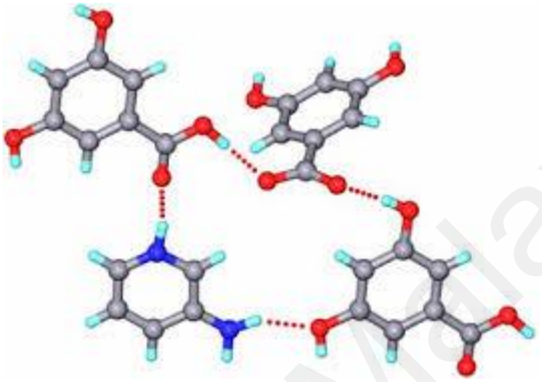

Figure 1.6: The intermolecular hydrogen bond synthon of 3-Aminopyridinium and 3,5-dihydroxybenzoate

There are also few similar articles focusing on the designing molecular salts. Most of the research reported that charged-assisted hydrogen bond synthons are most likely to occur resulted from protonation of hetero-N atom (Bhogala et al., 2005; Smith et al., 2001)

Thus, chemist had ventured multiple building blocks by showing interest in engineering of charged organic-organic compounds that developed in recent years where there will be protonation and deprotonation of molecules to happen. The presence of charged compounds will assist the hydrogen bond strength and make it a powerful tool for linking ions together in predictable manner. The synthesis of piperazine and benzoic acid is one of the example on supramolecular architecture of organic salts and **Figure 1.7** show the interactions of the compounds (Chen & Peng, 2011).

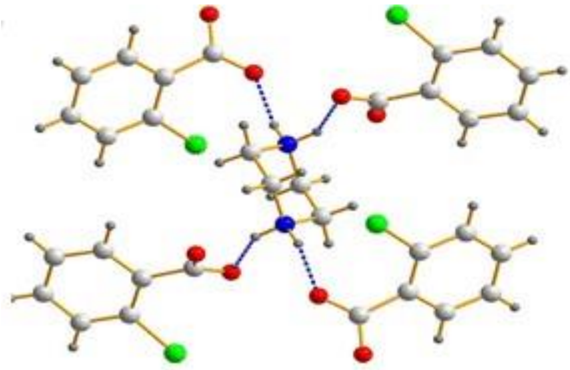

Figure 1.7: Hydrogen-bonding environment around the piperazine cation

1.3 Metal-Organic Framework and Coordination Polymer

The area of crystal engineering and supramolecular chemistry also precedes with coordination polymer (CP) and metal-organic framework (MOF). The discussion on terminologies of CP and MOF are still being continued since the preparation and analyzation result for both class of compounds almost similar kinds of new materials (Batten et al., 2012). The IUPAC Red Book define CP as “A coordination compound is any compound that contains a coordination entity (an ion or neutral molecule) that is composed of a central atom (metal) to which attached a surrounding array of atoms or groups of atom (ligand)” (Connelly et al., 2005). However CP are known to result only straight-chain polymers (1D) and MOF can form either 1D, 2D or 3D compounds.

MOF structures usually have two main components: the organic linkers and the metal centers. The organic linkers considered as organic secondary building unit (SBU), act as ‘struts’ that bridge metal centers considered as inorganic SBU, in which in turn act as ‘joint’ in the resulting MOF architecture. The two main components are connected to each other by coordination bonds, together with other molecular interactions to form a network with a definite topology as illustrated in **Figure 1.8**.

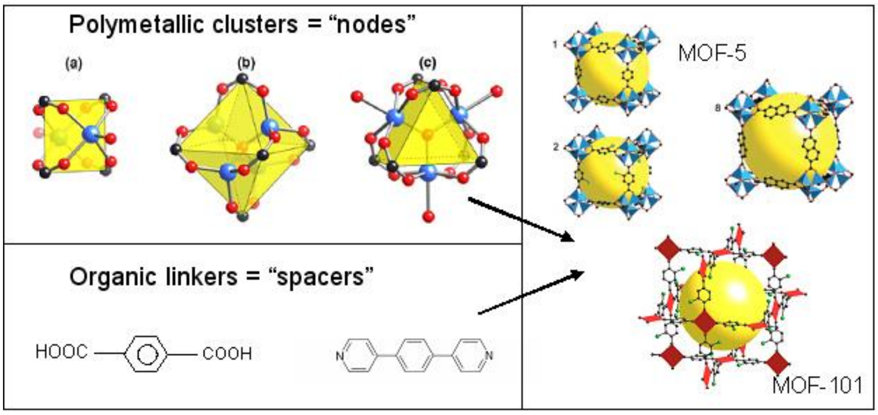

Figure 1.8: Single crystal structure of MOF-5 and MOF-101 with large yellow sphere represent the largest sphere

The important elements of MOFs are topology of framework, inorganic metal centers and organic ligands. MOFs constitute a new class of hybrid materials composed of inorganic building units connected by organic linker molecules, thereby forming three-dimensional periodic networks (Férey, 2008).

MOFs with various chemical composition and building units can be obtained by modifying already exist structure by increasing the chemical stability and its porosity to be used in gas storage, separations and catalysis (Furukawa et al., 2013). This is because the introduction of organic linker in a structure of a complex will improve the directionality and dimensionality in a solid state structure.

1.4 The Project and Objectives

Two different projects were conducted in this thesis highlighting the area of crystal engineering and supramolecular chemistry. The first project focused on the combination of 2-amino-4-chlorobenzoic acid and 1,2,4,5-benzenetetracarboxylic acid with common amine molecules as tectons: piperazine, 1-methylpiperazine, 1,10-phenanthroline and 2-dipyridylketone. A total of eight compounds have been prepared from these series which varies from co-crystal and crystalline organic salts.

The second project involved the exploration and modification of coordination entities using DTC compound with amine linkers. These results in modification of two-dimensional to three-dimensional supramolecular network.

The aims of study in this thesis are:

1) To design, synthesis, characterize formation of crystalline organic salts and co-crystals using carboxylic acid and selected amines (Chapter 2).
2) To modify the dimensionality in the crystal packing of DTC by introducing amine as organic linker (Chapter 3).
3) To compare products of mechanochemical grinding method with the normal stirring techniques.
4) To study the molecular interactions and factors affecting the self-assembly process in the crystal packing.

CHAPTER 2: SUPRAMOLECULAR STRUCTURES OF BA AND TCA WITH SELECTED AMINES

2.1 Introduction and Literature Review

Nowadays, the investigation on the co-crystal and salts by using carboxylic acid as one of the tecton to be combined with another tecton to generate a product with different molecular properties is growing. Carboxylic acid are known to be a versatile building blocks, its ability to act as mediator for two-dimensional supramolecular self-assembly and the presence of the carboxylic groups that resulted in interesting study of hydrogen bonds (Lackinger & Heckl, 2009).

Cambridge Structural Database (CSD) surveys revealed that 34% of the molecular carboxylic acids entries form supramolecular homosynthons in crystalline solids without the presence of competing hydrogen bond donors and/or acceptor (Shattock et al., 2008).

Besides that, there have been several attempts to establish the proton-transfer of carboxylic acids to amines such as combination of (malonic acid).(nicotinamide) and (pimelic acid).(nicotinamide) show different packing arrangement using the same combination of hydrogen bond interactions (Lemmerer et al., 2013).

Another related literature, (Sarma et al., 2009) was using meta- and para-substituted hydroxybenzoic acids and amino-pyridines in understanding the hydrogen bond motif with the presence of different functional groups such as amino and hydroxyl in the molecular structure which result show that the persistent formation of $PyNH^{+}\cdots{}^{-}OOC$ type of synthon to occur. Similar studies also being reported in constructing supramolecular architectures of piperazine in combination benzoic acid derivatives mainly in aliphatic chain carboxylic acids (Rao, 2001).

In contrast, the combination of piperazine with aromatic benzoic acid derivatives especially in the presence substituted functional group such as *m*-chlorobenzoic acid, *p*-chlorobenzoic acid and *o*-aminobenzoic acid which resulted in the formation of organic salts with various hydrogen bond networks (Chen & Peng, 2011; Del & Benites, 1998).

1, 2, 4, 5-benzenetetracarboxylic acid, also was reported by Luo et al. which can be partially or completely deprotonated, leading to various coordination modes (Luo et al., 2013). Moreover, the solid-state grinding of the methanol solvate phase of 1, 2, 4, 5-benzenetetracarboxylic acid leads selectively to two different transformation pathways under different atmospheric condition giving rise to different product phases(Fujii et al., 2010).

Herein, we report on the usage of 1, 2, 4, 5-benzenetetracarboxylic acid or 2-amino-4-chlorobenzoic acid as primary tecton in combination with other amines as tectons (**Scheme 2.1**). The selected amines that is to be used will control the deprotonation of the carboxylic acid. During the course of investigation of the structure of the addition compounds of amines with acids, grinding and stirring methods were used in compounds preparation. For grinding method, a small amount of methanol was added during grinding process to enhance the kinetic and facilitate co-crystal formation (Jones et al., 2006).

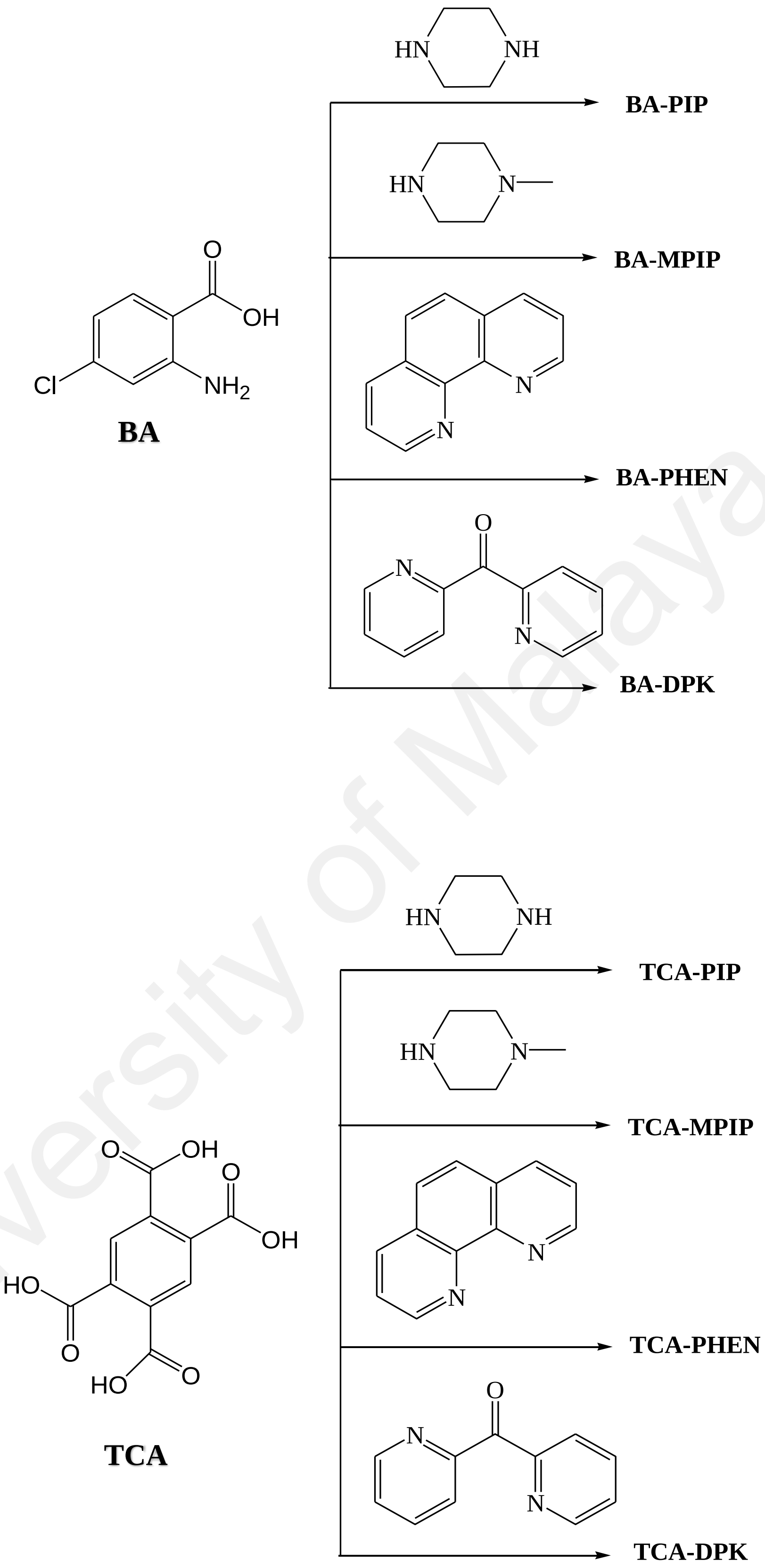

Scheme 2.1: Synthesis diagram of BA and TCA series

2.2 Methodology

2.2.1 Materials

All reagents and solvents used were commercially available and used as received without further purification: 2-amino-4-chlorobenzoic acid, 1,2,4,5-benzenetetracarboxylic acid and piperazine were obtained from Sigma Aldrich, 1-methylpiperazine and 1,10-phenanthroline from Merck and di(2-pyridyl) ketone from Acros Organic.

2.2.2 Experimental

2.2.2.1 Synthesis of 2-amino-4-chlorobenzoic acid series

BA-PIP, $C_7H_6ClNO_2 .C_4H_{10}N_2$

10 mL an ethanolic solution of **PIP** (1 mmol, 86 mg) was added into 20 mL ethanolic solution of **BA** (1 mmol, 172 mg). The solution mixture was reflux for four hours before it was kept in the dark (cupboard) at room temperature to allow crystallization process. Colorless block crystals **BA-PIP** were formed after a week and were analyzed by single crystal diffraction technique. (Yield: 167 mg, 72.17 %).

BA-MPIP, $C_7H_6ClNO_2 .C_5H_{12}N_2$

10 mL an ethanolic solution of **MPIP** (2 mmol, 200 mg) was added into 40 mL ethanolic solution of **BA** (2 mmol, 343 mg). The solution mixture was reflux for four hours before it was kept in the dark (cupboard) at room temperature to allow crystallization process. Colorless block crystals **BA-MPIP** were formed after a week and were analyzed by single crystal diffraction technique. (Yield: 90 mg, 16.56 %).

BA-PHEN, $C_7H_6ClNO_2 . C_{12}H_8N_2$

PHEN (1 mmol, 181 mg) and **BA** (1 mmol, 172 mg) were grounded together with 1:1 ratio for 30 minutes with a drop of methanol. 20 mg of the grounded mixture was taken and dissolved respectively in a minimum amount of ethanol and was left for recrystallization process. An X-ray powder diffraction measurement on the solid product showed the presence of a physical mixture of the starting materials since the crystal from the recrystallization process resulted could not be obtained. (Yield: 207 mg, 59.60 %).

BA-DPK, $C_7H_6ClNO_2 . C_{11}H_8N_2O$

10 mL methanolic solution of **DPK** (1 mmol, 187 mg) was added into a 10 mL methanolic solution of **BA** (1 mmol, 172 mg). The solution mixture was stirred for 1 hour before the solution was left at room temperature to allow crystallization process. (Yield: 147 mg, 41.31 %).

2.2.2.2 Synthesis of 1, 2, 4, 5-benzenetetracarboxylic acid series

TCA-PIP, $C_{10}H_6O_8 . C_4H_{10}N_2$

PIP (1 mmol, 138 mg) and **TCA** (1 mmol, 201 mg) were grounded together with 1:1 ratio for 30 minutes with a drop of methanol. 20 mg of the grounded mixture was taken and dissolved respectively in a minimum amount of ethanol and was left for recrystallization process. (Yield: 362 mg, 94.00 %).

TCA-MPIP, $C_{10}H_6O_8 . C_5H_{12}N_2$

10 mL methanolic solution of **MPIP** (1 mmol, 220 mg) was added into a methanolic solution (10 mL) of **TCA** (1 mmol, 255 mg). The solution mixture was stirred for 1 hour before the solution was left at room temperature to allow crystallization process. Unfortunately, PXRD cannot be performed in **TCA-MPIP** since the product is in liquid form and recrystallization process was unsuccessful.

TCA-PHEN, $C_{10}H_6O_8 . C_{12}H_8N_2$

PHEN (1 mmol, 146 mg) and **TCA** (1 mmol, 205 mg) were grounded together with 1:1 ratio for 30 minutes with a drop of methanol. 20 mg of the grounded mixture was taken and dissolved respectively in a minimum amount of ethanol and was left for recrystallization process. Needle crystals of **TCA-PHEN** were formed after a week and were analyzed by single crystal diffraction technique. (Yield: 73 mg, 24.43 %).

TCA-DPK, $C_{10}H_6O_8 . C_{11}H_8N_2O$

DPK (1 mmol, 299 mg) and **TCA** (1 mmol, 206 mg) were grounded together with 1:2 ratio for 30 minutes with a drop of methanol. 20 mg of the grounded mixture was taken and dissolved respectively in a minimum amount of ethanol and was left for recrystallization process. Needle crystals of **TCA-DPK** were formed after a week and were analyzed by single crystal diffraction technique. (Yield: 218 mg, 58.44 %).

2.2.3 Instrument and Measurement Parameters

Melting points were determined on a MEL-TEMP II melting point apparatus.

The elemental analyses were performed on a Perkin Elmer PE 2400 CHN Elemental Analyzer. In this technique percentage of carbon, hydrogen and nitrogen is determined that lead to the determination of empirical formula of the complex from which molecular formula of complex can be drawn.

Besides that, FT-IR spectra were measured on a Perkin Elmer Spectrum 400 FT Mid-IR/Far-IR spectrophotometer with diamond crystal plate in the frequency range of 4,000–400 cm^{-1}. FTIR is a type of infrared spectroscopy that sees IR radiation being passed through a sample. Some of the radiation will be absorbed in the test sample that builds the foundation of the resulting spectrum obtained and some will be transmitted. The resulting spectrum will be the compounds own special fingerprint.

Single crystal X-ray crystallography is one of the most widely used techniques for structural interpretation of complexes. Atomic positions and space groups can be determined from the intensities of hkl reflections measured from X-ray crystallography. Complete information about bonds nature, number of atoms and functional groups can only be determined by using single crystal x-ray technique. Based on the intensities and angles of the diffracted rays, a three-dimensional picture of the crystal electron density distribution will be interpreted and refined. Single crystal X-ray diffraction data for **BA-PIP** and **BA-MPIP** were collected on a Bruker AXS SMART APEX II diffractometer with a CCD area detector Mo K_α (λ = 0.71073 A°), monochromator = graphite. Also, high quality crystals were chosen under a polarizing microscope and had been mounted on a glass fiber. Data processing and absorption correction were carried out using the APEX II software package (Bruker, 2005).

Single crystal X-ray diffraction data for **TCA-PHEN** and **TCA-DPK** were collected at 100 K on Oxford Supernova Dual Wavelength diffractometer Mo K_α (λ = 0.71073 A°). Absorption correction was performed by multi-scan method using CrysAlis PRO, with empirical absorption correction using spherical harmonics, implemented in SCALE3 ABSPACK scaling algorithm (Ganapayya et al., 2013).

All the structures were solved by employing the charge flipping method using Superflip solution program (Palatinus & Chapuis, 2007). The hydrogen atoms were placed in geometrically-calculated position and included in the refinement process using the riding model with $U_{iso} = 1.2U_{eq}$ C(H,H) groups. Moreover, the full matrix least-squares refinement against $|F^2|$ was carried out via SHELXTL refinement program (Sheldrick, 2008) and the final refinement included atomic position for all the atoms, anisotropic thermal parameters for all the non-hydrogen atoms, and isotropic thermal parameters for all the hydrogen atoms. The programs Olex2 (Dolomanov et al., 2009), PLATON (Spek, 2009), and Mercury (Macrae et al., 2008) were also used throughout the study.

X-ray diffraction allows identifying crystal structures of solids in a simple and rapid way. Powder X-Ray Diffraction (PXRD) can be used to determine the crystallinity applying the Scherrer equation. Plane waves incident on a crystal lattice at angle θ are partially reflected by successive parallel crystal planes of spacing d. PXRD was carried out using PANalytical Empyrean XRD system, with Cu K_α radiation (λ = 1.54056 Å) in the range of $2\theta = 5°$ to $40°$ with a step size of 0.026°. Comparison between experimental and calculated (from CIFs) PXRD patterns was performed with X'Pert HighScore Plus 20 (PANalytical, 2009).

2.2.3.1 Spectroscopic Characterization of 2-amino-4-chlorobenzoic acid series

The elemental analyses data of all prepared compounds of **BA** series were performed and the experimental values agree quite well with the calculated values. This indicates that predicted compounds show similarity with the expected. However, the result obtained did not confirmed the product to be either co-crystal or organic salts. As a result, solubility test was conducted by dissolving 0.8 mg of each compounds with 2 mL of distilled water. Since **BA-PIP** and **BA-MPIP** dissolved in water, we can conclude that the compounds are organic salt and **BA-PHEN** as co-crystal since it insoluble in water.

The compounds of this series show variable melting point value in the range of (130-169) $^{\circ}$C. As we can see from the result, all compounds show quite sharp melting points value except for **BA-PIP**. This may be due to the presence of impurities in the bulk materials of the compound which is not as pure as product from recrystallization process.

The IR spectra recorded on prepared compounds were compared with the spectra of the tectons and significant shifts (v(N−H) region; the v(C=O) associated with –COOH moiety; and the v_{as} (COO-) and v_s (COO-) region) on the important peaks were observed. The IR spectrum of the free ligand **BA** shows a strong band around 1700cm^{-1} assignable to v(C=O) of the –COOH moiety. In **BA-PIP**, **BA-MPIP** and **BA-PHEN** compounds, new bands due to v_{as} (COO-) were observed in the region 1650-1700 cm^{-1} and that due to v_s (COO-) at about 1230-1250 cm^{-1}.

BA-PIP, $C_{10}H_6O_8$.$C_4H_{10}N_2$

Elemental analysis, Experimental (Calculated) (%):$C_7H_6ClNO_2.C_4H_{10}N_2$: C, 47.74(47.67); H, 6.92(6.86); N, 15.18(15.11) %. Melting point: (156-166) °C. IR (cm^{-1}): 3528 *ν*(N−H); 1705 *ν*(C=O), 1238 *ν*(C−O).

BA-MPIP, $C_{10}H_6O_8$.$C_5H_{12}N_2$

Elemental analysis, Experimental (Calculated) (%):$C_7H_6ClNO_2.C_5H_{12}N_2$: C, 53.04(53.10); H, 6.68(6.60); N, 15.46(15.40) %. Melting point: (135-138) °C. IR (cm^{-1}): 3079 *ν*(N−H); 1682 *ν*(C=O) , 1239 *ν*(C−O).

BA-PHEN, $C_7H_6ClNO_2$.$C_{12}H_8N_2$

Elemental analysis, Experimental (Calculated) (%):$C_7H_6ClNO_2.C_{12}H_8N_2$: C, 64.87(64.67); H, 4.01(3.89); N, 11.94(11.53) %. Melting point: (141-143) °C. IR (cm^{-1}): 3449 *ν*(N−H); 1666 *ν*(C=O), 1245 *ν*(C−O).

BA-DPK, $C_7H_6ClNO_2.C_{11}H_8N_2O$

The preparation for **BA-DPK** was unsuccessful. The detail will be discuss further in section **2.2.6.1**.

2.2.4 Spectroscopic Characterization of TCA series

Three different compounds were successfully obtained from this series. The elemental analyses data of **TCA-PHEN**, **TCA-DPK** and **TCA-PIP** compounds were performed and the resulted values agree quite well with the calculated values. This indicates that the predicted compounds show similarity with the expected. However, the result obtained did not confirmed the product to be either co-crystal or organic salts. According to literature, calculation of pKa values can differentiate these two forms of solids. The formation of organic salts only occurs if the difference in pKa value between the conjugate base and conjugate acid is more than or equal to 2.7. If the pKa difference is less than 2.7, co-crystals will form instead (Sekhon, 2009).

In this experiment we use a very simple approach where solubility test was conducted by dissolving 0.8 mg of each compounds with 2 mL of distilled water. Theoretically, salts are easier to dissolve in water compared to organic solids. Since **TCA-PHEN** dissolved in water, we can conclude that the compounds are organic salt and **TCA-DPK** and **TCA-PIP** as co-crystals since they were insoluble in water.

The compounds show variable melting point value in the range of (180-310) °C. The bulk materials used for melting point test was less pure due to the presence of impurities.

The IR spectra recorded on all compounds were compared with the spectra of the tectons and significant shifts (v(N−H) region; the v(C=O) associated with –COOH moiety; and the v_{as} (COO-) and v_{s} (COO-) region) on the important peaks were observed.

The IR spectrum of the free **TCA** shows a strong band around 1700 cm^{-1} assignable to v(C=O) of the –COOH moiety. However, the new strong absorption peaks observed at 1705 cm^{-1} and 1682 cm^{-1} upon compounds formation indicates the presence of COOH groups which is the frequency are shifted compared to free **TCA** molecule because of hydrogen bonding interactions. A broad band observed in the region 3400-3000 cm^{-1} due to v(N-H) peaks, but shifted to higher value during molecular recognition process of the title compounds where it shows two middle strong bands at 3079 and 3528, which correspond to the formation of N-H····O hydrogen bonds.

TCA-PIP, $C_{10}H_6O_8 .C_4H_{10}N_2$

Elemental analysis, Experimental (Calculated) (%):$C_{10}H_6O_8.C_4H_{10}N_2$: C, 49.41(49.55); H, 4.74(4.64); N, 8.23(8.34) %. Melting point: (305-307) °C. IR (cm^{-1}): 3527 s *v*(N−H); 1682 *v*(C=O) , 1239 *v*(C−O).

TCA-PHEN, $C_{10}H_6O_8 .C_{12}H_8N_2$

Elemental analysis, Experimental (Calculated) (%):$C_{10}H_6O_8.C_{12}H_8N_2$: C, 59.65(59.60); H, 3.53(3.48); N, 4.09(4.14) %. Melting point: (224-227) °C. IR (cm^{-1}): 3528 s *v*(N−H); 1705 *v*(C=O), 1238 *v*(C−O).

TCA-DPK, $C_{10}H_6O_8 .C_{11}H_8N_2O$

Elemental analysis, Experimental (Calculated) (%):$C_{10}H_6O_8.C_{11}H_8N_2O$: C, 65.22(65.17); H, 3.50(3.55); N, 4.09(4.16) %. Melting point: (186-188) °C. IR (cm^{-1}): 3079 s *v*(N−H); 1682 *v*(C=O) , 1239 *v*(C−O).

2.2.5 Single Crystal X-Ray Crystallography (SCXRD)

A total of four single crystals were obtained from the slow evaporation technique in both series: **BA-PIP**, **BA-MPIP**, **TCA-PHEN**, **and TCA-DPK.** The crystal refinement data were collected and tabulated in **Table 2.3**.

BA-PIP organic salt

Single crystal X-ray diffraction reveals that crystal **BA-PIP** crystallized in the $P\overline{1}$ space group with triclinic crystal system. The asymmetric unit consist of ½ molecule of the protonated **PIP**, [**PIP**]$^+$ cation which lies in the center of inversion, a deprotonated **BA**, [**BA**]$^-$ anion and a solvated water molecule, as shown in **Figure 2.1**.

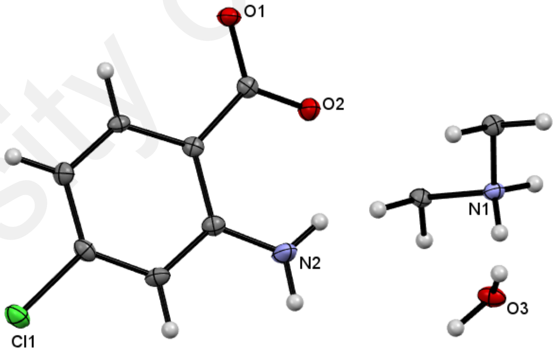

Figure 2.1: Asymmetric unit of BA-PIP

In the molecular structure, the [**BA**]$^-$ moiety shows two different hydrogen bond synthons around the amino group; intermolecular (N(2)-H(2B)····O(1) distance is 2.986 Å, angle N(2)–H(2B)····O(1)= 149°) and intramolecular (N(2)-H(2A)····O(2) distance is 2.691 Å, angle N(2)–H(2A)····O(2) = 129°) connecting the **[BA]**$^-$ molecules represented by the graph set C_1^1 [3]. **Figure 2.2** illustrates these interactions and displaying the center of inversion.

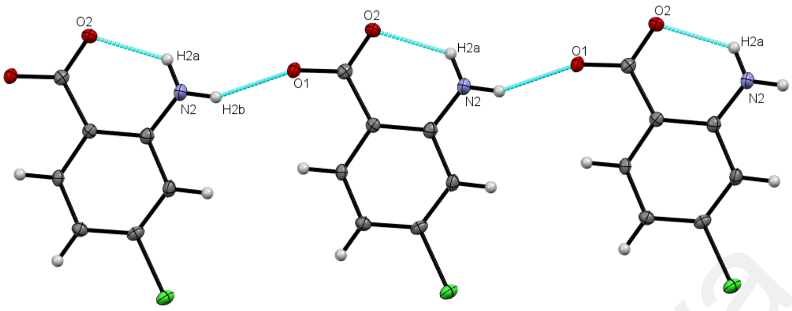

Figure 2.2: The hydrogen bond synthons environment of $[BA]^-$

Apart from that, the cation environment similarly is making two different hydrogen bonding; (N(1)-H(1A)····O(3) is 2.7711 Å, angle N(1)–H(1A)····O(3) = 156°; N(1)-H(1B)····O(2) is 2.6626 Å, angle N(1)–H(1B)····O(2) = 157°); connecting the protonated amine to a water molecule and the carboxylate anion respectively. The N–H····O hydrogen bond synthons contribute to C_1^1 [3] graph set as illustrated in **Figure 2.3**.

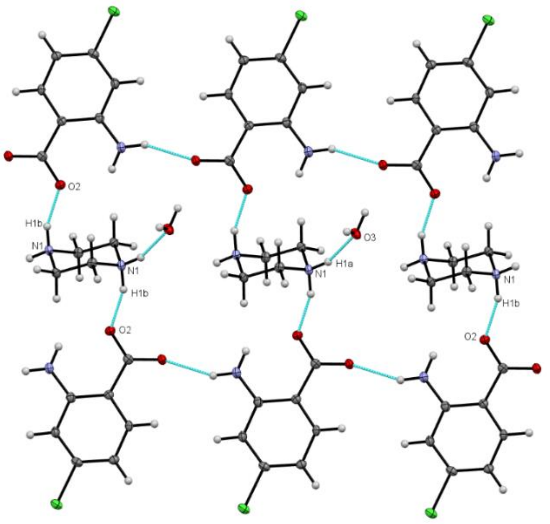

Figure 2.3: The intermolecular hydrogen bond synthons of [PIP]$^+$

All mentioned hydrogen bond synthons are the normal linear hydrogen except for one bifurcated hydrogen bond synthon (O–H····O and O–H····O), which the formation of the synthons was contributed by O atom from the carboxyl functional group and H atom from the water molecules. The two synthons; (O(3)-H(3A)····O(1) is 2.753 Å, angle O(3)–H(3A)····O(1) = 174°; O(3)-H(3B)····O(1) is 2.882 Å, angle O(3)–H(3B)····O(1) = 168°); connecting both oxygen atoms of the [**BA**]$^-$ to the hydrogen atom of water molecule. **Figure 2.4** displays the hydrogen bond synthons environment.

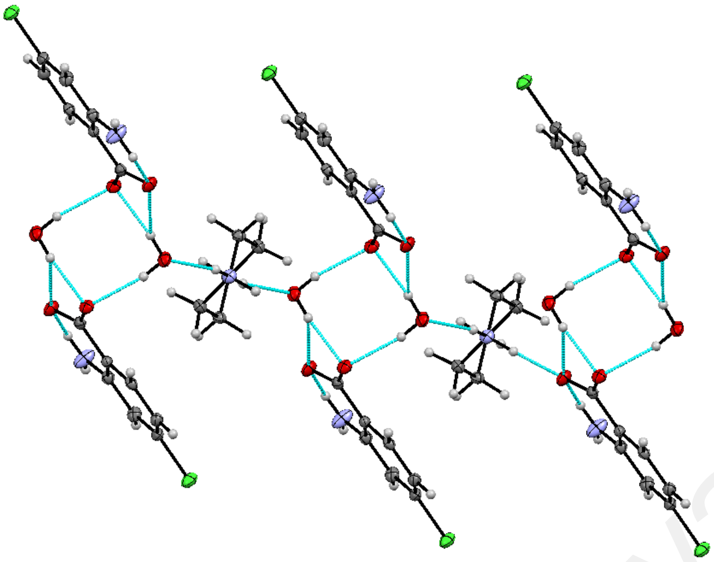

Figure 2.4: The intermolecular (O-H····O) hydrogen bond synthons of [BA]$^-$ and water molecules

Figure 2.5 depicts the square pores resulted from the intermolecular O–H····O hydrogen bond synthons with R_4^4 [10] graph set initiated by the two molecules of water and two molecules of [**BA**]$^-$.

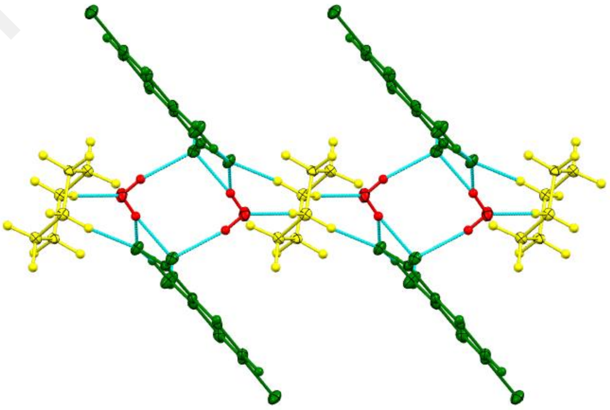

Figure 2.5: Square pores resulted from the intermolecular interactions along *a* axis

Besides that, another view of porous structure can also be seen from the alternate layer of **BA-PIP** that leads to a two-dimensional supramolecular chain. The pores formed by the interactions between four molecules of [**BA**]$^{-}$, four water molecules and two [**PIP**]$^{+}$ as illustrate in **Figure 2.6**.

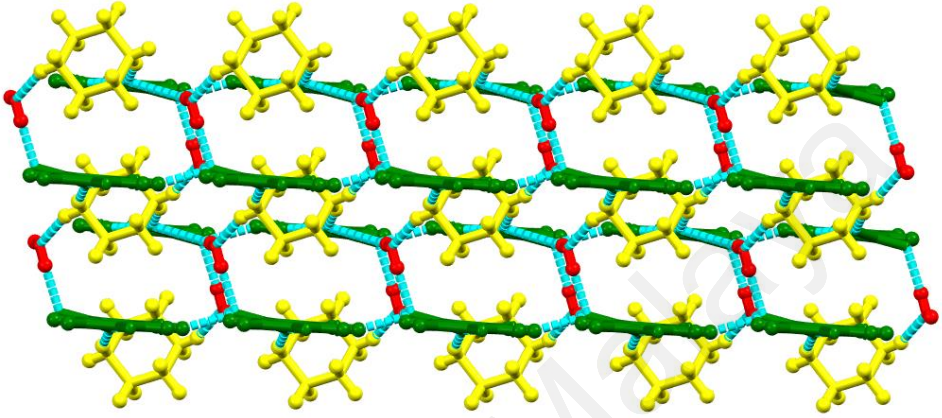

Figure 2.6: Crystal packing of BA-PIP showing two-dimensional square pores

BA-MPIP organic salt

The colourless block crystal of **BA-MPIP** crystallized in $P\overline{1}$ space group in the triclinic crystal system. The structure consist of one molecule of [**MPIP**]$^{+}$ cation and [**BA**]$^{-}$ anion in the asymmetric unit which also represent the molecular structure as illustrated in **Figure 2.7**.

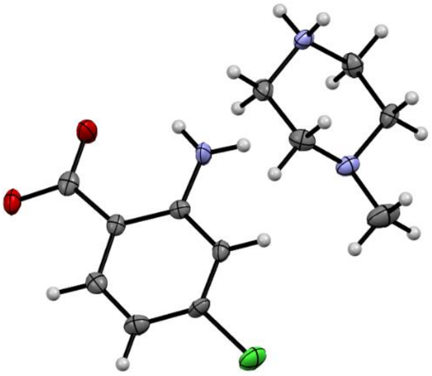

Figure 2.7: Asymmetric unit crystal structure of BA-MPIP

Moreover, the cation environment shows two hydrogen bond synthons; (N(1)-H(1A)····O(2) is 2.7610 Å, angle N(1)–H(1A)····O(2) = 166 °) and; ($N_{N(1)-H(1B)}$····O(1) distance is 2.6728 Å, angle N(1)–H(1B)····O(1) = 168 °) contribute to R_4^4 [12] graph set . **Figure 2.8** shows the cation environment with two sets of each hydrogen bonds generated by the centre of inversion.

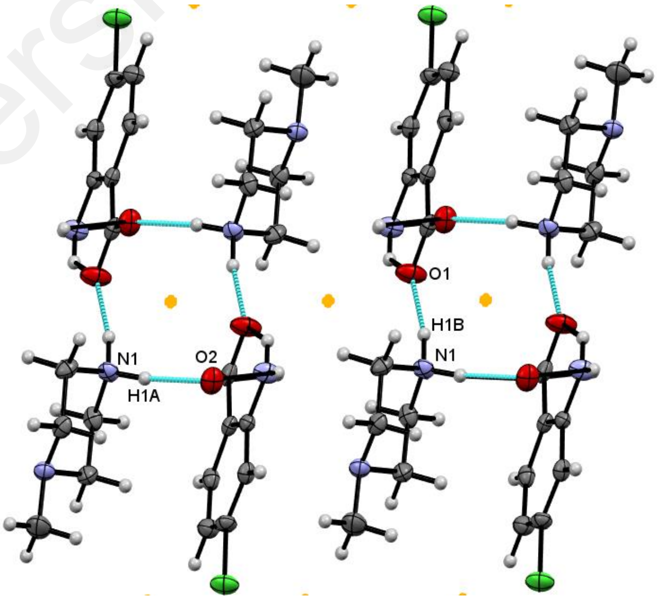

Figure 2.8: The structure of two molecules of BA-MPIP related by the centre of inversion (yellow dots) along *a* axis

The anion moiety in this structure also shows intramolecular; (N(3)-H(3E)····O(1) is 2.6525 Å, 130°) and intermolecular; (N(3)-H(3D)····O(2) is 2.9174 Å, 122°) N–H····O hydrogen bond synthons. **Figure 2.9** illustrates the intermolecular and intramolecular synthons environment for **BA-MPIP** molecules with graph set C_1^1 [3].

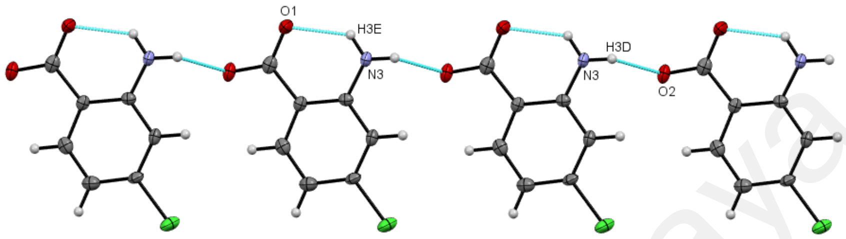

Figure 2.9: Intermolecular and intramolecular hydrogen bond synthons similar to crystal BA-PIP

The arrangement of these intermolecular and intramolecular hydrogen bond synthons (blue lines) lead to square pores of two dimensional supramolecular networks as depicted in **Figure 2.10 (a)** and **Figure 2.10 (b)**.

(a)

(b)

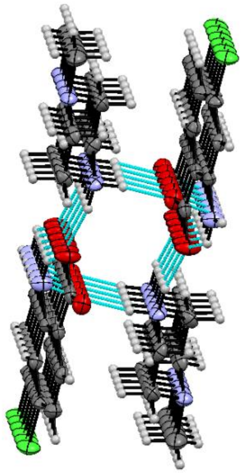

Figure 2.10: Crystal packing view along the *a* (a) and *c* (b) axis respectively.

TCA-PHEN organic salt

The **TCA-PHEN** was crystallized in the $P2_1/c$ space group with monoclinic crystal system. The asymmetric unit comprises of one **TCA** molecules and a molecule of **PHEN** as depicted in **Figure 2.11**.

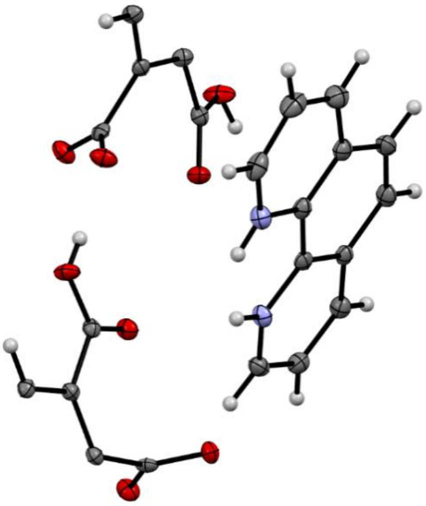

Figure 2.11: Asymmetric unit of TCA-PHEN

The molecular structure of **TCA-PHEN** show the presence of two molecules of **TCA** together with a molecule of **PHEN**. **Figure 2.12** showing layered molecules **TCA-PHEN** in the presence of inversion centre along *b* axis.

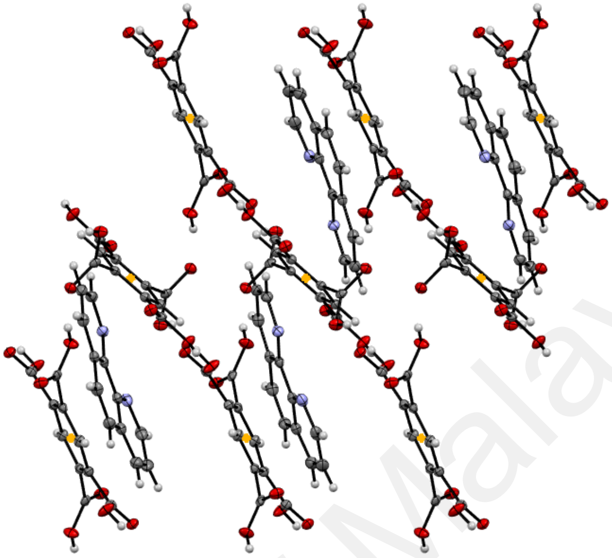

Figure 2.12: Molecular structure of TCA-PHEN with the presence of center of inversion (yellow dots)

Figure 2.13 display the intermolecular N–H····O type of hydrogen bond synthons was observed around the in **PHEN** molecule represented by graph set C_1^1 [3]. The N–H····O (N(4)-H(4)····O(20) is 2.884 Å, 137°) connecting the tecton **TCA** molecule to other **PHEN** molecule.

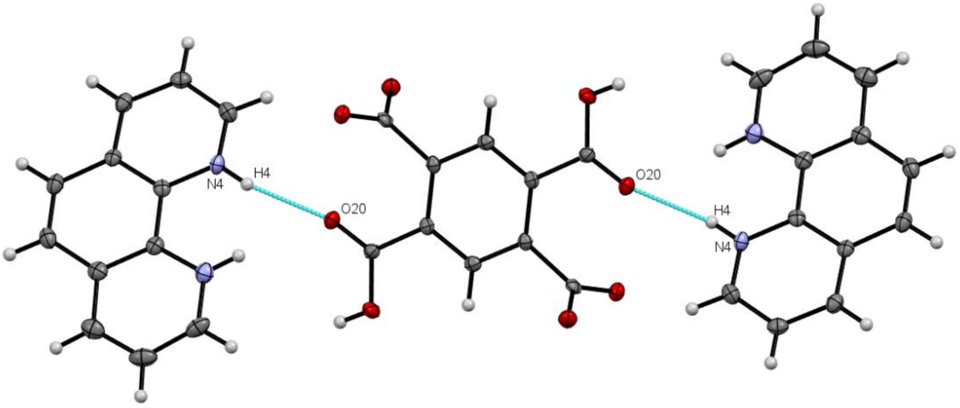

Figure 2.13: Intermolecular interaction of PHEN with TCA

Besides that, another O–H····O type of hydrogen bond synthon was contributed by the O atom from the carboxyl functional group of **TCA** and formed intermolecular interaction with hydroxyl of another **TCA** molecules (O(6)-H(6)····O(9) is 2.618 Å, 165°; O(7)-H(7)····O(18) is 2.527 Å, 166°). The intermolecular interactions environment of O–H····O between the **TCA** molecules contributed to R_4^4 [12] and was illustrated in **Figure 2.14**.

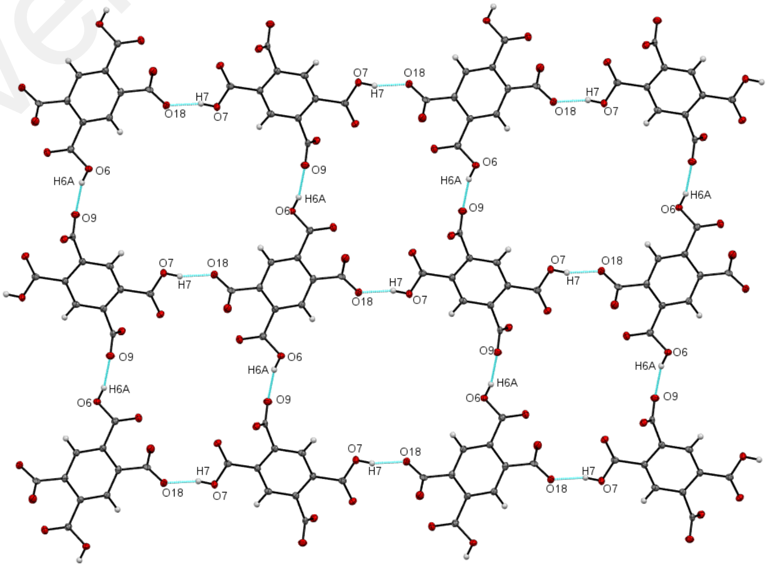

Figure 2.14: Intermolecular hydrogen bonding environment between TCA molecules

These O–H····O and N–H····O hydrogen bond synthons interactions led to three-dimensional crystal packing with layered **TCA** molecules which contribute to square pores and being enclose with two molecules of **PHEN** inside the pores as shown in **Figure 2.15.**

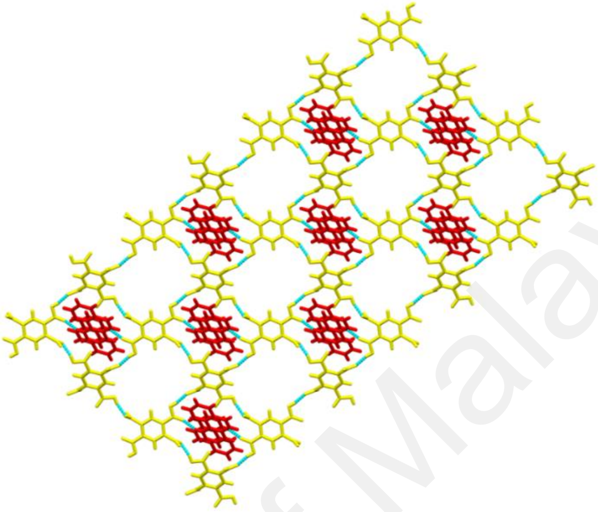

Figure 2.15: Crystal packing of compound TCA-PHEN

TCA-DPK co-crystal

The colourless needle crystal crystallized in $P2_1/n$ space group with the triclinic crystal system. Each asymmetric units consist half of **TCA** molecule and half **DPK** molecule as shown in **Figure 2.16**.

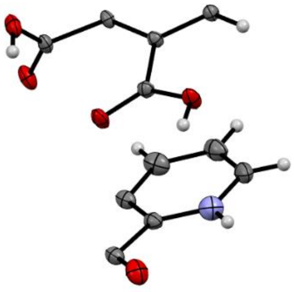

Figure 2.16: The asymmetric unit of TCA-DPK

The molecular structure of **TCA-DPK** consist of one **TCA** molecule and a molecule of **DPK** showing centre of inversion (yellow dots) in the middle of each molecules as portrays in **Figure 2.17.**

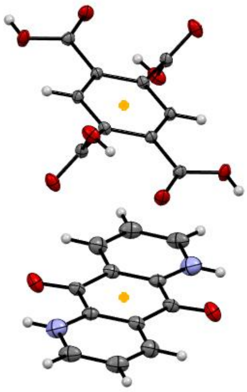

Figure 2.17: Molecular structure of TCA-DPK

TCA molecules in this structure arranged themselves and shows intermolecular O–H····O hydrogen bond synthons; (O(15)-H(15)····O(4) is 2.537 Å, 169°) which contribute to porous structure with R_4^4 [12] graph set as depicted in **Figure 2.18.**

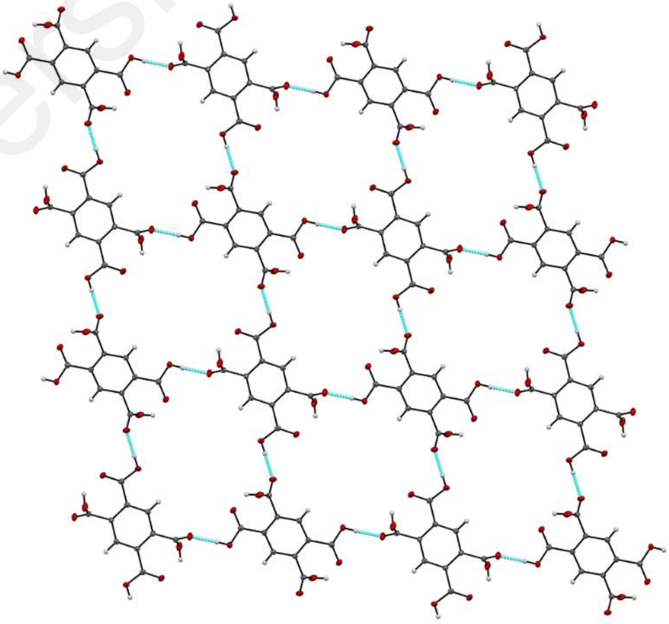

Figure 2.18: The TCA molecules showing an intermolecular hydrogen bonding

There are no π-π stacking interactions obtained from the crystal packing of the molecules since the centroid-centroid distance calculated is 6.875 Å which is larger from the accepted value of 3.3-3.8 Å (Janiak, 2000). Also, crystal packing of compound **TCA-DPK** lead to the formation of a complex of two dimensional supramolecular networks. The pores initiated by the O–H····O hydrogen bond synthons of **TCA** molecules being occupied with two molecules of **DPK** which actually overlay with each other inside the pores. **Figure 2.19** illustrate the crystal packing.

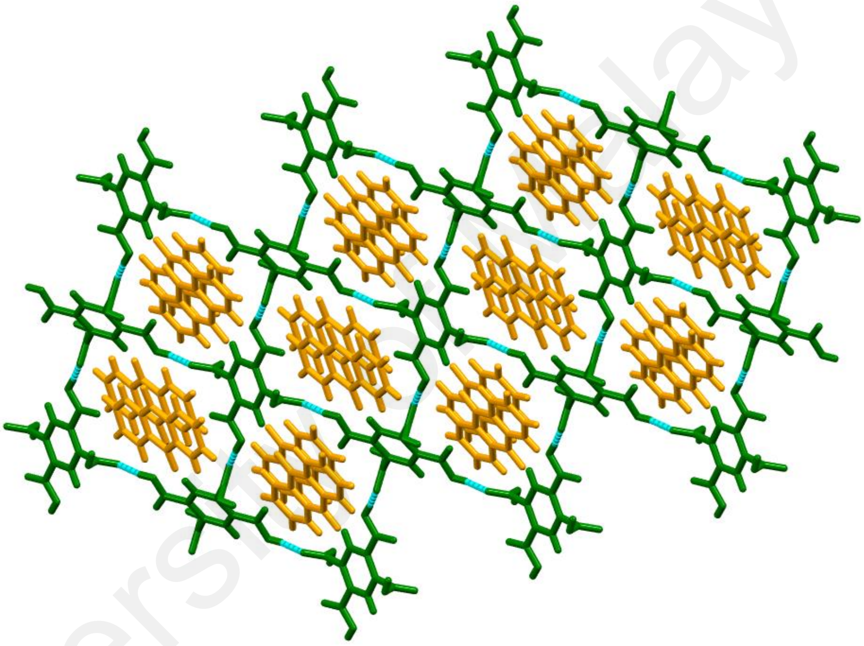

Figure 2.19: Crystal packing of compound TCA-DPK

Table 2.1: Crystallographic and refinement details for (BA-PIP), (BA-MPIP), (TCA-PHEN) and (TCA-DPK)

Parameter	**BA-PIP**	**BA-MPIP**	**TCA-PHEN**	**TCA-DPK**
Empirical formula	$C_{10}H_6O_8$.$C_4H_{10}N_2$	$C_{10}H_6O_8$.$C_5H_{12}N_2$	$C_{10}H_6O_8$.$C_{12}H_8N_2$	$C_{10}H_6O_8$.$C_{11}H_8N_2O$
Formula weight	230.66	271.74	435.36	232.94
Temperature/K	296.15	100.15	100.2(9)	100(1)
Crystal system	Triclinic	Triclinic	Monoclinic	Monoclinic
Space group	$P\bar{1}$	$P\bar{1}$	$P2_1/c$	$P2_1/n$
a/Å	7.070(3)	6.6559(3)	11.8842(16)	6.8750(5)
b/Å	7.800(3)	7.3309(4)	13.5559(14)	12.3146(9)
c/Å	9.712(4)	14.1291(6)	12.2015(17)	11.3737(9)
α/°	93.553(5)	93.970(3)	90.00	90.00
β/°	103.709(5)	98.594(4)	110.403(16)	105.661(8)
γ/°	91.236(6)	94.709(3)	90.00	90.00
Volume/Å^3	519.0(3)	677.04(6)	1842.4(4)	927.18(12)
Z	2	2	4	4
ρ_{calc}g/cm^3	1.476	1.333	1.570	1.6686
μ/mm^{-1}	0.354	0.281	0.122	0.135
F(000)	242.0	288.0	900.0	479.4
Radiation	Mo Kα (λ = 0.71073)	Mo Kα (λ = 0.71073)	Mo Kα (λ = 0.71073)	Mo Kα (λ = 0.71073)
2θ range for data collection/°	4.32 to 61.74	2.92 to 55.46	6.02 to 52.96	6.28 to 60.74
Reflections collected	3193	4858	9709	11890
Independent reflections	2549	3078	3800	2560
Data/restraints/parameters	2549/0/144	3078/0/163	3800/0/293	2560/0/156
Goodness-of-fit on F^2	1.054	0.964	1.069	1.075
Final R indexes [I>=2σ (I)]	R_1 = 0.0504, wR_2 = 0.1373	R_1 = 0.0622, wR_2 = 0.1308	R_1 = 0.0498, wR_2 = 0.1120	R_1 = 0.0966, wR_2 = 0.2925
Final R indexes [all data]	R_1 = 0.0662, wR_2 = 0.1506	R_1 = 0.1267, wR_2 = 0.1610	R_1 = 0.0810, wR_2 = 0.1351	R_1 = 0.1094, wR_2 = 0.3090
Largest diff. peak/hole / e Å^{-3}	0.86/-0.41	0.35/-0.37	0.74/-0.50	0.80/-1.55
CCDC reference	Not submitted	Not submitted	Not submitted	Not submitted

2.2.6 Powder X-Ray Diffraction (PXRD)

PXRD experiments were performed to examine the structural homogeneity of bulk samples by comparing the experimental with the simulated patterns (CIF) calculated from the single crystal (SCXRD) experiments measured at 273 K. As both pairs of patterns matched, the SCXRD results are representative of the bulk materials. The agreement indices, which were in the form of R profile after fitting mode refinement with the calculated powder pattern from crystallographic information file (CIF) of the crystal structure, was found to be coherent with the generally accepted R profile<30%. This suggested that the single crystal had been similar with the bulk materials.

PXRD experiments were conducted on all **BA** and **TCA** products from bulk material and compared with the simulated patterns calculated from the single crystal (SCXRD) experiments measured at 273K. As both pairs of patterns matched for **BA-PIP**, **BA-MPIP**, **TCA-PHEN** and **TCA-DPK** the SCXRD results (blue) are the representative of the bulk materials (red).

2.2.6.1 PXRD for 2-amino-4-chlorobenzoic acid series

Besides that, the PXRD experiments for **BA-PHEN** and **BA-DPK** was also conducted with their starting material compounds since the crystal from the recrystallization process could not be obtained and the pattern obtained for **BA-PHEN** distinct from each other and new peaks began to appear from the starting materials. This indicate that new compounds had formed from **BA** and **PHEN** from mechanochemical grinding as shown in **Figure 2.20**. Unfortunately, the powder pattern for **BA-DPK** instead resulted in physical mixtures of starting materials of **BA** and this indicate that the preparation is unsuccessful.

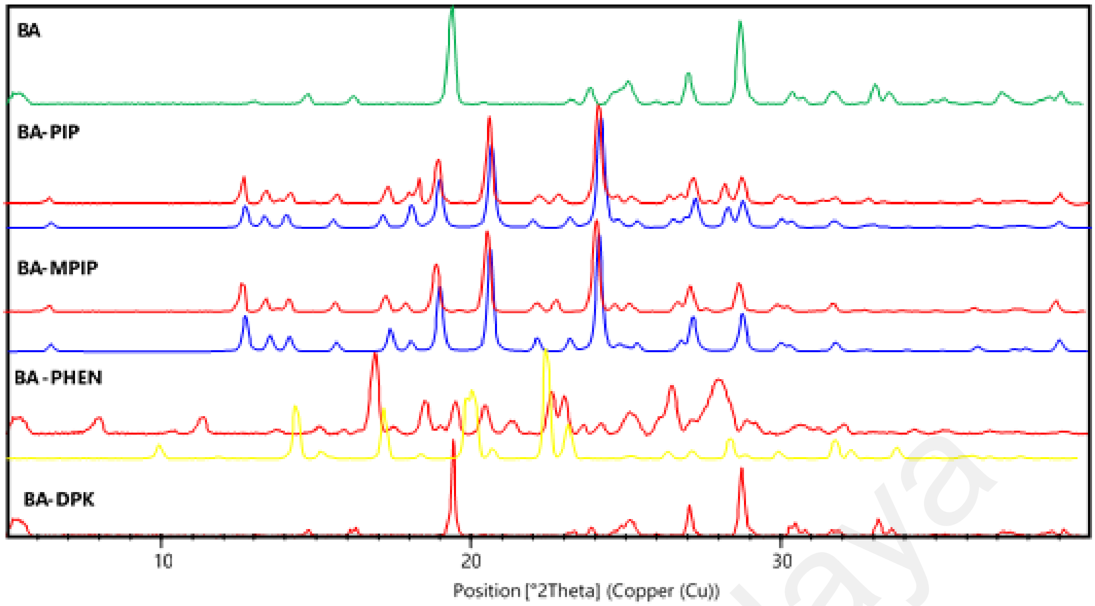

Figure 2.20: Red = bulk product from mechanochemical grinding, blue = simulated single crystal at 273 K, yellow = starting material of pure 1, 10-phenanthroline and green = starting material of pure BA

2.2.6.2 PXRD for 1, 2, 4, 5-benzenetetracarboxylic acid series

Besides that, the PXRD experiments for **TCA-PIP** was also conducted with their starting material compounds since the crystal from the recrystallization process could not be obtained and the pattern obtained were distinct from each other and new peaks began to appear from the starting materials. This indicate that new compound had formed from **TCA** and **PIP** from mechanochemical grinding as shown in **Figure 2.21.**

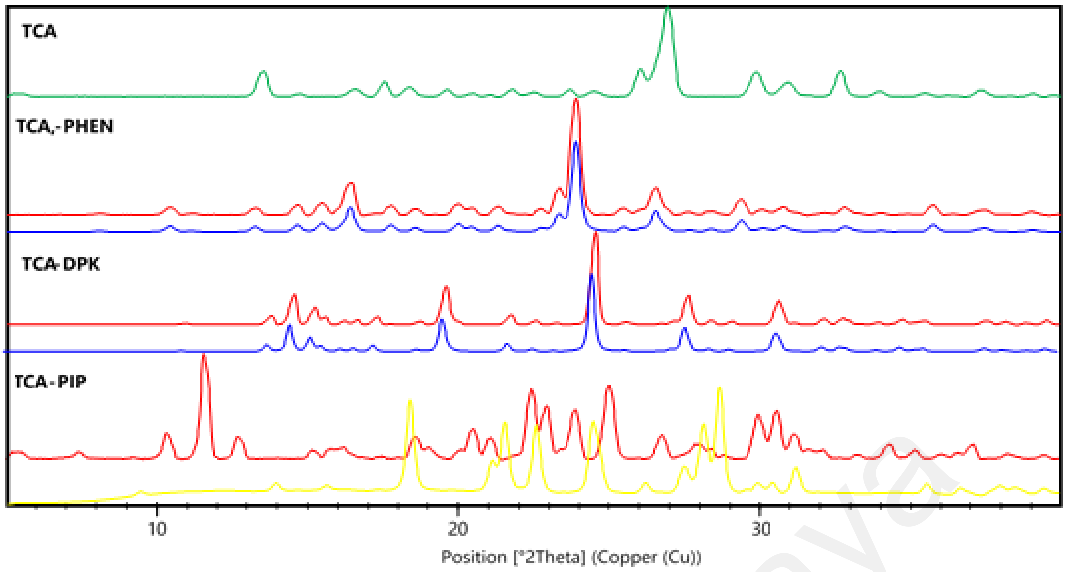

Figure 2.21: Red = bulk product from mechanochemical grinding, blue = simulated single crystal at 273 K, yellow = starting material of pure piperazine and green = starting material of pure TCA

2.3 Conclusion

In this chapter, a total of eight compounds was successfully prepared. **BA-PIP**, **BA-MPIP** and **TCA-PHEN** formed an organic salts while **BA-PHEN** and **TCA-DPK** resulted in formation of co-crystal. However, only two compounds from 2-amino-4-chlorobenzoic acid (**BA-PIP** and **BA-MPIP**) were structurally characterized together with another two compounds from 1, 2, 4, 5-benzenetetracarboxylic acid series (**TCA-PHEN** and **TCA-DPK**).

Common laboratory analytical tools such as CHN elemental analyzer, melting point and FTIR were used to confirm the formation of the organic salts or co-crystals. Based on the elemental analyses result, it shows that the predicted show similarity with the expected compounds. Also, all five compounds obtained shows various range of melting point values. This might be due to the presence of impurities in the bulk materials used since it is less pure compared to crystals. As a result, the compound start to melt at one temperature and not be completely transformed into liquid phase until the temperature risen by several degrees.

Besides that, SCXRD was used in the structure determination of compounds and also to understand the supramolecular architectures. The space group of **BA-PIP** and **BA-MPIP** were same and both organic salts obtained crystallized in triclinic crystal system. The value of unit cell for **BA-PIP** and **BA-MPIP** does not show similarity even both of the compounds crystallized in same crystal system and space group. Meanwhile, the space group of **TCA-PHEN** and **TCA-DPK** were different but both compounds crystallized in the same crystal system which is monoclinic.

In the crystal structures of all four complexes, the interaction is dominated by hydrogen bond synthons rather than π-π stacking interactions and were observed in variable manner. The interactions result depends on both **BA** and **TCA** chosen as tecton which were arranged differently due to their molecular structures and the arrangements that contributed to the stability of the crystal structures.

In addition, the approach of crystal engineering in designing the molecular structure co-crystals or organic salts resulted in various supramolecular structure of crystal packing from the intermolecular and intramolecular hydrogen bond synthons within the molecules of both series. The combinations both series resulted in co-crystal formation instead of organic salts if the association between the two different tectons acid and amines in the aggregate is strong enough to survive the crystallization process.

From the structure of **BA** series, the packing of the molecules resulted in square pores. As for **BA-PIP**, the pores was initiated by the water and **BA** molecules while **BA-MPIP** pores was from the interaction of **BA** and **MPIP** molecules. On the other hand, porous structure formed in **TCA** series initiated from the synthons interactions of **TCA** molecules and being occupied with **PHEN** or **DPK** amines respectively.

Apart from that, PXRD performed on all compounds of both series showed that single-crystal data collected functioned as the representative of the bulk material at room temperature. As for crystals with no crystal data, PXRD analysis was also performed and the results obtained provided the evidence for the formation of either organic salts or co-crystals since the peaks from the bulk materials were different with starting materials.

CHAPTER 3: CRYSTAL ENGINEERING OF DITHIOCARBAMATE COMPLEXES: 2D TO 3D STRUCTURES

3.1 Introduction and Literature Review

The interest in coordination chemistry of nitrogen-sulphur donor ligand has been in much interest and the complexation of these ligands with transition metal ions keep growing in recent decades (Tarafder et al., 2001). Dithiocarbamate (DTC) ligand was first identified as the nucleophilic attack of primary or secondary amines with carbon disulfide in basic solution as shown in **Scheme 3.1**. The preparation for dithiocarbamatic acid salts and their S-alkylated derivatives had been reported by Aly et al., to possess in various biological activities such as in treatment of cancer and antifungal activity (Aly et al., 2012).

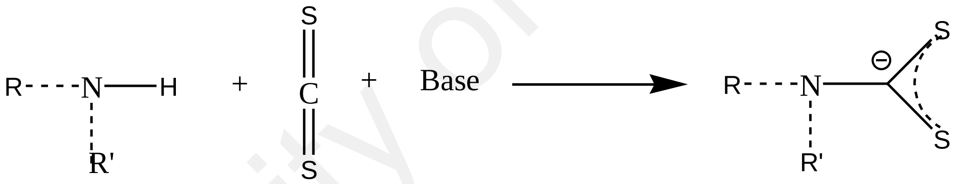

R=H, Alkyl, Aryl: R’=Alkyl, Aryl

Scheme 3.1

The usage of the coordination entities dithiocarbamate (DTC) ligands in research of designing new supramolecular architectures have been developed recently due to its structure-redox properties (Wilton-Ely et al., 2008). As reported in the literature, the dithiocarbamate ligand $^{-}S_2CNRR'$, is well known as an effective chelator of transition metals, main group elements and lanthanides (Heard, 2005; G Hogarth, 2005). Seemingly, small modification to the ligand can lead to significant changes in the structure behaviour of the complexes formed (Sherwood et al., 2015).The use dithiocarbamate (DTC) ligand as building block in preparation of metal complexes can usually form different motifs of crystalline structures depending on the ligands and solvents involved in the reaction.

For example, *N*-hydroxyethyl-*N*-isopropyldithiocarbamate, *N*, *N'*-dihydroxyethyldithiocarbamate (CAS: 2801-04-9) and *N*-hydroxyethyl-*N*-methyldithiocarbamate are already commercially available and also being used (**Scheme 3.2).**

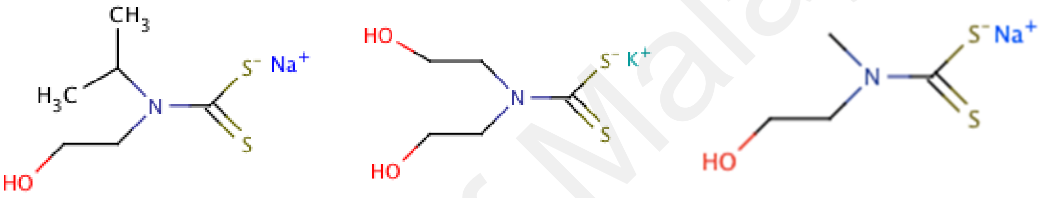

Scheme 3.2: Chemical structure of DTC series used

DTC mixed-ligand complexes with organic linkers been growing due to their structural, biological, electrochemical and thermal properties (Tarique, 2015). In 2011, a case study using *N*-isopropyl-*N*-methyldithiocarbamato as ligand with zinc metal as the precursor to construct a molecular structure with 1,10-phenanthroline (Wahab et al., 2011). This research is in extension studies of the precursor and the presence of 1,10-pehnanthroline as linker resulted to a distorted octahedron geometry (**Figure 3.1**).

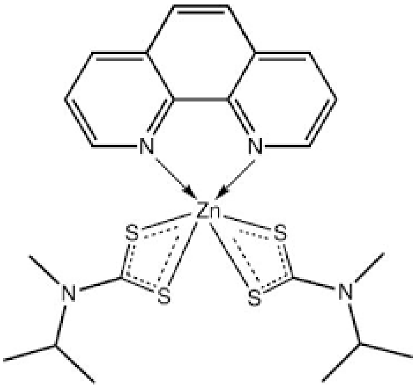

Figure 3.1: Molecular structure of Zn($C_5H_{10}NS_2$)$_2$-($C_{12}H_8N_2$)

Similar case study also reported by with different metal precursor but the geometry obtained was similar to the previous case mentioned before and also an on-going structural studies of nitrogen donor adducts of cadmium dithiocarbamate. The precursor was then react with pyridine and a title compound of Cd($C_6H_{11}N_2S_2$)$_2$(C_5H_5N)$_2$ as shown in **Figure 3.2** was obtained from slow evaporation process after few days (Valarmathi et al., 2012).

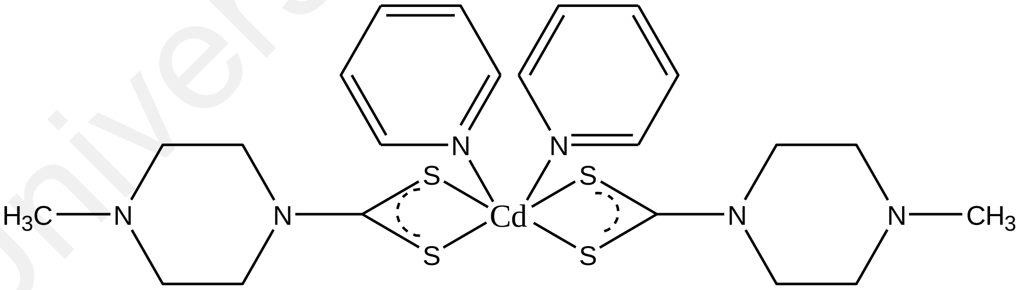

Figure 3.2: Molecular structure of Cd($C_6H_{11}N_2S_2$)$_2$(C_5H_5N)$_2$

Apart from providing various type of molecular structures, the growing interest in using amine as linker is due to wide range of application in gas storage and separation, heterogeneous catalysis or chemical sensing (Fischer & Hoffmann, 2010). Apparently, it is believed that small modification to the ligand can lead to significant changes in the structure behaviour of the complexes formed (Sherwood et al., 2015).

Herewith we report crystal engineering studies of DTC complexes with the presence of organic linkers in designing various supramolecular network. A total of four known precursor had been prepared in this study (**Scheme 3.3**).

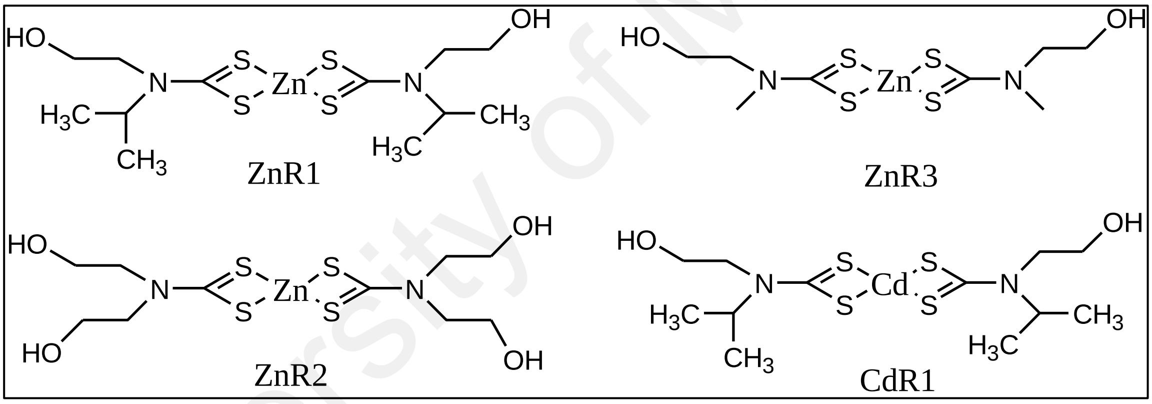

Scheme 3.3: Chemical structure of four reported precursor used

These precursor were then added with organic linker (L = **BIPY, PHEN, PIP** or **PYR**) as depicted in **Scheme 3.4** and **Scheme 3.5** to prepare mixed-ligand complexes which will be discussed herein.

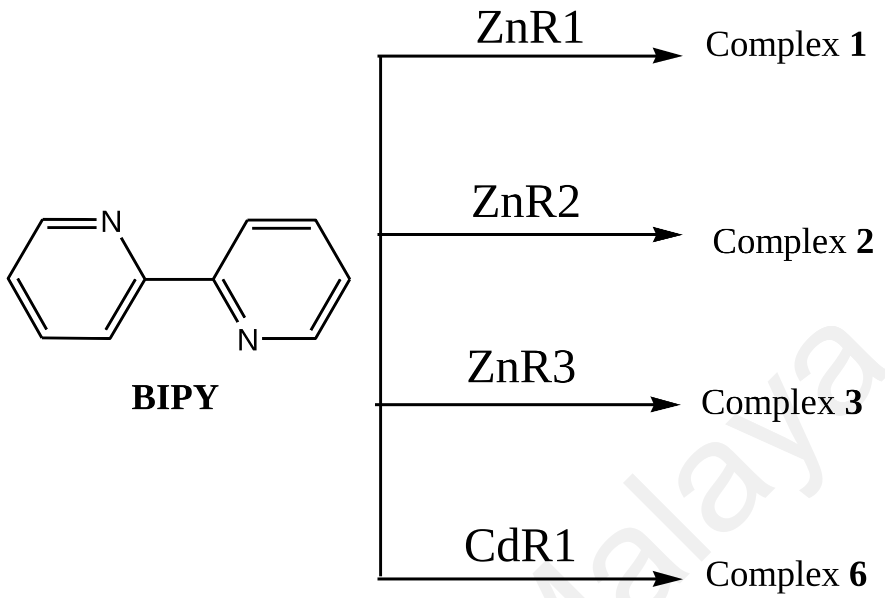

Scheme 3.4: Synthesis diagram of BIPY with metal precursor

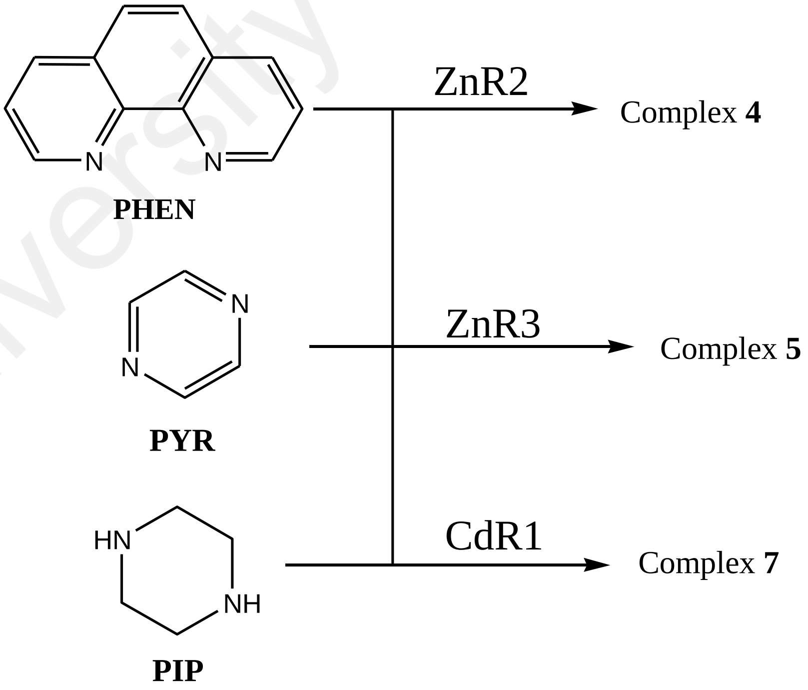

Scheme 3.5: Synthesis diagram of PHEN, PYR and PIP organic linker with metal precursor

3.2 Methodology

3.2.1 Materials

All reactions were carried out under ambient conditions. All reagents and solvents used were commercially available and used as received without further purification.

3.2.2 Experimental

3.2.2.1 Syntheses of Dithiocarbamate Ligands

***N*-hydroxyethyl-*N*-isopropyldithiocarbamate, R1**

50% (w/v) NaOH was prepared by dissolving NaOH (50.00g) into 100mL volumetric flask with distilled water. Carbon disulfide (0.05mol, 3.00mL) was added to a stirred solution of ethanolic 2-(isopropylamine) (0.05mol, 5.80mL) in an ice bath. Few drops of acetone were added into the mixture and the reaction was left for 1 minute before adding 50% (w/v) NaOH (2.00mL) solution. This step was repeated twice to give white precipitate. The precipitate were isolated upon filtration, washed with acetone and dried in the dessicator. (Yield: 4.22 g, 72.38 %).

***N, N'*-dihydroxyethyldithiocarbamate, R2**

50% (w/v) KOH was prepared by dissolving KOH (50.00g) into 100mL volumetric flask with distilled water. Carbon disulfide (0.05 mol, 3.00 mL) was added to a stirred solution of diethanolamine (0.05 mol, 4.80 mL) in an ice bath. The reaction was left for 1 minute before adding 50% (w/v) KOH (0.05mol, 5.60 mL) and the solution was continued stirred for overnight. The precipitate were isolated upon filtration, washed with acetone and dried in the dessicator. (Yield: 2.12 g, 44.31%).

_N_-hydroxyethyl-_N_-methyldithiocarbamate, R3

Chloroform (5.00 mL) was added into 2-methylaminoethanol (0.05mol, 4.00mL) and stirred in an ice bath at about 8°C. This is followed by adding carbon disulphide (0.05 mol, 3.00mL) and 50% (w/v) NaOH (0.05mol, 4.00mL). The temperature was maintained for 1 hour and white precipitate formed. The precipitate formed was isolated upon filtration and washed with acetone. To remove the impurities ethanol was added to the precipitate and stirred it for a while. Again, the white precipitate formed was isolated upon filtration, washed with acetone and dried in the desiccator. (Yield: 1.65 g, 41.31%).

3.2.2.2 Syntheses of *di* R1, R2 and R3 metal complexes

Bis[_N_-(2-hydroxyethyl)-_N_-isopropyldithiocarbamato]zinc, ZnR1

Both **R1** (10.00 mmol, 2.06 g) and zinc chloride (5.00 mmol, 0.70 g) were dissolved in minimum amount distilled water separately. Zinc chloride solution was added into ligand solution drop wisely to give white precipitate. The white precipitate formed was isolated upon filtration and washed with distilled water, followed by diethyl ether. The product was pale orange powder and dried in desiccator. (Yield: 0.52 g, 76.01%).

Bis [*N*,*N'*-bis*(*2-hydroxyethyl)dithiocarbamato]zinc dihydrate, ZnR2

Both **R2** (10.00 mmol, 2.29 g) and zinc chloride (5.00 mmol, 0.70 g) were dissolved in minimum amount distilled water separately. Zinc chloride solution was added into ligand solution drop wisely to give white precipitate. The white precipitate formed was isolated upon filtration and washed with distilled water, followed by diethyl ether. The product of white powder was dried in desiccator. (Yield: 1.84 g, 80.15%).

Bis[*N*-(2-hydroxyethyl)-*N*-methyldithiocarbamato]zinc, ZnR3

Both **R3** (10.00 mmol, 1.73 g) and zinc chloride (5.00 mmol, 0.70 g) were dissolved in minimum amount of distilled water separately. Aqueous zinc chloride was added into the ligand solution drop wisely to give white precipitate. The white precipitate formed was filtered and stirred with ether. The precipitate formed was isolated upon filtration and washed with ether. The product was white powder and dried in the desiccator. (Yield: 0.20g, 15.56%).

Bis[*N*-(2-hydroxyethyl)-*N*-isopropyldithiocarbamato]cadmium, CdR1

Both **R1** (10.00 mmol, 2.03 g) and cadmium acetate (5.00 mmol, 1.03 g) were dissolve in 20 mL and 25 mL of distilled water respectively. Aqueous cadmium acetate was added into the ligand solution drop wisely followed by 20 mL of warm chloroform while stirring. The mixture was continued stirring for 30 minutes to give out white precipitate which then separated from the chloroform by filtration. The white product was dried in the desiccator. (Yield: 1.42g, 70.15%).

3.2.2.3 Synthesis of mixed-ligand complexes

Zn[S_2CN(*i*Pr)CH_2CH_2OH]$_2$(BIPY) – Crystal 1

ZnR1 (0.47 mmol, 0.20 g) and **BIPY** (0.47 mmol, 0.07 g) were dissolved in 30 mL of chloroform and 10 mL of acetone respectively. **BIPY** solution was added dropwise into **ZnR1** solution and was stirred for about 30 minutes. The color of the mixture changed from colorless to light yellow. The mixture was left at room temperature to allow crystallization process. Needle crystals of **1** were formed after three days and were analyzed by single crystal diffraction technique. (Yield: 0.20g, 15.56%).

Zn[S_2CN(CH_2CH_2OH)$_2$]$_2$(BIPY) – Crystal 2

ZnR2 Complex **2** (0.47 mmol, 0.20 g) and **BIPY** (0.47 mmol, 0.07 g) were dissolved in 30 mL of acetone and 10 mL of ethanol respectively. **BIPY** solution was added dropwise into **ZnR2** solution and was stirred for about 30 minutes. The color of the mixture changed from colorless to light yellow solution. The mixture was left to allow crystallization process. Block crystals of **2** were formed after a week and were analyzed by single crystal diffraction technique. (Yield: 0.11g, 56.00%).

Zn[S_2CN(CH_2CH_2OH)(CH_3)]$_2$(BIPY) – Crystal 3

ZnR3 (0.55 mmol, 0.20 g) and **BIPY** (0.55 mmol, 0.08 g) were dissolved in 30 mL of acetone and 10 mL of ethanol respectively. **BIPY** solution was added dropwise into **ZnR3** solution and was stirred for about 30 minutes. The color of the mixture changed from colorless to light yellow solution. The mixture was left at room temperature to allow crystallization process. Needle crystals of **3** were formed after a week and were analyzed by single crystal diffraction technique. (Yield: 0.09g, 45.30%).

$Zn[S_2CN(CH_2CH_2OH)_2]_2(PHEN)$ – Crystal 4

ZnR2 (0.50 mmol, 0.20 g) and **PHEN** (0.50 mmol, 0.09 g) were dissolved in 20 mL acetone and 5 mL chloroform respectively. The colour of the mixture changed from colourless to yellow. The mixture was stirred for 30 minutes and then filtered by gravity before it was left at room temperature to allow crystallization process. Yellow crystal color of **4** formed in few days and were analyzed by single crystal diffraction technique. (Yield: 0.08g, 39.50%).

$Zn[S_2CN(CH_2CH_2OH)(CH_3)]_2(PYR)$ – Crystal 5

ZnR3 (0.55 mmol, 0.20g) and **PYR** (1.09 mmol, 0.09 g) were dissolved in 30 mL of acetone and 10 mL of ethanol respectively. **PYR** solution was added drop wisely into aqueous **ZnR3** and was stirred for about 30 minutes. The mixture was left at room temperature to allow crystallization process. Colorless crystals **3** formed after a week and were analyzed by single crystal diffraction technique. (Yield: 0.05g, 25.30%).

$Cd[S_2CN(\textit{i}Pr)CH_2CH_2OH]_2(BIPY).CHCl_3$ – Crystal 6

CdR1 (0.43 mmol, 0.20 g) and **BIPY** (0.43 mmol, 0.07 g) were dissolved in 25 mL of chloroform and 10 mL of acetone respectively. The cadmium complex solution was stirred and the solution of the ligand complex was added dropwise while stirring. The mixture was continued stirring for 30 minutes to obtain a clear yellow solution before it was filtered and left in fume hood. Colorless needle crystals of **6** formed after two days and were analyzed by single crystal diffraction technique. (Yield: 0.03g, 16.00%).

Cd[S_2CN(***i***Pr)CH_2CH_2OH]$_2$(PIP) – Crystal 7

CdR1 (0.44 mmol, 0.21 g) and **PIP** (0.43 mmol, 0.08 g) were dissolved in 15 mL of chloroform and 5 mL acetonitrile respectively. **PIP** solution was added drop wisely into **CdR1** solution and the mixture was stirred for an hour at room temperature. The clear solution mixture then was left for slow evaporation to give colorless crystals and were analyzed by single crystal diffraction technique. (Yield: 0.04g, 22.30%).

3.2.3 Measurements

Melting points were determined on a MEL-TEMP II melting point apparatus and the elemental analyses were performed on a Perkin Elmer PE 2400 CHN Elemental Analyzer.

FT-IR spectra were measured on a Perkin Elmer Spectrum 400 FT Mid-IR/Far-IR spectrophotometer with diamond crystal plate in the frequency range of 4,000–400 cm^{-1}.

Single crystal X-ray diffraction data for, complex **4** and complex **6** were collected on a Bruker AXS SMART APEX II diffractometer with a CCD area detector Mo K_α (λ = 0.71073 A°). High quality crystals were chosen under a polarizing microscope and had been mounted on a glass fibre. Data processing and absorption correction were carried out using the APEX II software package (Bruker, 2005).

Single crystal X-ray diffraction data for complex **1**, **2**, **3**, **5** and **7** were collected at 100 K on Oxford Supernova Dual Wavelength diffractometer Mo K_α (λ = 0.71073 A°). Absorption correction was performed by multi-scan method using CrysAlis PRO, with empirical absorption correction using spherical harmonics, implemented in SCALE3 ABSPACK scaling algorithm (Ganapayya *et al*., 2013).

All the structures were solved by employing the charge flipping method using Superflip solution program (Palatinus & Chapuis, 2007). The hydrogen atoms were placed in geometrically-calculated position and included in the refinement process using the riding model with $U_{iso} = 1.2U_{eq}$ C(H,H) groups. Moreover, the full matrix least-squares refinement against $|F^2|$ was carried out via SHELXTL refinement program (Sheldrick, 2008) and the final refinement included atomic position for all the atoms, anisotropic thermal parameters for all the non-hydrogen atoms, and isotropic thermal parameters for all the hydrogen atoms. The programs Olex2 (Dolomanov et al., 2009), PLATON (Spek, 2009), and Mercury (Macrae *et al*., 2008) were also used throughout the study.

Powder X-Ray Diffraction (PXRD) was carried out using PANalytical Empyrean XRD system, with Cu K_α radiation (λ = 1.54056 Å) in the range of 2θ = 5° to 40° with a step size of 0.026°. Comparison between experimental and calculated (from CIFs) PXRD patterns was performed with X'Pert HighScore Plus 20 (PANalytical, 2009).

3.3 Results and Discussion

3.3.1 General spectroscopic characterization of complexes 1-7

Since the yield was low, the remaining solution was reduced and the precipitates obtained were examined by PXRD. Powder pattern for PXRD of the bulk materials of the crystals were found to be consistent with the calculated pattern generated using single crystal X-ray diffraction and therefore further characterizations were done using these particular precipitate. However, as for crystal **4** and **7**, the PXRD pattern were quite different from the simulated pattern due to the presence of impurities and detailed discussion in section **3.3.3**.

The elemental analyses data of all prepared compounds were performed and the experimental values agree quite well with the calculated values which indicates that the expected product was successfully obtained. Melting point values for all compounds shows (130-180)°C in range. From the result, all compounds does not show a sharp melting points value. As mentioned in first paragraph, the presence of impurities in bulk materials obtained from the precipitation process also affects the melting point values.

IR spectra shows that all compounds are having almost the same important frequencies. The important IR peak values are in the accepted range for all compounds; 900–1200 for *ν*(C−S) and 1250–1360 for *ν*(C−N) (Nabipour et al., 2010; Virginia & Kaplan, 1962). However, new absorption bands are expected to form since there is presence of new amine bond between precursor and mixed-ligands.

Complex 1

Elemental analysis, Experimental (Calculated) (%):$C_{22}H_{32}N_4O_2S_4Zn$: C, 45.22(45.70); H, 5.50(5.58); N, 9.15(9.70) %. Melting point: (148-152) °C. IR (cm^{-1}): 1159 s *ν*(C−N); 1134 *ν*(C=S) , 1053 *ν*(C−O).

Complex 2

Elemental analysis, Experimental (Calculated) (%):$C_{20}H_{32}N_4O_6S_4Zn$: C, 35.55(38.86); H, 4.95(5.22); N, 8.94(9.06) %. Melting point: (176-180) °C. IR (cm^{-1}): 1170 s *ν*(C−N); 1073 *ν*(C=S) , 1059 *ν*(C−O).

Complex 3

Elemental analysis, Experimental (Calculated) (%):$C_{18}H_{24}N_4O_2S_4Zn$: C, 38.99(41.41); H, 4.15(4.63); N, 10.23(10.73) %. Melting point: (156-160) °C. IR (cm^{-1}): 1249 s *ν*(C−N); 1155 *ν*(C=S) , 1056 *ν*(C−O).

Complex 4

Elemental analysis, Experimental (Calculated) (%):$C_{30}H_{18}N_{12}S_2Zn$: C, 43.11(43.60); H, 4.44(4.66); N, 9.01(9.24) %. Melting point: (150-158) °C. IR (cm^{-1}): 1249 s *ν*(C−N); 1155 *ν*(C=S) , 1056 *ν*(C−O).

Complex 5

Elemental analysis, Experimental (Calculated) (%):$C_{20}H_{36}N_6O_4S_8Zn_2$: C, 25.45(29.59); H, 4.04(4.47); N, 9.95(10.35) %. Melting point: (132-136) °C. IR (cm^{-1}): 1236 s *ν*(C−N); 1157 *ν*(C=S) , 1036 *ν*(C−O).

Complex 6

Elemental analysis, Experimental (Calculated) (%):$C_{23}H_{33}N_4O_2S_4CdCl_3$: C, 36.93(37.10); H, 4.34(4.46); N, 7.26(7.52) %. Melting point: (146-149) °C. IR (cm^{-1}): 1012 s *ν*(C−N); 1129 *ν*(C=S) , 1158 *ν*(C−O).

Complex 7

Elemental analysis, Experimental (Calculated) (%):$C_{16}H_{34}CdN_4O_2S_4$: C, 34.42(34.62); H, 5.79(6.17); N, 9.77(10.10) %. Melting point: (142-144) °C. IR (cm^{-1}): 1027 s *ν*(C−N); 1027 *ν*(C=S) , 1156 *ν*(C−O).

3.3.2 Single Crystal X-Ray Diffraction Analysis

A total of seven mixed-ligand complexes were successfully obtained from stirring technique using two types of metal precursor and four amines. The crystals of the complexes **1**–**7** obtained by slow evaporation process of the solution remaining after filtration of the reaction mixtures. Single crystals of all seven complexes were acquired from ethanol or chloroform solvents after a few days and analyzed by SCXRD then being compared with the precursor. However, only two out of four precursor will be discussed only to highlight the differences in geometry of the precursor and mixed-ligand complexes. Herein, the crystal structure of **ZnR2** and **ZnR3** precursor and seven mixed-ligand complexes were discussed thoroughly.

3.3.2.1 Crystal description of ZnR2 and ZnR3 precursor

ZnR2 crystal

Crystal **ZnR2** crystallized in monoclinic crystal system with *C2/c* space group as shown in **Figure 3.3.**

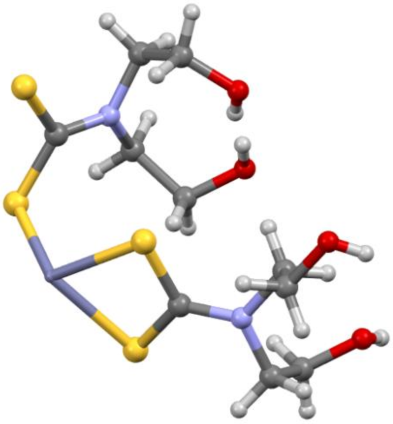

Figure 3.3: Asymmetric unit of ZnR2

The zinc atom displays octahedral coordination geometry *via* four different ligand. Each zinc ion is six-coordinated by two bidentate and two monodentate **R2** ligands respectively. The bond angle of S2-Zn1-S1 and S1-Zn1-S3^{1} are 75.38° and 149.48°C respectively which deviated marginally from the ideal 90.00°, hence showing the distorted octahedral geometry of the structure. **Figure 3.4** display molecular structure of **ZnR2**.

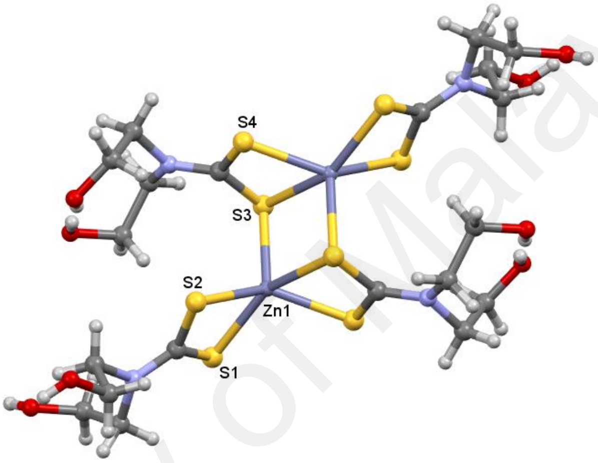

Figure 3.4: Molecular structure of ZnR2

There is a O–H····O intermolecular interaction between the adjacent molecules; O(2)–H(2A)····O(3) = (2.615 Å,180°). Besides that, another O–H····O hydrogen bond synthons observed in supramolecular chain of **ZnR2** molecules; O(1)–H(1A)····O(2) = (2.653 Å ,179°) connecting hydrogen bond donor of **R1** ligand to oxygen atom of **R1** ligand of another **ZnR1** compounds. The hydrogen bond synthons generate graph set of C_{1}^{1} [3] as display in **Figure 3.5**.

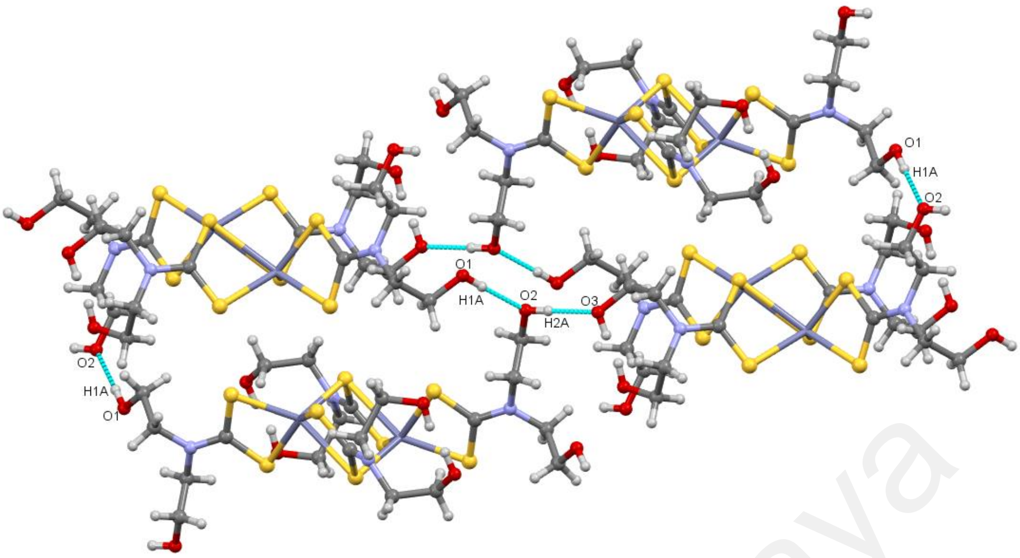

Figure 3.5: Hydrogen bond synthon between the molecules

The arrangements of monodentate and a bidentate manner of the sulphur atom at each ligand aligned them into one dimensional crystal packing along *b* axis as shown in **Figure 3.6**.

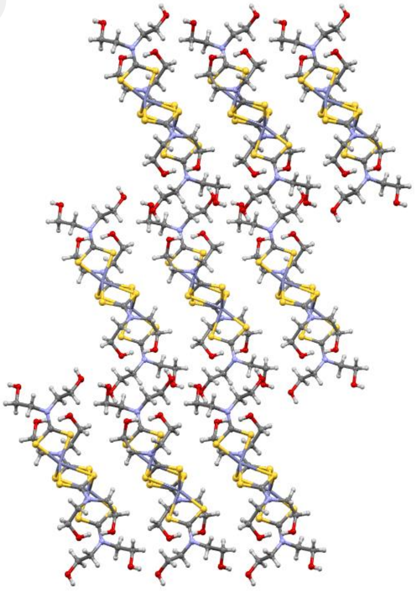

Figure 3.6: Crystal packing of ZnR2

ZnR3 crystal

ZnR3 crystallized in triclinic crystal system with $P\overline{1}$ space group. The asymmetric unit comprises of half independent molecule of compound **ZnR3** with the presence of a solvated molecule (**Figure3.7**).

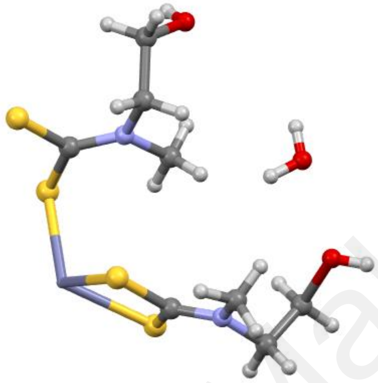

Figure 3.7: Asymmetric structure of ZnR3

The zinc atom displays tetrahedral coordination geometry *via* three different ligands. Each zinc ion is coordinated as bidentate ligand to one molecule of **R3** through the sulphur atom and the other side show bridging-chelating with **R3** ligand with presence of a solvated water molecules. The bond angle of S3-Zn1-S1, S3-Zn1-S2 and S4-Zn1-S1 are 113.45°, 112.36° and 135.18° respectively which deviated from the ideal angle of 109.5°, hence showing distorted tetrahedral geometry of the structure. **Figure 3.8** show the presence of center of inversion (yellow dots) in the molecular structure of **ZnR3** along *a* axis**.**

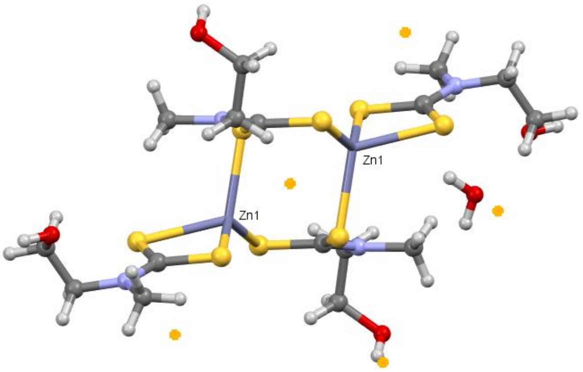

Figure 3.8: Molecular structure of ZnR3

ZnR3 molecules show two different O–H····O hydrogen bond synthons; O(1)–H(1)····O(2) = (2.676 Å, 159°) and O(2)–H(2)····O(2) = (2.677 Å, 160°) connecting to another **ZnR3** precursor. Another O–H····O hydrogen bond synthon resulted from the interaction of hydrogen bond of the water molecule with oxygen atom of the ligand; O(1W)–H(1WB)····O(1) = (2.49 Å, 155°). Similar to previous discuss structure, the O–H····O in this molecules also resulted in C_1^1 [3] graph set as portray in **Figure 3.9**.

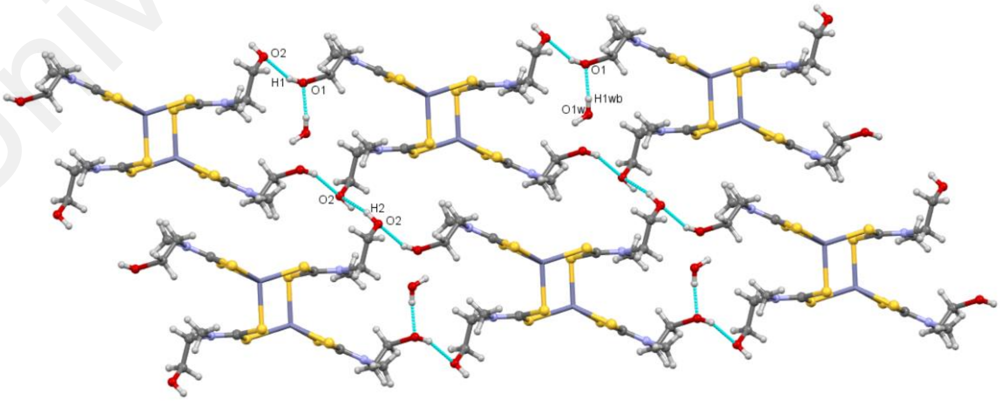

Figure 3.9: O–H····O hydrogen bond synthon environment of ZnR3

Crystal packing of **ZnR3** long *a* axis show a pores obtained due to the presence of the O–H····O hydrogen bond synthon together with C–H····O and C–H····S short contacts (**Figure 3.10**).

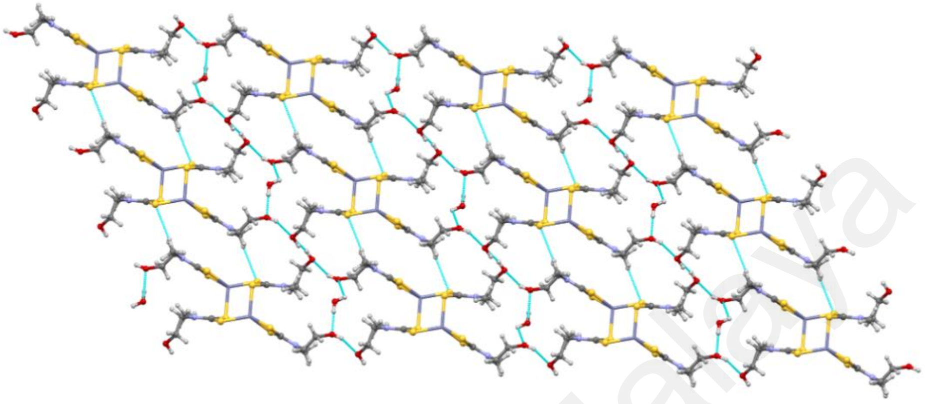

Figure 3.10: Crystal packing of ZnR3

3.3.2.2 Crystal structure description of mixed-ligand complexes

Crystal 1

Colourless needle of crystal 1 was obtained from the slow evaporation technique in chloroform. The molecular structure of **1** crystallized in monoclinic crystal system with *C*2/*c* space group. The asymmetric unit contains a pair of independent half-molecules of the complex as shown in **Figure 3.11.**

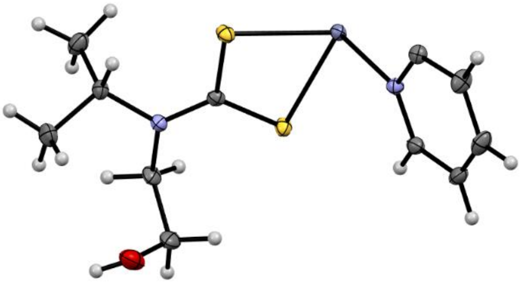

Figure 3.11: Asymmetric crystal structure of 1

In the molecular structure of crystal **1**, the zinc cation is located on a two-fold rotation axis and is chelated by two symmetry equivalent dithiocarbamate ligands and a **BIPY** ligand, which is bisected by the two-fold rotation axis as shown in **Figure 3.12.** The angle between the triangular faces is 1.50 (5)° and the twist angle is approximately 30°, again indicating a highly distorted coordination geometry.

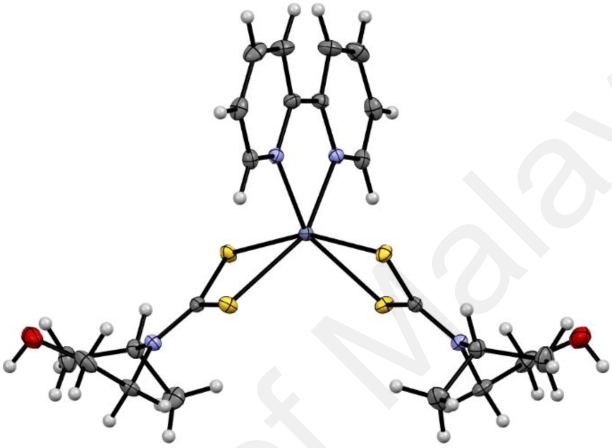

Figure 3.12: Molecular structure of crystal 1

In the molecular packing of crystal **1**, O–H····S hydrogen bonds lead to two dimensional supramolecular chain. The O(1)–H(1)····S(2) = (3.244 Å, 159°); connecting hydrogen atoms from **R1** ligand to the sulphur of another complex **1** represent by C_1^1 [3] graph set. **Figure 3.13** displays the environment of hydrogen bond synthons.

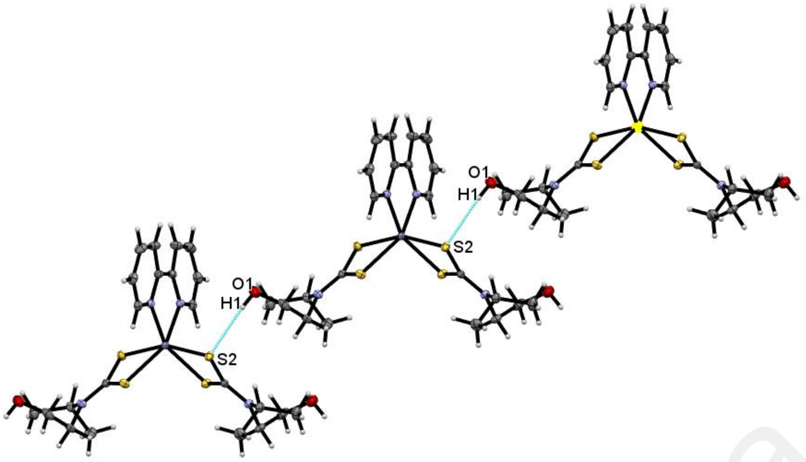

Figure 3.13: Environment of hydrogen bond synthon environment

The bond angles of S1^{1}-Zn1-S2^{1}, S1-Zn1-S2^{1}, and S2-Zn1-S2^{1} are 71.346(13) °, 95.817(14) °, and 159.92(2) ° respectively. The additional stabilization to this arrangement is provided by weak intermolecular C–H····S interaction from **BIPY** as illustrated in **Figure 3.14.**

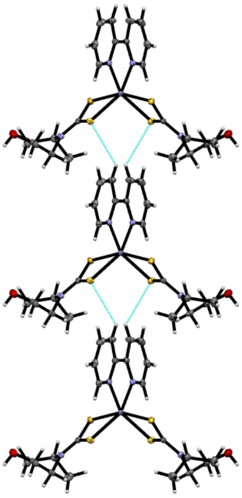

Figure 3.14: View of C–H····S intermolecular interactions along *c* axis

Connections between layers of pyridyl-C–H····S consolidate to three-dimensional crystal packing of crystal **1** along *c* axis as illustrated in **Figure 3.15**.

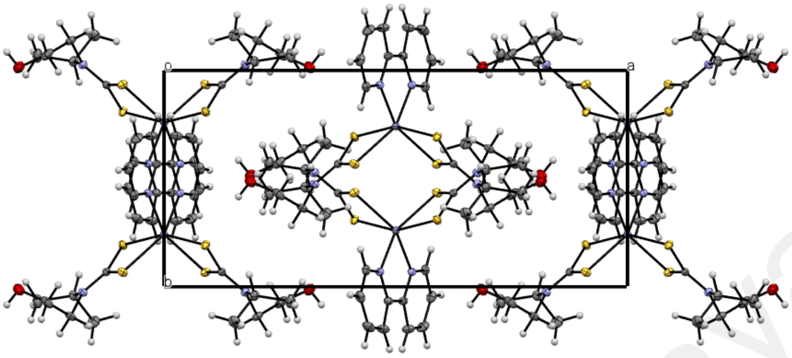

Figure 3.15: Crystal packing of crystal 1 along *c* axis

Crystal 2

Yellow needle crystal **2** was obtained from slow evaporation process in ethanol. Crystal **2** crystallized in an orthorhombic crystal system with *Pccn* space group. The asymmetric unit comprises of half independent molecule of complex **2** with the presence of a solvated water molecule (**Figure 3.16**).

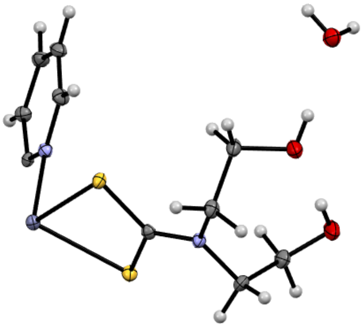

Figure 3.16: Asymmetric unit of crystal 2

In the molecular structure of **2**, the dithiocarbamate ligand chelates in a symmetric mode with the difference between the Zn—S_{long} and Zn—S_{short} bond lengths being 0.02 A°. The shorter Zn—S bond is approximately trans to the pyridyl-N atom. The zinc cation is located on a two-fold rotation axis and is chelated by two symmetry-equivalent dithiocarbamate ligands and one **BIPY** ligand, which is bisected by the two-fold rotation axis and a water molecule as shown in **Figure 3.17**.

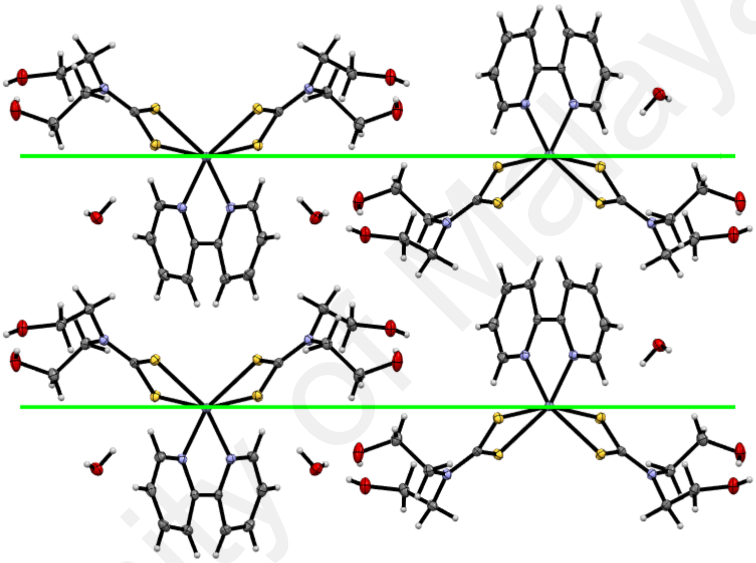

Figure 3.17: Molecular structure of crystal 2 view along *a* axis

There is an intramolecular O–H····O; O(1)–H(1)····O(1W) = (2.713 Å, 174°) hydrogen bond as well as intermolecular O–H····O; O(2)–H(2)····O(1) = (2.696 Å, 178°) hydrogen bonds found in crystal **2**. This mode of association results in one-dimensional jagged chains with graph set C_{1}^{1} [3] as shown in **Figure 3.18**.

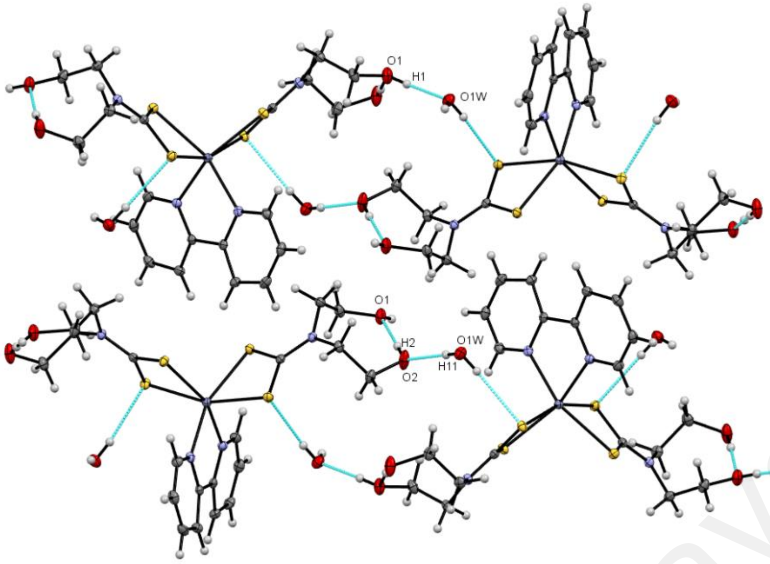

Figure 3.18: O–H····O hydrogen bond synthons environment in the molecular structure

The water molecules are the central molecule in connecting the chain into a supramolecular layer parallel to the ab plane by forming water-O–H····S interactions as shown in **Figure 3.19**. Globally, the crystal structure comprises alternating layers of hydrophilic and hydrophobic regions with the former arranged as supramolecular rods, indicating significant hydrogen bonding in this region of the crystal structure.

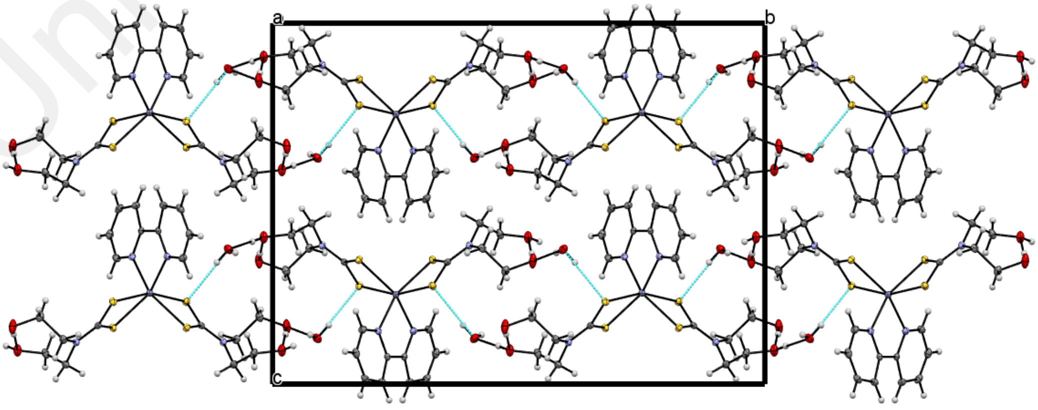

Figure 3.19: A view of unit cell content showing O–H····S interactions of crystal 2

Crystal 3

Single crystal X-ray diffraction reveals that crystal **3** obtained from ethanol solvent crystallized in the space group *Pn* with monoclinic crystal system. The asymmetric unit consist of zinc ion which chelated by two symmetry-equivalent dithiocarbamate ligands and a **BIPY** ligand which also represent the molecular structure for crystal **3** as shown in **Figure 3.20**.

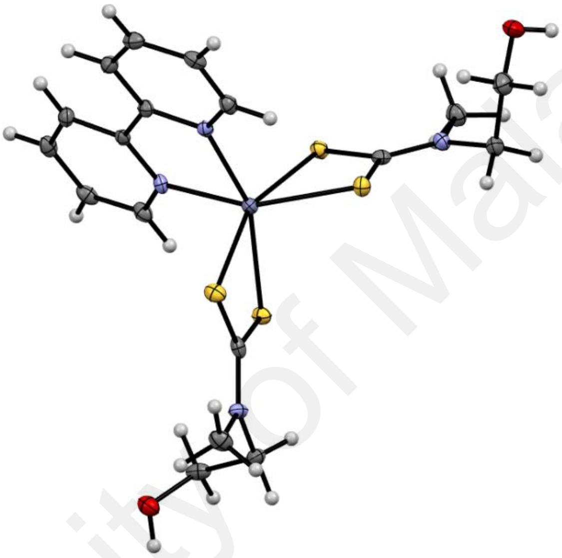

Figure 3.20: Asymmetric unit of crystal 3

Besides that, O–H····S; O(1)–H(1)····S(4) = (2.537 Å, 169°) and O(2)–H(2)····S(1) = (2.747 Å, 100°) hydrogen bonds synthon were observed in crystal **3** and contributed to C_1^1 [3] graph set (**Figure 3.21**).

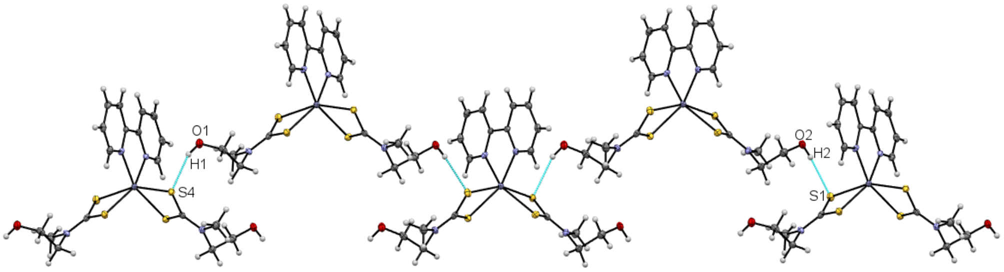

Figure 3.21: Intermolecular interactions of crystal 3 along *b* axis

Similar to crystal **1**, additional stabilization to this arrangement is provided by methyl-C–H····O and C–H····S interactions. These interactions was illustrated in **Figure 3.22**.

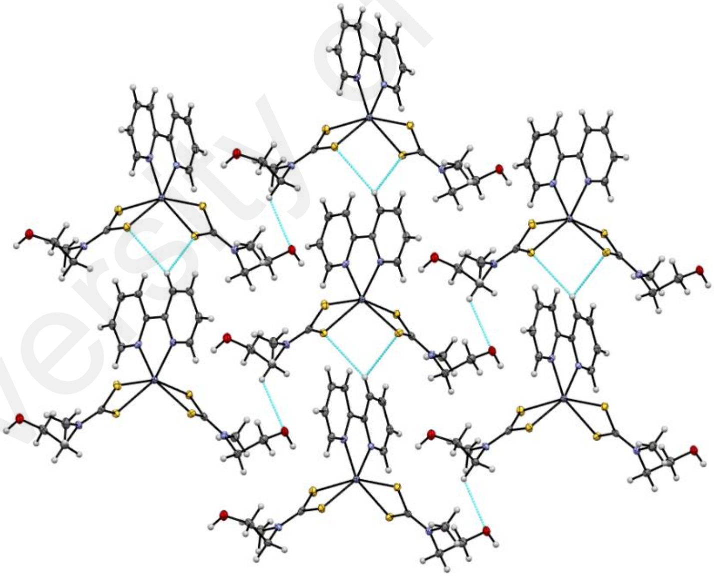

Figure 3.22: Intermolecular interactions of crystal 3 along *b* axis

All mentioned interactions lead to two-dimensional crystal packing as shown in **Figure 3.23**.

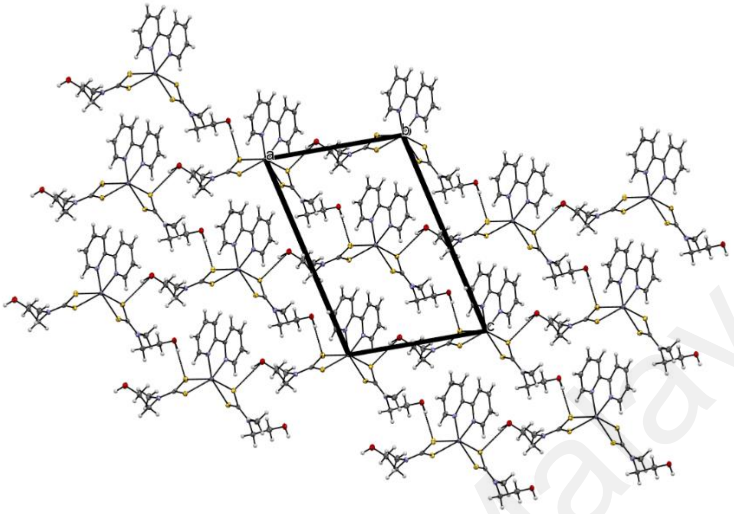

Figure 3.23: Crystal packing of crystal 3

Crystal 4

Crystal **4** was obtained from slow evaporation in chloroform and crystallized in monoclinic crystal system with space group *C*2/*c*. **Figure 3.24** display the asymmetric unit, which consist of half independent molecule of crystal **4.**

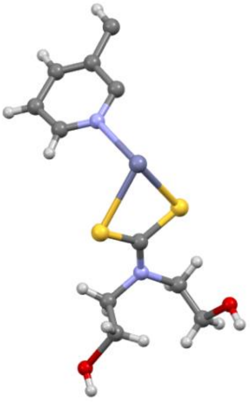

Figure 3.24: Asymmetric unit of crystal 4

In the molecular structure of crystal **4,** the zinc atom is chelated by two symmetrically coordinating dithiocarbamate ligands and also symmetrically by the **PHEN** ligand. The zinc ions are coordinated with four sulphur atoms from two **R2** dithiocarbamate ligands and two nitrogen atom of **PHEN** which show 6-coordination metal centre (**Figure 3.25**).

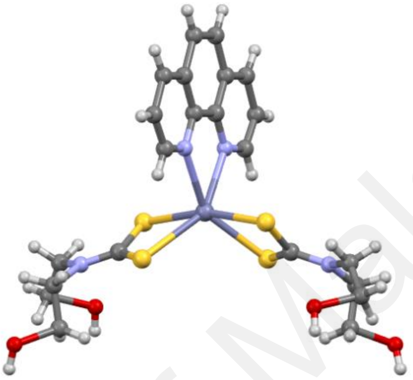

Figure 3.25: Asymmetric unit and molecular structure of crystal 4

The geometry of crystal **4** can be described as distorted octahedral resulted from the restricted bite distances of the chelating ligands. **Figure 3.26** display the molecular structure of crystal **4** and the rotation axis.

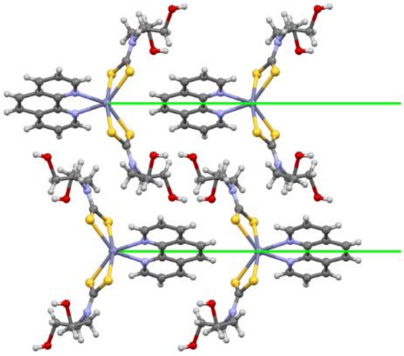

Figure 3.26: Rotation axis in molecular structure of crystal 4

Two O–H····O hydrogen bond synthons exist in the structure; O(1)–H(1A)····O(2) = (2.65 Å, 168°) and O(2)–H(2B)····O(1) = (2.65 Å, 167°) which resulted to a chain of molecular structure of complex **4** represented by graph set R_2^2 [4] (**Figure 3.27**).

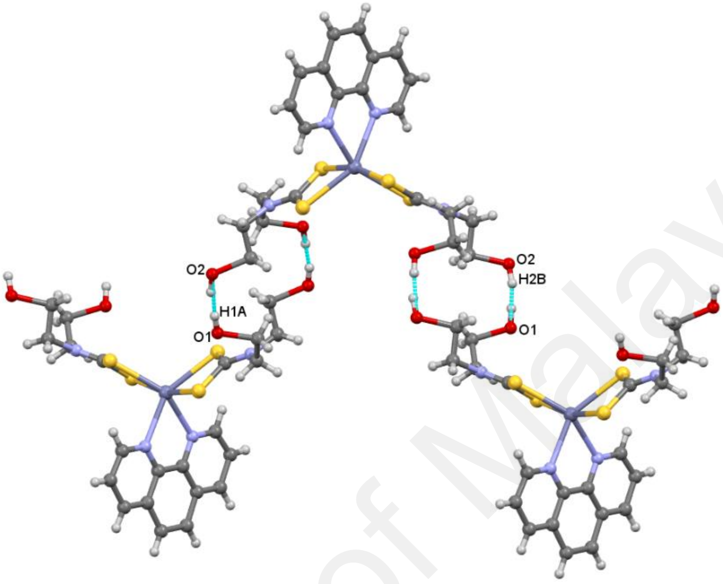

Figure 3.27: Environment of hydrogen bond synthons crystal 4

The presence of weak C–H····S and C–H····O intermolecular interactions stabilize the structure of crystal **4**. These weak interactions was display in **Figure 3.28**. Also, there are occurrences of π–π interactions between the centrosymmetrically related pyridyl rings (ring centroid····ring centroid distance = 3.795 Å) as shown in **Figure 3.29**.

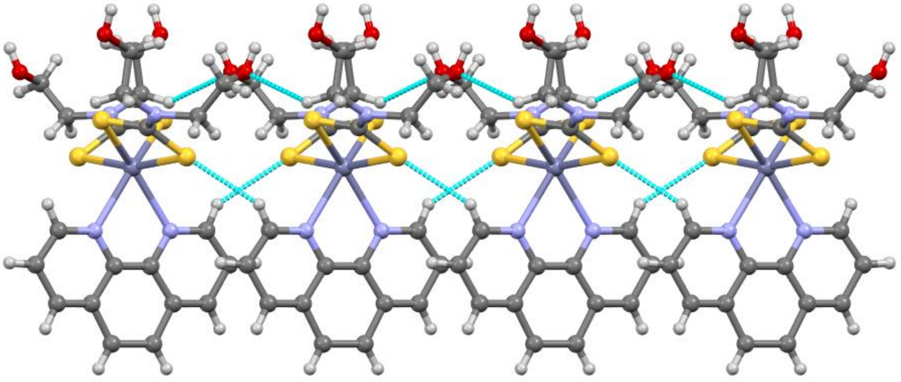

Figure 3.28: C–H····S and C–H····O short contacts presence as weak intermolecular interactions

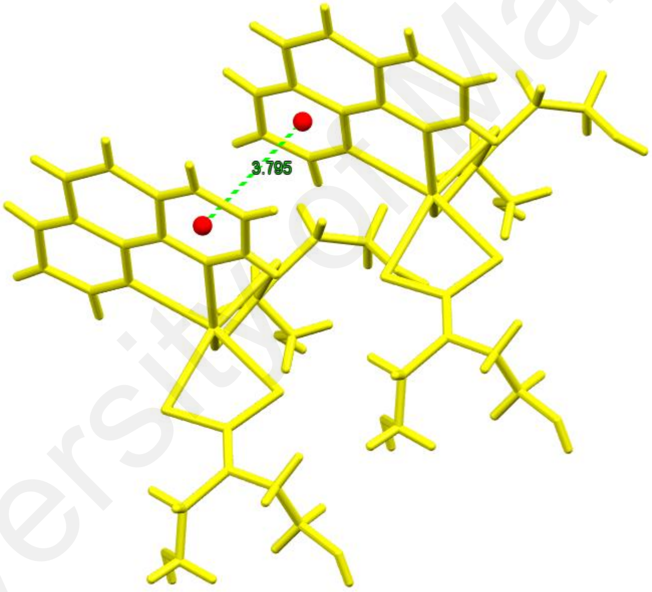

Figure 3.29: π-π interactions between pyridyl rings of PHEN

Figure 3.30 displays alternate layer of the crystal **4** that lead to two-dimensional crystal packing resulted from interactions discussed earlier.

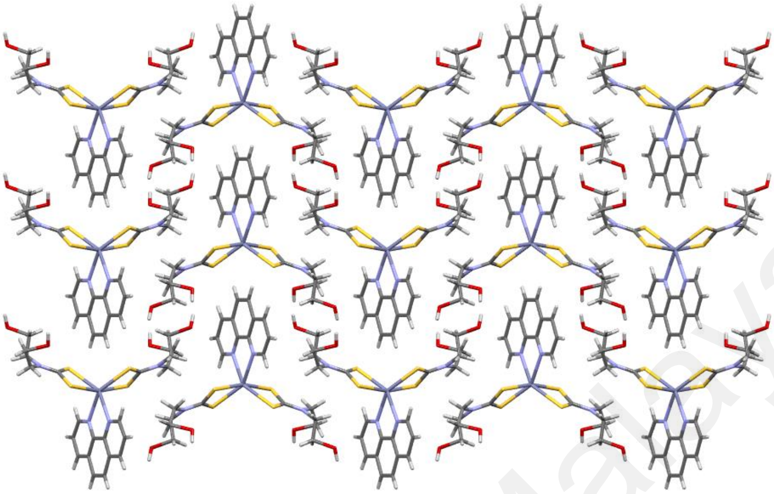

Figure 3.30: Crystal packing of crystal 4

Crystal 5

Crystal **5** was obtained from crystallization process in ethanol and crystallized in triclinic crystal system, with space group of $P\overline{1}$. **Figure 3.31** show the asymmetric unit of crystal **5** with zinc atom is chelated by two symmetrically coordinating dithiocarbamate ligands and half molecule of **PYR**.

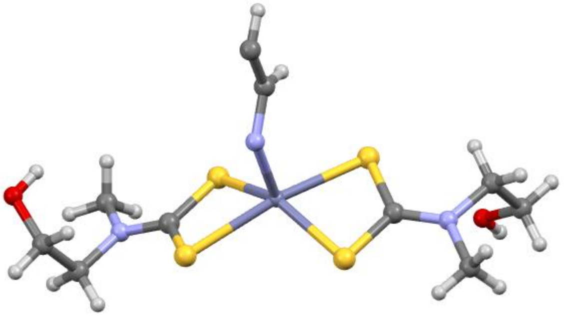

Figure 3.31: Asymmetric unit of crystal 5

The zinc is 5-coordinated with four sulphur atoms of two **R3** dithiocarbamate ligands and one nitrogen atom from **PYR**. **PYR** is sitting on the center of inversion as display in **Figure 3.32**.

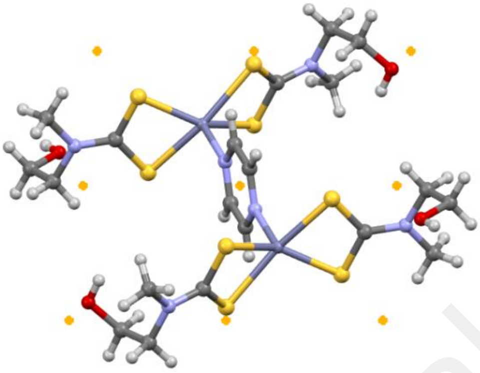

Figure 3.32: Molecular structure of crystal 5 showing the center of inversion (yellow dots)

There is no hydrogen bond synthon in the extended molecular structure of crystal **5**. However there are short contact O–H····S and C–H····O short contact interactions which resulted to porous structure (**Figure 3.33**).

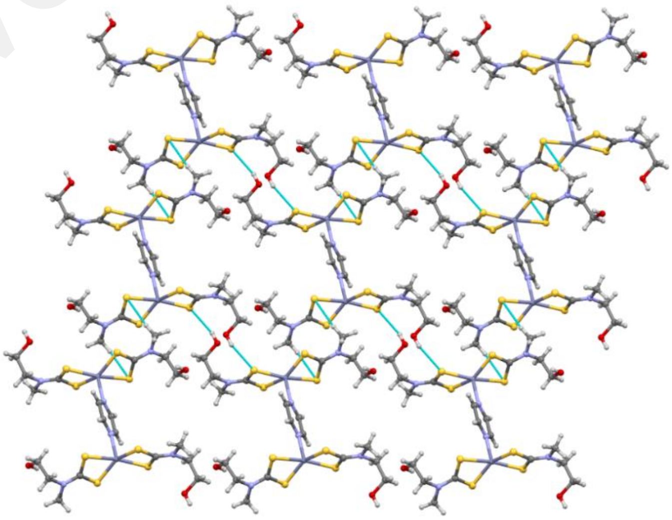

Figure 3.33: **O–H····S and C–H····O weak interactions in crystal 5**

Figure 3.34 show crystal packing of **5** which resulted in two-dimensional crystal structure of layered molecules.

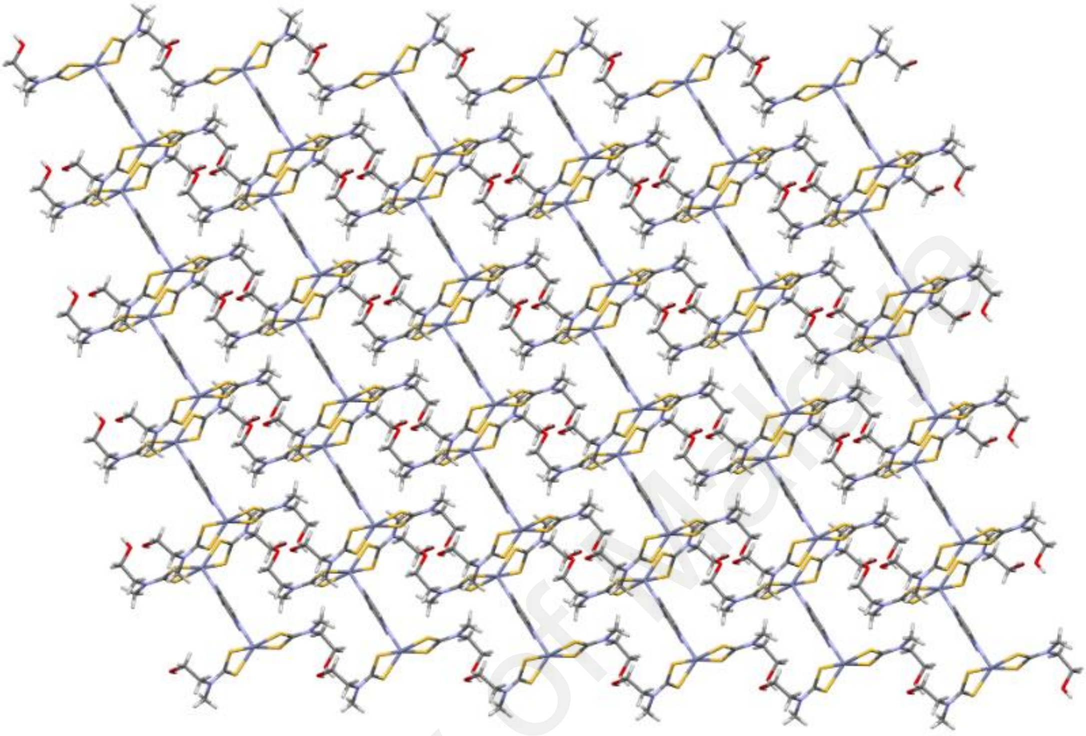

Figure 3.34: Crystal packing of crystal 5

Crystal 6

The colourless crystal **6** was obtained from chloroform, crystallized in monoclinic crystal system and space group *P*2_1/*c*. In **Figure 3.35**, zinc atom is chelated by two bidentate **R1** dithiocarbamate and a **BIPY** ligand. The zinc ions are 6-coordinated with four sulphur atoms from two **R1** dithiocarbamate ligands and two nitrogen atom from **BIPY** with $CHCl_3$ appeared as solvated molecule in the structure. Crystal **6** display an octahedral geometry.

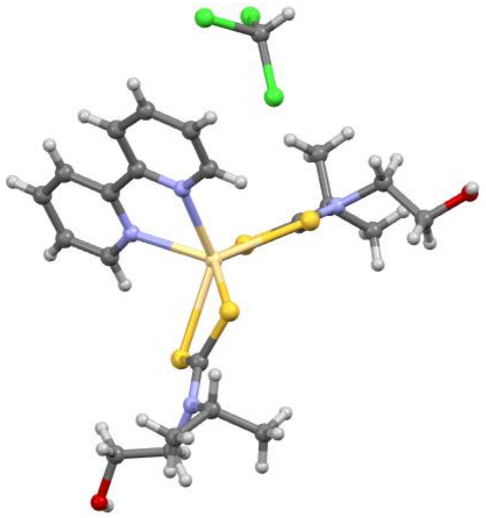

Figure 3.35: Molecular structure of crystal 6 which resembles the asymmetric unit

In the structure, O–H····O hydrogen bond synthons; (O$_{\text{O(2)-H(2B)}}$····O(5) distance is 2.684 Å, angle O(2)–H(2B)····O(5) = 167° and O$_{\text{O(5)-H(5A)}}$····O(2) distance is 2.684 Å, angle O(5)–H(5A)····O(2) = 170°) lead to the formation of supramolecular chain along *a* axis. These interaction contribute to C_1^1 [3] graph set. **Figure 3.36** portray the intermolecular interactions for crystal **6**.

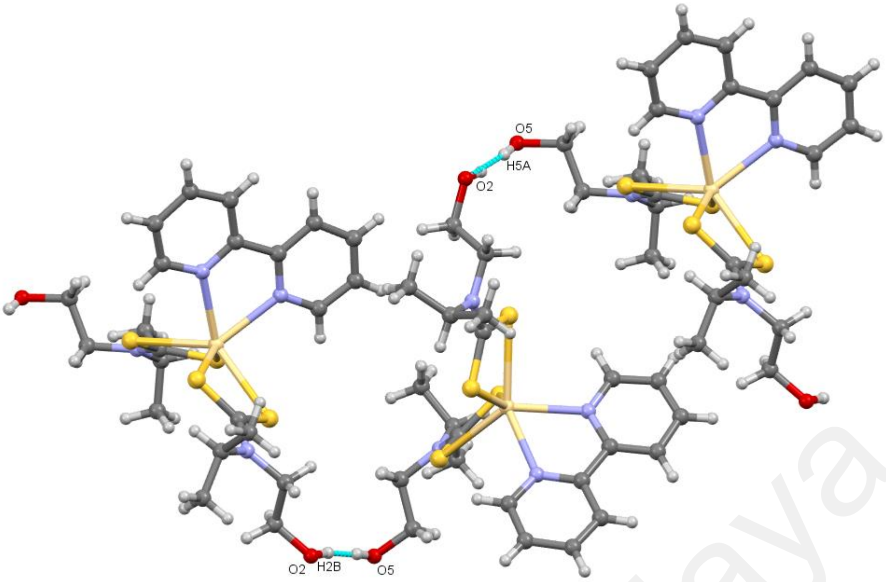

Figure 3.36: Environment of O–H····O hydrogen bond synthons of crystal 6

Figure

The stability of crystal **6** obtained by the presence of weak C–H····S intermolecular interactions (**Figure 3.37**). Besides that, there are occurrences of π–π interactions between the centrosymmetrically related pyridyl rings (ring centroid····ring centroid = 3.814 Å) as shown in **Figure 3.38**.

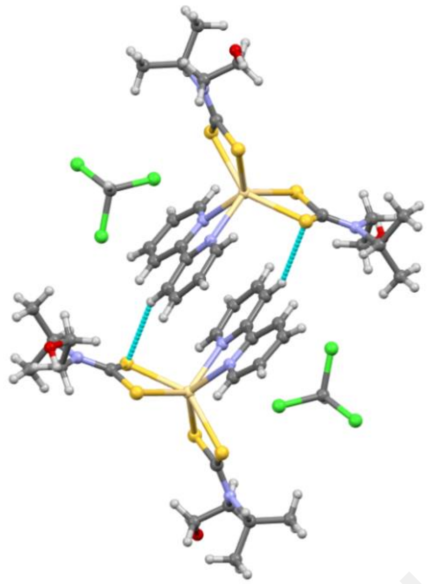

Figure 3.37: C–H····S short contacts between molecules in crystal 6

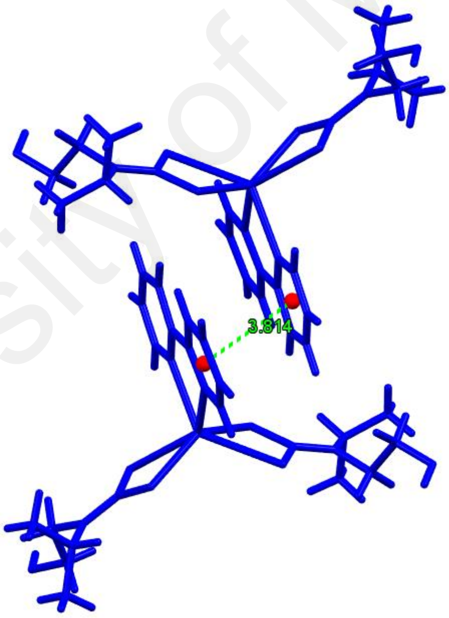

Figure 3.38: The centroid····centroid distance between pyridyl ring of BIPY showing π-π interaction

All mentioned interactions lead to layered of three-dimensional supramolecular crystal packing as shown in **Figure 3.39.**

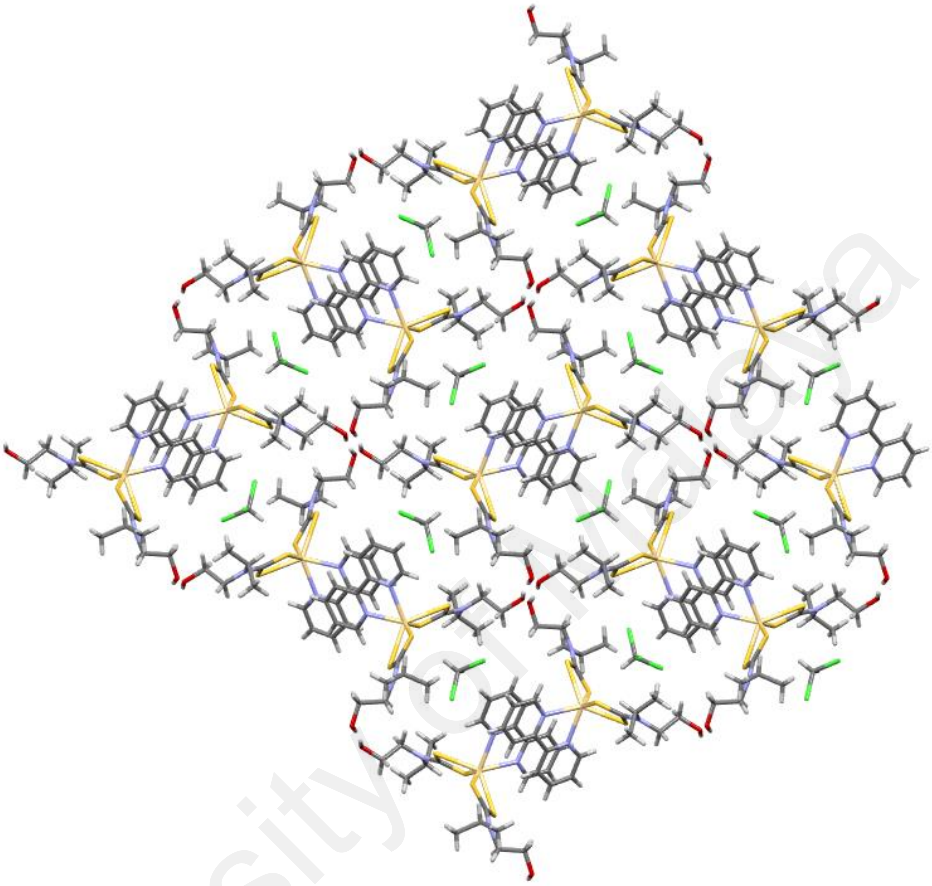

Figure 3.39: Three dimensional crystal packing of crystal 6

Crystal 7

Colorless needle of crystal **7** was obtained from slow evaporation technique in chloroform, crystallized in monoclinic crystal system with $P2_1/c$ space group. The asymmetric unit of crystal **7** comprises of penta-coordinated cadmium atom, being chelated by two bidentate dithiocarbamate ligands and one nitrogen atom from **PIP** molecule. **Figure 3.40** portray the asymmetric structure of crystal **7** which also represent its molecular structure.

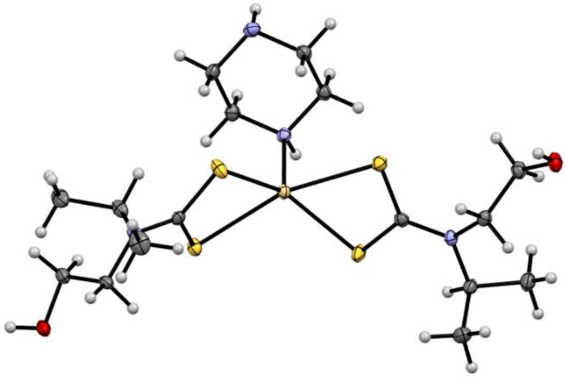

Figure 3.40: Asymmetric and molecular structure of crystal 7

The coordination geometry of crystal **7** can be described as distorted square pyramidal with the nitrogen atom in apical position. The distortions from the ideal geometry are related to the acute chelate angles subtended by the chelating ligands, *i.e*. 68-69°, and the angle of N–Cd–S angles is 98-116°. **Figure 3.41** display the symmetry operation exist in crystal **7**.

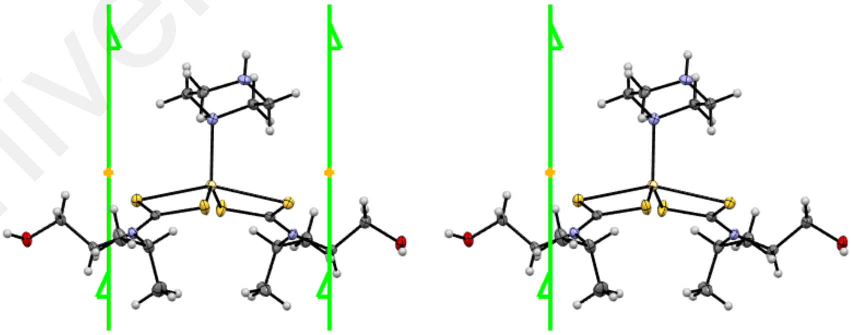

Figure 3.41: Symmetry operation (yellow dots) and rotation axis perpendicular to *c* axis in crystal 7

O–H····O; O(1)–H(1)····O(2) = (2.673 Å, 155°) hydrogen bonds synthon were observed between the ligand. This form a one dimensional layer with graph set C_{1}^{1} [3] as shown in **Figure 3.42**.

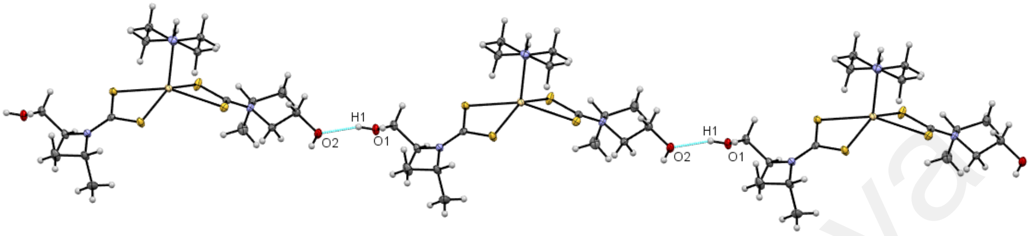

Figure 3.42: O–H····O hydrogen bond synthon of crystal 7

There are also N–H····O and O–H····N interactions between the **PIP** and the metal precursor of another molecules. The N(4)–H(4)····O(2) = (3.501 Å, 162°) and O(2)–H(2)····N(4) = (2.749 Å, 169°) intermolecular hydrogen bond synthons to formation of supramolecular layers as shown in **Figure 3.43**. Both interactions contribute to C_{1}^{1} [3] graph set.

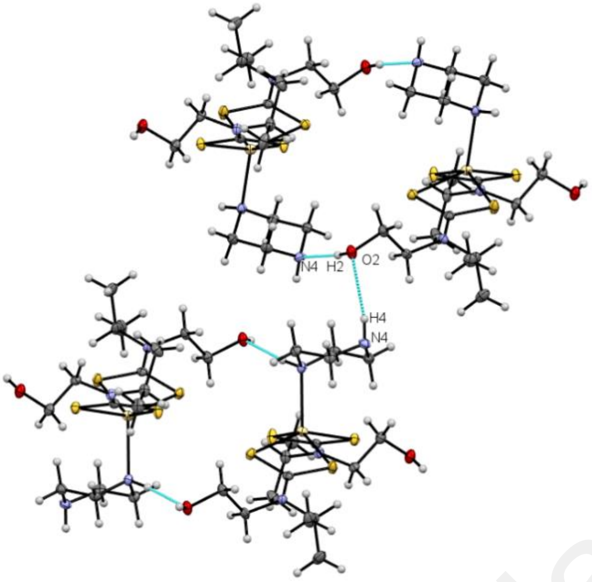

Figure 3.43: Environment of intermolecular interactions (N–H····O and O–H····N) of crystal 7

The presence of methyl-C–H····S short contacts interactions stabilize the extended crystal structure of crystal **7** as illustrated in **Figure 3.44**.

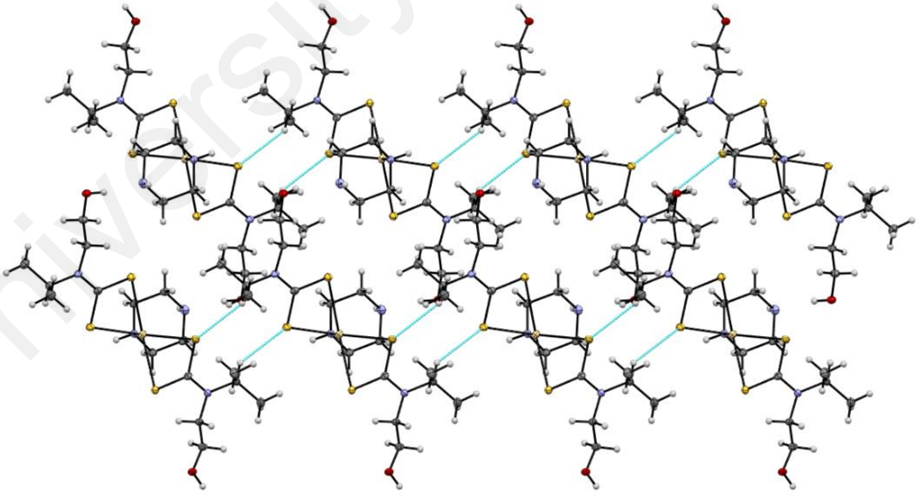

Figure 3.44: Stabilization provided by weak interaction of C–H····S short contacts

Figure 3.45 displays the crystal packing resulted from the N–H····O and O–H····N interactions with the presence of methyl-C–H····S short contacts which formed layers that stack along *c* axis.

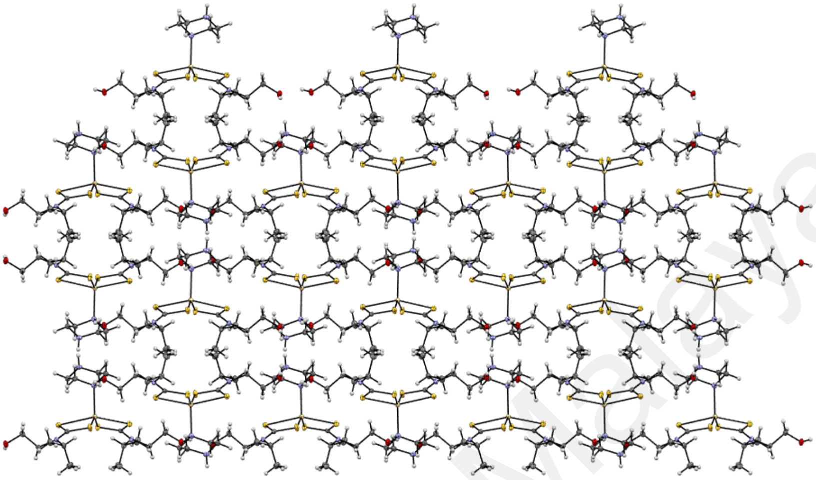

Figure 3.45: Crystal packing of crystal 7

Table 3.1: Crystallographic and refinement details for complex 1, 2, 3 and 6

Parameter	**1**	**2**	**3**	**6**
Empirical formula	$C_{22}H_{32}N_4O_2S_4Zn$	$C_{20}H_{32}N_4O_6S_4Zn$	$C_{18}H_{24}N_4O_2S_4Zn$	$C_{23}H_{33}CdCl_3N_4O_2S_4$
Formula weight	578.13	618.11	522.02	744.52
Temperature/K	100(2)	100(2)	100(2)	296(2)
Crystal system	Monoclinic	Orthorhombic	Monoclinic	Monoclinic
Space group	*C*2/*c*	*Pccn*	*Pn*	$P2_1/c$
a/Å	19.4903(7)	6.7685(2)	10.4796(3)	9.2776(4)
b/Å	8.9963(3)	23.1089(7)	6.6987(2)	20.3849(9)
c/Å	15.5401(5)	16.9441(5)	16.0057(5)	17.5354(8)
α/°	90.00	90.00	90.00	90.00
β/°	98.045(4)	90.00	103.100(3)	104.157(3)
γ/°	90.00	90.00	90.00	90.00
Volume/$Å^3$	2697.99(16)	2650.27(14)	1094.35(6)	3215.6(2)
Z	4	4	2	4
$\rho_{calc}g/cm^3$	1.423	1.549	1.584	1.538
μ/mm^{-1}	1.246	1.285	1.527	1.215
F(000)	12.08	1288.0	540.0	1512.0
Radiation	Mo Kα (λ = 0.71073)	Mo Kα (λ = 0.71073)	Mo Kα (λ = 0.71073)	Mo Kα (λ = 0.71073)
2θ range for data collection/°	5.8 to 55.16	5.96 to 55.12	6.08 to 55.24	4.52 to 53.02
Reflections collected	11846	13397	13280	27845
Independent reflections	3111	3065	4039	6591
Data/restraints/parameters	3111/0/151	3065/10/172	4039/2/267	6591/0/334
Goodness-of-fit on F^2	0.949	1.016	1.069	1.341
Final R indexes [I>=2σ (I)]	$R_1 = 0.0264$, $wR_2 = 0.0683$	$R_1 = 0.0297$, $wR_2 = 0.0712$	$R_1 = 0.0281$, $wR_2 = 0.0808$	$R_1 =0.0899$, $wR_2 = 0.3303$
Final R indexes [all data]	$R_1 = 0.0304$, $wR_2 = 0.0714$	$R_1 = 0.0342$, $wR_2 = 0.0745$	$R_1 = 0.0287$, $wR_2 = 0.0814$	$R_1 =0.1118$, $wR_2 = 0.3481$
Largest diff. peak/hole / e $Å^{-3}$	0.47/-0.49	1.05/-0.74	0.71/-0.53	1.97/-1.18
CCDC reference	1447174	1447175	Not submitted	Not submitted

Table 3.2: Crystallographic and refinement details for complex 4, 5 and 7

Parameter	**4**	**5**	**7**
Empirical formula	$C_{30}H_{18}N_{12}O_2S_2Zn$	$C_{20}H_{36}N_6O_4S_8Zn_2$	$C_{16}H_{34}CdN_4O_2S_4$
Formula weight	708.05	811.77	555.11
Temperature/K	296(2)	100(2)	100(2)
Crystal system	Monoclinic	Triclinic	Monoclinic
Space group	$C2/c$	$P\bar{1}$	$P2_1/c$
a/Å	6.782(3)	8.6567(5)	19.1822(17)
b/Å	18.846(8)	9.2932(5)	16.9915(7)
c/Å	19.278(7)	10.3319(7)	9.0308(8)
α/°	90.00	104.088(5)	90.00
β/°	91.75(4)	94.768(5)	128.183(14)
γ/°	90.00	94.062(5)	90.00
Volume/$Å^3$	2462.7(17)	799.82(8)	2313.7(3)
Z	2	1	4
$\rho_{calc}g/cm^3$	0.955	1.685	1.594
μ/mm^{-1}	0.616	2.060	1.324
F(000)	720.0	418.0	1144.0
Radiation	Mo Kα (λ = 0.71073)	Mo Kα (λ = 0.71073)	Mo Kα (λ = 0.71073)
2θ range for data collection/°	4.32 to 53.52	5.94 to 55.14	5.18 to 55.12
Reflections collected	8526	6667	19918
Independent reflections	2539	3681	5336
Data/restraints/parameters	2539/0/160	3681/0/183	5336/0/246
Goodness-of-fit on F^2	1.707	1.049	0.942
Final R indexes [I>=2σ (I)]	$R_1 = 0.1547$, $wR_2 = 0.4290$	$R_1 = 0.0468$, $wR_2 = 0.1075$	$R_1 = 0.0259$, $wR_2 = 0.0561$
Final R indexes [all data]	$R_1 = 0.1891$, $wR_2 = 0.4557$	$R_1 = 0.0649$, $wR_2 = 0.1221$	$R_1 = 0.0358$, $wR_2 = 0.0626$
Largest diff. peak/hole / e $Å^{-3}$	2.61/-0.68	0.95/-0.80	0.44/-0.48
CCDC reference	Not submitted	Not submitted	1445316

3.3.3 Powder X-Ray Diffraction (PXRD)

PXRD experiments were performed on compound **1-7** to examine the structural homogeneity of bulk samples by comparing the experimental with the simulated patterns (CIF) calculated from the single crystal (SCXRD) experiments measured at 273 K. As both pairs of patterns matched, the SCXRD results are representative of the bulk materials. The agreement indices, which were in the form of R profile after fitting mode refinement with the calculated powder pattern from crystallographic information file (CIF) of the crystal structure, was found to be coherent with the generally accepted R profile<30%. This suggested that the single crystal had been similar with the bulk materials. The powder pattern for the two series were shown in **Figure 3.46** and **3.47**.

PXRD experiments were conducted on all prepared mixed-ligands from bulk material and compared with the simulated patterns calculated from the single crystal (SCXRD) experiments measured at 273K. As both pairs of patterns matched for crystal **1, 2, 5** and **6** the SCXRD results (blue) are the representative of the bulk materials (red).

Besides that, the PXRD experiments for crystal **4** and **7** was also conducted with their starting material compounds and the PXRD pattern obtained for both crystals were distinct from the simulated patterns. This indicate that impurities content in the bulk materials quite high.

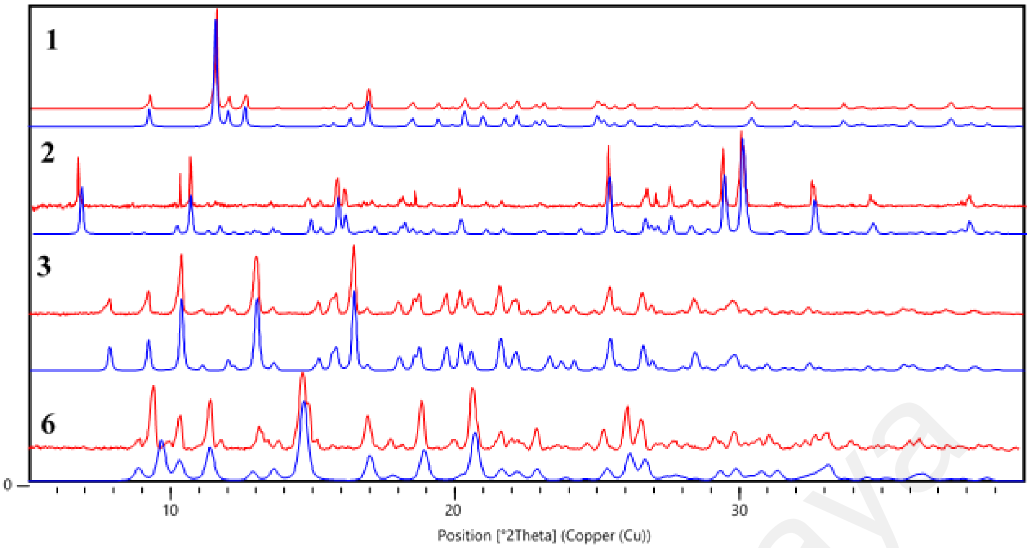

Figure 3.46: PXRD patterns for mixed-ligand complexes with BIPY. Red = bulk product calculated from stirring, blue = simulated at 273 K

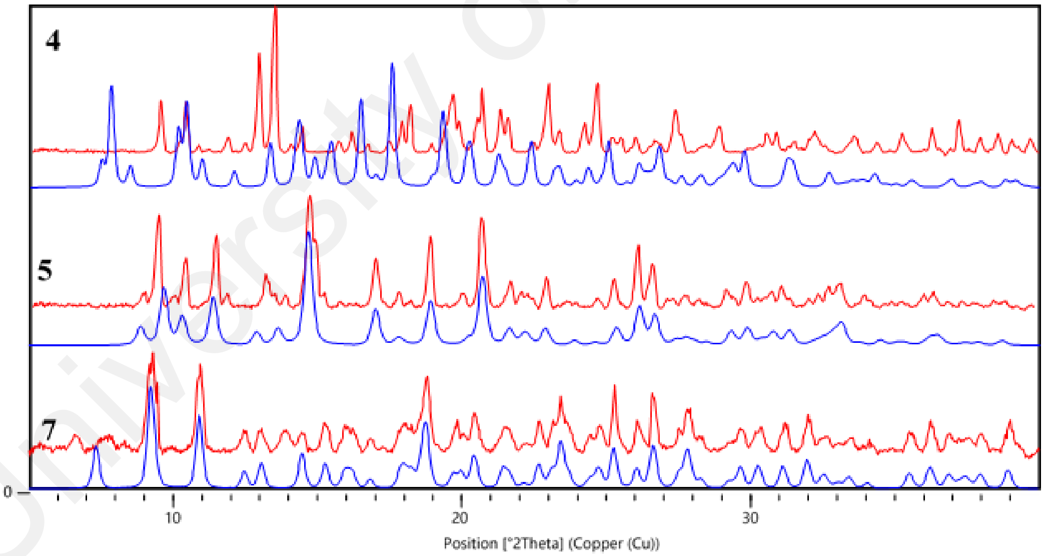

Figure 3.47: PXRD patterns of complexes 4,5 and 7. Red = bulk product calculated from stirring, blue = simulated at 273 K

3.4 Conclusion

In this chapter, seven mixed-ligands have been isolated from four different precursor and four amines. Out of seven complexes, four of them are from the **BIPY** amine linker and the other three are combination of precursor with **PHEN**, **PYR** and **PIP** respectively.

Common laboratory analytical tools such as CHN elemental analyzer, melting point and FTIR were used in characterize all complexes where all experimental are in agreement with literature. Melting point values of complexes **1**-**7** are in the range of (130-180)°C. However, crystal **1** and **4** show broad range of melting point value which is (148-152) °C and (10-158) °C respectively. This may be due to the purity of the bulk materials from the mother liquor which is less than from recrystallization process as mentioned before in section **3.3.1**.

In terms of geometry, both precursor are distinct with each other where **ZnR2** display an octahedral geometry and **ZnR3** show coordination geometry of tetrahedral. However, the geometry of complex **1**-**7** are different after the insertion of amine as linker due to the self-assembly and recognition process within molecules.

Supramolecular architectures also one of the aspect of interest other than π-π stacking interactions present in the extended molecular structures of complexes **1**-**7**. Crystal structure display that crystal **1**,**3**,**4**,**6** and **7** crystallized in the same crystal system but with different space group except for crystal **6** and **7** which shared $P2_1/c$ space group. The different space group resulted may be due to the different solvent that used in recrystallization process which affect the self-assembly of the complex in solid state. As for crystal **2** and **5**, contain different crystal system and space group which is orthorhombic (*Pccn* space group) and triclinic ($P\overline{1}$ space group) respectively.

The interactions in all seven complexes varies from hydrogen bond synthon, π-π interaction, C–H···S and C–H···O short contacts which resulted in different molecular crystal packing. All interactions are within the acceptable range where the average distances for O–H···O hydrogen bond synthons is 2.57-3.27 Å, C–H···S and C–H···O is 2.53-2.81 Å which is within the sum of van der Waals radii whilst π-π interaction is 3.3-3.8 Å (Janiak, 2000).

In the crystal structures of all seven complexes, the interaction is dominated by weak C–H···S and C–H···O interactions in achieving the stabilisation of the complex formed. Also, the occurrence of crystal structure overlapping also lead to the formation of π-π interaction between the pyridyl ring of organic linker in complex **4** and **6** where the centroid···centroid distance is within the accepted range of 3.3-3.8 Å.

Crystal packing of precursor aligned in 2D layered forms of molecules. Most of mixed-ligand complexes shows 2D crystal packing except for crystal 1 and 6, where the molecules are arranged in 3D network. This can explain that the insertion of amine linkers can modify the crystal structure of compounds from 2D into 3D crystal packing.

Apart from that, PXRD performed on all complexes showed that single-crystal data collected functioned as the representative of the bulk material at room temperature. PXRD pattern for crystal **1, 2, 3, 5** and **6** were found to be coherent with the simulated pattern from SCXRD. However, as for crystal **4** and **7**, due to the presence of impurities in the bulk materials, some peaks were not overlapping.

CHAPTER 4: CONCLUSIONS

In summary, the approach of crystal engineering and supramolecular chemistry has been applied by conducting two different projects with a total of 13 compounds have been successfully prepared. However, only 11 out of 13 compounds were successfully structurally characterized by SCXRD. All compounds were characterized with common analytical tools such as CHN elemental analyzer, melting point and FTIR.

As the sample examined was prepared by precipitate out from the mother liquor solution, the melting point for some crystals in both chapters showed a broad range of melting point values. This may due to the presence of impurities of the bulk powder.

The combination of carboxylic acid and amines resulted in either co-crystal or organic salt based on the aggregations between the two different tectons either it is strong enough to survive during the crystallization process. The dominant types of hydrogen bond synthons in this chapter were N–H···O and O–H···O which presence in all crystal of **BA-PIP**, **BA-MPIP**, **TCA-PHEN** and **TCA-DPK**.

On the other hand, **BA-DPK** the expected interaction to be happen within the molecules was unsuccessful since the PXRD pattern show the peaks of starting material of **BA**. This may be due to difficulty of hydrogen bonds to be formed along with the presence of π-π stacking interactions which resulted in formation of starting material.

The insertion of amine linker to the precursor resulted in various dimension of crystal packing from 2D to 3D. The observed interactions in all complexes **1-7** are within the accepted distance ranges which is O–H···O hydrogen bond synthons is 2.57-3.27 Å, C–H···S and C–H···O is 2.53-2.81 Å which is within the sum of van der Waals radii whilst π-π interaction is 3.3-3.8 Å (Janiak, 2000). Also, the stabilization of complexes were obtained from weak interactions of C–H···S and C–H···O short contacts along with π-π stacking.

In general, the concept of crystal engineering and supramolecular chemistry offer many possible applications to the drug development and delivery including medicinal industry for their potential to function as anti-cancer agents (Hogarth, 2012). This is due to the crystalline arrangement which can be design, planned and control. The intermolecular interactions will generate different chemical and physical properties of the resulting crystal structures from the individual components (Peterson, Hickey, & Michael, 2006). Apart from that, the modification of existing structure by changing chemical stability and porosity will increase its potential to be apply as gas adsorption for alternative fuels and offer many advantages in catalysis (Furukawa et al., 2013).

REFERENCES

Aakeröy, C. B. (1997). Crystal engineering: strategies and architectures. *Acta Crystallographica Section B: Structural Science*, *53*(4), 569-586.

Almarsson, Ö., & Zaworotko, M. J. (2004). Crystal engineering of the composition of pharmaceutical phases. Do pharmaceutical co-crystals represent a new path to improved medicines?. *Chemical Communications*, (17), 1889-1896.

Aly, A. A., Brown, A. B., Bedair, T. M., & Ishak, E. A. (2012). Dithiocarbamate salts: biological activity, preparation, and utility in organic synthesis. *Journal of Sulfur Chemistry*, *33*(5), 605-617.

Andricopulo, A. D., Salum, L. B., & Abraham, D. J. (2009). Structure-based Drug Design Strategies In Medicinal Chemistry. *Current topics in Medicinal Chemistry*, *9*(9), 771-790.

Anthony, A., Desiraju, G. R., Jetti, R. K. R., Kuduva, S. S., Madhavi, N. N. L., Nangia, A., Thaimattam, R., & Thalladi, V. R. (1998). Crystal Engineering: Some Further Srategies. *Crystal Engineering*, *1*(1), 1-18.

Batten, S. R., Champness, N. R., Chen, X. M., Garcia-Martinez, J., Kitagawa, S., Öhrström, L., O'Keeffe, M., Suh, M. P., & Reedijk, J. (2012). Coordination polymers, metal–organic frameworks and the need for terminology guidelines. *Crystal Engineering Communication*, *14*(9), 3001-3004.

Berge, S. M., Bighley, L. D., & Monkhouse, D. C. (1977). Pharmaceutical salts. *Journal of Pharmaceutical Sciences*, *66*(1), 1-19.

Bhogala, B. R., Basavoju, S., & Nangia, A. (2005). Tape and layer structures in cocrystals of some di- and tricarboxylic acids with 4, 4′-bipyridines and isonicotinamide. From binary to ternary cocrystals. *Crystal Engineering Communication*, *7*(90), 551-562.

Brook, D. R., & Koch, T. (1997). Structure and properties of some new dihydropyrazine tetracyanoquinodimethane charge transfer salts. *Journal of Materials Chemistry*, *7*(12), 2381-2385.

Bruker. (2005). APEX2. *Bruker, AXS Inc., Madison, Wisconsin, USA.*

Chen, Z. Y., & Peng, M. X. (2011). Supramolecular Architectures Constructed from Piperazine and Substituted Benzoic Acids. *Journal of Chemical Crystallography*, *41*(2), 137-142.

Connelly, N. G. (2005). *IUPAC Recommendations 2005*. Royal Society of Chemistry.

Desiraju, G. R. (1995). Supramolecular synthons in crystal engineering—a new organic synthesis. *Angewandte Chemie International Edition in English*, *34*(21), 2311-2327.

Dolomanov, O. V., Bourhis, L. J., Gildea, R. J., Howard, J. A., & Puschmann, H. (2009). OLEX2: a complete structure solution, refinement and analysis program. *Journal of Applied Crystallography*, *42*(2), 339-341.

Férey, G. (2008). Hybrid porous solids: past, present, future. *Chemical Society Reviews*, *37*(1), 191-214.

Fischer, M., Kuchta, B., Firlej, L., Hoffmann, F., & Fröba, M. (2010). Accurate prediction of hydrogen adsorption in metal− organic frameworks with unsaturated metal sites via a combined density-functional theory and molecular mechanics approach. *The Journal of Physical Chemistry C*, *114*(44), 19116-19126.

Fujii, K., Ashida, Y., Uekusa, H., Guo, F., & Harris, K. D. (2010). Selective transformation pathways between crystalline forms of an organic material established from powder X-ray diffraction analysis. *Chemical Communications*, *46*(24), 4264-4266.

Furukawa, H., Cordova, K. E., O'Keeffe, M., & Yaghi, O. M. (2013). The chemistry and applications of metal-organic frameworks. *Science*, *341*(6149), 1230444.

Ganapayya, B., Jayarama, A., & Dharmaprakash, S. M. (2013). Crystal structure and optical properties of a New Nonlinear optical Chalcone Crystal. *Molecular Crystals and Liquid Crystals*, *571*(1), 87-98.

Heard, P. J. (2005). Main group dithiocarbamate complexes. *Progress in Inorganic Chemistry*, *53*, 1.

Hogarth, G. (2005). Transition metal dithiocarbamates: 1978–2003. *Progress in Inorganic Chemistry, 53*, 71-561.

Hogarth, G. (2012). Metal-dithiocarbamates complexes: *Mini-Reviews in Medicinal Chemistry, 12*, 1202-1215.

Janiak, C. (2000). A critical account on π–π stacking in metal complexes with aromatic nitrogen-containing ligands. *Journal of the Chemical Society, Dalton Transactions*, (21), 3885-3896.

Jones, J. T. A., Hasell, T., Wu, X., Bacsa, J., Jelfs, K. E., Schmidtmann, M., & Cooper, A. I. (2011). Modular and predictable assembly of porous organic molecular crystals. *Nature, 474*(7351), 367–371.

Jones, J. T., Hasell, T., Wu, X., Bacsa, J., Jelfs, K. E., Schmidtmann, M., & Cora, F. (2011). Modular and predictable assembly of porous organic molecular crystals. *Nature*, *474*(7351), 367-371.

Kuleshova, L. N., & Zorky, P. M. (1980). Graphical enumeration of hydrogen-bonded structures. *Acta Crystallographica Section B: Structural Crystallography and Crystal Chemistry*, *36*(9), 2113-2115.

Lackinger, M., & Heckl, W. M. (2009). Carboxylic acids: versatile building blocks and mediators for two-dimensional supramolecular self-assembly. *Langmuir*, *25*(19), 11307-11321.

Lehn, J. (1995). Supramolecular Chemistry. *Supramolecular Chemistry*, 1–970.

Lemmerer, A., Adsmond, D. A., Esterhuysen, C., & Bernstein, J. (2013). Polymorphic co-crystals from polymorphic co-crystal formers: competition between carboxylic acid··· pyridine and phenol··· pyridine hydrogen bonds. *Crystal Growth & Design*, *13*(9), 3935-3952.

Luo, Y., Bernot, K., Calvez, G., Freslon, S., Daiguebonne, C., Guillou, O., & Roisnel, T. (2013). 1, 2, 4, 5-Benzene-tetra-carboxylic acid: a versatile ligand for high dimensional lanthanide-based coordination polymers. *Crystal Engineering Communication*, *15*(10), 1882-1896.

Margaret E. Etter. (1991). Hydrogen Bonds as Deslgn Elements in Organic Chemistry. *Jopurnal of Physical Chem*, *95*(8), 4601–4610.

Macrae, C. F., Bruno, I. J., Chisholm, J. A., Edgington, P. R., McCabe, P., Pidcock, E., & Wood, P. A. (2008). Mercury CSD 2.0–new features for the visualization and investigation of crystal structures. *Journal of Applied Crystallography*, *41*(2), 466-470.

Morgado, J., Santos, I. C., Veiros, L. F., Henriques, R. T., Duarte, M. T., Almeida, M., & Alcácer, L. (1997). Perylene derivative charge transfer salts: synthesis, crystal structure and characterisation of (pet) 3 [Ni (mnt) 2] 2. *Journal of Materials Chemistry*, *7*(12), 2387-2392.

Nabipour, H., Ghammamy, S., Ashuri, S., & Aghbolagh, Z. S. (2010). Synthesis of a new dithiocarbamate compound and study of its biological properties. *Org Chem J*, *2*, 75-80.

Nangia, A. (2009). Supramolecular chemistry and crystal engineering. *Current Trends in Science – Platinum Jubilee Special*, *122*(figure 1), 35–51.

Öhrström, L., & Larsson, K. (2004). What kinds of three-dimensional nets are possible with tris-chelated metal complexes as building blocks?. *Dalton Transactions*, (3), 347-353.

Palatinus, L., & Chapuis, G. (2007). Superflip–a computer program for the solution of crystal structures by charge flipping in arbitrary dimensions. *Journal of Applied Crystallography*, *40*(4), 786-790.

PANalytical, B. V. (2009). *X'Pert HighScore Plus* (Vol. 3). Version.

Peterson, M. L., Hickey, M. B., Zawarotko, M. J., & Almarsson, O. (2006) Expanding the scope of crystal form evaluation in pharmaceutical science. *J Pharm Pharmaceut Sci*, *9*(3), 317-326.

Stahly, G. P. (2009). A survey of cocrystals reported prior to 2000. *Crystal Growth & Design*, *9*(10), 4212-4229.

Rao, C. N. R. (2001). Basic building units, self-assembly and crystallization in the formation of complex inorganic open architectures. *Journal of Chemical Sciences*, *113*(5-6), 363-374.

Sarma, B., Nath, N. K., Bhogala, B. R., & Nangia, A. (2009). Synthon competition and cooperation in molecular salts of hydroxybenzoic acids and aminopyridines. *Crystal Growth and Design*, *9*(3), 1546-1557.

Schmidt, G. M. J. (1971). Photodimerization in the solid state. *Pure and Applied Chemistry*, *27*(4), 647-678.

Sekhon, B. S. (2009). Pharmaceutical co-crystals-a review. *ARS Pharmaceutica*, (50), 99-117.

Shan, N., & Zaworotko, M. J. (2010). Polymorphic crystal forms and cocrystals in drug delivery (crystal engineering). *Burger's Medicinal Chemistry and Drug Discovery*.

Shattock, T. R., Arora, K. K., Vishweshwar, P., & Zaworotko, M. J. (2008). Hierarchy of supramolecular synthons: persistent carboxylic acid··· pyridine hydrogen bonds in cocrystals that also contain a hydroxyl moiety. *Crystal Growth and Design*, *8*(12), 4533-4545.

Sheldrick, G. M. (2008). A short history of SHELX. *Acta Crystallographica Section A: Foundations of Crystallography*, *64*(1), 112-122.

Sherwood, R., Gonzàlez de Rivera, F., Wan, J. H., Zhang, Q., White, A. J., Rossell, O., & Wilton-Ely, J. D. (2015). Multimetallic Complexes Based on a Diphosphine-Dithiocarbamate "Janus" Ligand. *Inorganic Chemistry*, *54*(9), 4222-4230.

Smith, G., Wermuth, U. D., & White, J. M. (2001). The 1: 1 proton-transfer compound of sulfanilamide with 3, 5-dinitrosalicylic acid. *Acta Crystallographica Section E: Structure Reports Online*, *57*(11), o1036-o1038.

Spek, A. L. (2009). Structure validation in chemical crystallography. *Acta Crystallographica Section D: Biological Crystallography*, *65*(2), 148-155.

Tarafder, M. T. H., Asmadi, A., Talib, S. M., Ali, A. M., & Crouse, K. A. (2001). Studies on coordination chemistry of a nitrogen–sulfur donor ligand with lighter and heavier metal ions and biological activities of its complexes. *Transition Metal Chemistry*, *26*(1-2), 170-174.

Tarique, M. (2015). Advances in the coordination chemistry of transition metal compounds applying nitrogen and sulphur containing ligand : Synthesis , Structural and properties consideration ., *1*(1), 34–37.

Taylor, M. J., Tanna, S., & Sahota, T. (2010). In vivo study of a polymeric glucose-sensitive insulin delivery system using a rat model. *Journal of Pharmaceutical Sciences*, *99*(10), 4215-4227.

Valarmathi, P., Thirumaran, S., Kapoor, K., Gupta, V. K., & Kant, R. (2012). cis-Bis (4-methylpiperazine-1-carbodithioato-κ2S, S′) bis (pyridine-κN) cadmium. *Acta Crystallographica Section E: Structure Reports Online*, *68*(1), m89-m89.

Veerakanellore, G. B., Captain, B., & Ramamurthy, V. (2016). Solid-state photochemistry of cis-cinnamic acids: a competition between [2+ 2] addition and cis–trans isomerization. *Crystal Engineering Communication*.

McCormick, B. J., Stormer, B. P., & Kaplan, R. I. (1969). Complexes of cationic dithiocarbamate ligands. *Inorganic Chemistry*, *8*(11), 2522-2524.

Vishweshwar, P., Nangia, A., & Lynch, V. M. (2003). Supramolecular synthons in phenol–isonicotinamide adducts. *Crystal Engineering Communication*, *5*(31), 164-168.

Wahab, N. A. A., Baba, I., Mohamed Tahir, M. I., & Tiekink, E. R. (2011). Bis (N-isopropyl-N-methyldithiocarbamato-κ2S, S′)(1, 10-phenanthroline-κ2N, N′) zinc. *Acta Crystallographica Section E: Structure Reports Online*, *67*(5), m553-m554.

Wilton-Ely, J. D., Solanki, D., Knight, E. R., Holt, K. B., Thompson, A. L., & Hogarth, G. (2008). Multimetallic assemblies using piperazine-based dithiocarbamate building blocks. *Inorganic Chemistry*, *47*(20), 9642-9653.

Wood, P. A., Feeder, N., Furlow, M., Galek, P. T., Groom, C. R., & Pidcock, E. (2014). Knowledge-based approaches to co-crystal design. *Crystal Engineering Communication*, *16*(26), 5839-5848.

Yang, X. D., Chen, Y. G., Mirzaei, M., Salimi, A. R., & Yao, F. (2009). Synthesis, structure and analysis of intermolecular interactions of organic–inorganic hybrid compound based on Anderson-type polyoxometalates and piperazine. *Inorganic Chemistry Communications*, *12*(3), 195-197.

LIST OF PUBLICATIONS AND PAPERS PRESENTED

List of Publication

1. Siti Artikah M. Safbri, Siti Nadiah Abdul Halim, Edward R. T. Tiekink. Crystal structures of (2,2'-bipyridyl-κ^2 *N*,*N*') bis[*N*,*N*-bis(2-hydroxyethyl)dithiocarbamato- κ^2 *S*,*S*']zinc dihydrate and (2,2'-bipyridyl- κ^2 *N*,*N*')bis[*N*-(2-hydroxyethyl)-*N*-isopropyldithiocarbamato- κ^2 *S*,*S*']-zinc. *Acta Crystallographica E*. (Accepted, *Acta Cryst*. 2016, E72, 203-208).
2. Siti Artikah M. Safbri, Siti Nadiah Abdul Halim, Mukesh M. Jotani, Edward R. T. Tiekink. Bis[*N*-(2-hydroxyethyl)-*N*-isopropyldithiocarbamato- κ^2 *S*,*S*'](piperazine-κN) cadmium : crystal structure and Hirshfeld analysis. *Acta Crystallographica E*. (Accepted, *Acta Cryst*. 2016, E72, 158-163).

List of conference/ symposium/ seminar attended:

1. 4th Asian Conference of Coordination Chemistry, Jeju International Convention Center, Jeju South Korea, 2013. (Poster presenter).
2. University of Malaya Chemical Crystallography Symposium, UM, 2014. (Poster presenter).
3. University of Malaya Pharmaceutical Co-crystal Symposium, UM, 2014. (Poster presenter).
4. Seminar Kimia Analisis ke-28 Ipoh, 2015. (Poster presenter).
5. #UM111 Chemistry Symposium, UM, 2016. (Poster presenter).

APPENDIX

Table of bond lengths, Å for crystals BA-PIP, BA-MPIP, TCA-PHEN and TCA-DPK

Atom	Atom	Length/Å	Atom	Atom	Length/Å
BA-PIP					
N1	C1	1.489(2)	C4	O2	1.267(2)
N1	C2	1.491(2)	C5	N2	1.361(2)
C1	C2^1	1.514(2)	C5	C6	1.414(2)
C2	C1^1	1.514(2)	C6	C7	1.379(3)
C3	C4	1.502(2)	C7	Cl1	1.7478(18)
C3	C5	1.420(3)	C7	C8	1.388(3)
C3	C9	1.393(2)	C8	C9	1.381(2)
C4	O1	1.265(2)			
BA-MPIP					
N1	C1	1.494(4)	C6	C12	1.406(4)
N1	C5	1.488(4)	C7	O1	1.263(4)
C1	C2	1.514(4)	C7	O2	1.265(4)
C2	N2	1.458(4)	C8	N3	1.375(4)
N2	C3	1.464(4)	C8	C9	1.405(4)
N2	C4	1.467(4)	C9	C10	1.373(4)
C4	C5	1.505(5)	C10	Cl1	1.745(3)
C6	C7	1.505(4)	C10	C11	1.385(5)
C6	C8	1.407(4)	C11	C12	1.379(5)
TCA-PHEN					
O3	C82	1.270(3)	C19	C21^2	1.383(3)
O6	C61	1.327(3)	C19	C28	1.399(3)
O7	C41	1.321(3)	C19	C77	1.510(3)
O9	C77	1.235(3)	C21	C19^2	1.383(3)
O18	C82	1.238(3)	C21	C28	1.397(3)
O20	C41	1.216(3)	C28	C41	1.486(3)
O22	C61	1.206(3)	C35	C55	1.432(3)
O28	C77	1.287(3)	C35	C57	1.402(3)
N4	C55	1.363(3)	C37	C3^1	1.386(3)
N4	C87	1.332(3)	C37	C59	1.399(3)
N5	C35	1.360(3)	C37	C61	1.505(3)
N5	C74	1.325(3)	C40	C80	1.376(3)
C3	C37^1	1.386(3)	C50	C57	1.437(3)
C3	C59	1.390(3)	C51	C64	1.367(4)
C6	C17	1.426(3)	C51	C74	1.398(4)
C6	C50	1.350(3)	C57	C64	1.402(3)
C17	C40	1.403(3)	C59	C82	1.502(3)
C17	C55	1.403(3)	C80	C87	1.389(3)
TCA-DPK					
O0AA	C7	1.215(4)	C7	C11	1.498(4)
O4	C21	1.228(4)	N10	C33	1.391(5)
O11	C21	1.285(4)	C11	C24	1.397(4)
O15	C7	1.314(4)	C11	C31	1.390(4)
C17	C3	1.347(5)	C21	C24	1.505(4)
C17	N10	1.355(5)	C24	C31^2	1.391(4)
C17	C5	1.530(7)	C28	C37	1.388(6)
C3	C28	1.353(5)	C33	C37	1.392(6)
C3	C5^1	1.445(8)	C5	O1	1.250(9)

Table of hydrogen bond lengths, Å for crystals BA-PIP and BA-MPIP

BA-PIP				
D — H···A	**D — H, Å**	**H···A, Å**	**D···A, Å**	**D — H···A,º**
N(1)--H(1A)..O(3)	0.87	1.95	2.771(2)	156
N(1)--H(1B)..O(2)	0.93	1.78	2.663 (2)	158
N(2)--H(2A)..O(2)	0.88	2.05	2.691(2)	129
N(2)--H(2B)..O(1)	0.88	2.20	2.986(2)	149
O(3)--H(3A)..O(1)	0.86	1.90	2.753(2)	174
O(3) --H(3B)..O(1)	0.83	2.00	2.822(2)	168
C(1)--H(1D)..O(2)	0.99	2.59	3.258(2)	125
C(2)--H(2C)..O(2)	0.99	2.6	3.237(2)	126
C(9)--H(9)..O(1)	0.95	2.43	2.771(2)	101
BA-MPIP				
N(1)--H(1A)..O(2)	0.92	1.86	2.7610	166
N(1)--H(1B)..O(1)	0.92	1.77	2.6728	168
N(3)--H(3D)..O(2)	0.88	2.36	2.9174	122
N(3)--H(3E)..O(1)	0.88	2.00	2.6525	130
C(5)--H(5A)..N(3)	0.99	2.60	3.5602	163
C(12)--H(12A)..O(2)	0.95	2.45	2.7878	101

Table of hydrogen bond lengths, Å for crystals TCA-PHEN and TCA-DPK

TCA-PHEN				
D — H···A	**D — H, Å**	**H···A, Å**	**D···A, Å**	**D — H···A,º**
N(4)--H(4)..O(20)	0.86	2.19	2.884(3)	137
N(4)--H(4)..N(5)	0.86	2.38	2.731(3)	105
N(5)--H(5)..N(4)	0.86	2.42	2.731(3)	102
O(6)--H(6)..O(9)	0.82	1.82	2.618(2)	165
O(7)--H(7)..O(18)	0.82	1.72	2.527(2)	166
C(3--H(3A)..O(6)	0.93	2.44	2.757(3)	100
C(6)--H(6)..O(6)	0.93	2.55	3.346(3)	144
C(21)--H(21)..O(7)	0.93	2.38	2.713(3)	101
C(50)--H(50)..O(18)	0.93	2.48	3.393(3)	168
C(51)--H(51)..O(9)	0.93	2.51	3.374(3)	155
C(64)--H(64)..O(7)	0.93	2.53	3.429(3)	163
C(80)--H(80)..O(22)	0.93	2.49	3.154(3)	128
C(87)--H(87)..O(28)	0.93	2.59	3.174(3)	121
TCA-DPK				
O15--H15..O4	0.82	1.73	2.537(3)	169
C31--H31..O15	0.93	2.43	2.747(3)	100
C37--H37..O0AA	0.93	2.46	3.137(4)	130
C37--H37..O11	0.93	2.59	3.428(4)	149

Table of bond angle for crystals BA-PIP, BA-MPIP, TCA-PHEN and TCA-DPK

			BA-PIP				
Atom	**Atom**	**Atom**	**Angle/°**	**Atom**	**Atom**	**Atom**	**Angle/°**
C1	N1	C2	111.92(14)	N2	C5	C3	122.64(16)
N1	C1	C2^1	110.02(14)	N2	C5	C6	119.04(17)
N1	C2	C1^1	111.01(15)	C6	C5	C3	118.31(16)
C5	C3	C4	122.96(16)	C7	C6	C5	119.82(17)
C9	C3	C4	118.05(16)	C6	C7	Cl1	118.24(14)
C9	C3	C5	118.97(16)	C6	C7	C8	122.73(17)
O1	C4	C3	118.18(16)	C8	C7	Cl1	119.04(14)
O1	C4	O2	123.24(17)	C9	C8	C7	117.23(17)
O2	C4	C3	118.58(16)	C8	C9	C3	122.93(17)
			BA-MPIP				
C5	N1	C1	111.4(3)	O1	C7	O2	123.5(3)
N1	C1	C2	109.8(3)	O2	C7	C6	118.4(3)
N2	C2	C1	110.6(3)	N3	C8	C6	122.4(3)
C2	N2	C3	110.7(3)	N3	C8	C9	118.0(3)
C2	N2	C4	109.4(3)	C9	C8	C6	119.6(3)
C3	N2	C4	109.6(3)	C10	C9	C8	119.5(3)
N2	C4	C5	111.0(3)	C9	C10	Cl1	118.0(3)
N1	C5	C4	110.1(3)	C9	C10	C11	122.7(3)
C8	C6	C7	123.2(3)	C11	C10	Cl1	119.3(3)
			TCA-PHEN				
C87	N4	C55	122.3(2)	C6	C50	C57	121.2(2)
C74	N5	C35	115.9(2)	C64	C51	C74	118.7(2)
C37^1	C3	C59	121.9(2)	N4	C55	C17	119.6(2)
C50	C6	C17	120.9(2)	N4	C55	C35	118.8(2)
C40	C17	C6	123.6(2)	C17	C55	C35	121.4(2)
C55	C17	C6	118.5(2)	C35	C57	C50	119.6(2)
C55	C17	C40	117.9(2)	C35	C57	C64	117.0(2)
C21^2	C19	C28	119.2(2)	C64	C57	C50	123.3(2)
C21^2	C19	C77	116.89(19)	C3	C59	C37	119.2(2)
C28	C19	C77	123.8(2)	C3	C59	C82	117.2(2)
C19^2	C21	C28	121.9(2)	C37	C59	C82	123.6(2)
C19	C28	C41	120.3(2)	O6	C61	C37	112.61(19)
C21	C28	C19	119.0(2)	O22	C61	O6	124.1(2)
C21	C28	C41	120.7(2)	O22	C61	C37	123.2(2)
N5	C35	C55	117.5(2)	C51	C64	C57	119.5(2)
N5	C35	C57	124.3(2)	N5	C74	C51	124.6(2)
C57	C35	C55	118.2(2)	O9	C77	O28	123.5(2)
C3^1	C37	C59	118.9(2)	O9	C77	C19	118.8(2)
C3^1	C37	C61	119.5(2)	O28	C77	C19	117.5(2)
C59	C37	C61	121.3(2)	C40	C80	C87	119.3(2)
C80	C40	C17	120.6(2)	O3	C82	C59	114.9(2)
O7	C41	C28	112.78(19)	O18	C82	O3	126.7(2)
O20	C41	O7	124.3(2)	O18	C82	C59	118.3(2)
O20	C41	C28	123.0(2)	N4	C87	C80	120.2(2)

TCA-DPK

N10	C17	C3	122.5(3)	O11	C21	O4	123.8(3)
C5	C17	C3	116.4(4)	C24	C21	O4	118.4(3)
C5	C17	N10	120.9(4)	C24	C21	O11	117.7(3)
C28	C3	C17	119.5(3)	C21	C24	C11	123.2(3)
C5^1	C3	C17	119.5(4)	C31^2	C24	C11	119.7(3)
C5^1	C3	C28	121.0(4)	C31^2	C24	C21	117.1(3)
O15	C7	O0AA	124.6(3)	C37	C28	C3	120.8(4)
C11	C7	O0AA	121.8(3)	C24^2	C31	C11	120.7(3)
C11	C7	O15	113.5(3)	C37	C33	N10	119.1(4)
C33	N10	C17	119.1(4)	C33	C37	C28	119.0(3)
C24	C11	C7	119.6(3)	C3^1	C5	C17	123.8(5)
C31	C11	C7	120.9(3)	O1	C5	C17	118.6(6)
C31	C11	C24	119.5(3)	O1	C5	C3^1	117.6(6)

Table of bond lengths, Å for crystals 1-4

1

Atom	Atom	Length/Å	Atom	Atom	Length/Å
Zn1	S1^{1}	2.5068(4)	N1	C4	1.494(2)
Zn1	S1	2.5068(4)	N2	C7	1.340(2)
Zn1	S2^{1}	2.5236(4)	N2	C11	1.345(2)
Zn1	S2	2.5236(4)	C2	C3	1.525(2)
Zn1	N2	2.1711(13)	C4	C5	1.522(2)
Zn1	N2^{1}	2.1711(13)	C4	C6	1.525(2)
S1	C1	1.7218(17)	C7	C8	1.387(2)
S2	C1	1.7298(16)	C8	C9	1.378(3)
O1	C3	1.420(2)	C9	C10	1.388(2)
N1	C1	1.339(2)	C10	C11	1.391(2)
N1	C2	1.478(2)	C11	C11^{1}	1.488(3)

2

Zn1	S1	2.5152(5)	N2	C6	1.338(2)
Zn1	S1^{1}	2.5152(5)	N2	C10	1.350(2)
Zn1	S2	2.5365(5)	O1	C3	1.432(2)
Zn1	S2^{1}	2.5365(5)	O2	C5	1.420(2)
Zn1	N2^{1}	2.1663(15)	C2	C3	1.512(3)
Zn1	N2	2.1663(15)	C4	C5	1.523(3)
S1	C1	1.7270(18)	C6	C7	1.386(3)
S2	C1	1.7182(19)	C7	C8	1.350(2)
N1	C1	1.340(2)	C8	C9	1.3998
N1	C2	1.472(2)	C9	C10	1.415(2)
N1	C4	1.475(2)	C10	C10^{1}	1.486(4)

3

Zn1	S1	2.5773(10)	N2	C7	1.461(5)
Zn1	S2	2.5046(10)	N3	C9	1.335(5)
Zn1	S3	2.5568(10)	N3	C13	1.360(5)
Zn1	S4	2.5099(10)	N4	C14	1.341(5)
Zn1	N3	2.156(3)	N4	C18	1.345(5)
Zn1	N4	2.177(3)	C3	C4	1.511(6)
S1	C1	1.729(4)	C7	C8	1.533(6)
S2	C1	1.719(4)	C9	C10	1.390(6)
S3	C5	1.723(4)	C10	C11	1.387(6)
S4	C5	1.723(4)	C11	C12	1.385(5)
O1	C4	1.420(5)	C12	C13	1.385(5)
O2	C8	1.424(5)	C13	C14	1.493(5)
N1	C1	1.335(6)	C14	C15	1.392(5)
N1	C2	1.457(5)	C15	C16	1.394(5)
N1	C3	1.487(5)	C16	C17	1.385(6)
N2	C5	1.331(5)	C17	C18	1.384(6)
N2	C6	1.480(5)			

4

Zn1	N1^{1}	2.463(17)	C1	N2	1.31(3)
Zn1	N1	2.463(17)	C8	C9	1.36(4)
Zn1	S2	2.633(7)	N2	C2	1.48(3)
Zn1	S2^{1}	2.633(7)	N2	C3	1.54(4)
Zn1	S3	2.700(5)	C2	C12	1.41(5)
Zn1	S3^{1}	2.700(5)	C3	C4	1.40(6)
S2	C1	1.76(2)	C6	C10	1.30(4)

S3	C1	1.66(2)	C6	C5	1.47(4)
N1	C8	1.32(2)	C5	C5^1	1.51(7)
N1	C7	1.33(2)	C10	C9	1.46(5)
C7	C7^1	1.36(4)	O1	C4	1.67(6)
C7	C6	1.44(3)	O2	C12	1.74(8)

Table of bond lengths, Å for crystals 5-7

5

Atom	Atom	Length/Å	Atom	Atom	Length/Å
Zn1	S1	2.3467(10)	N1	C2	1.466(4)
Zn1	S2	2.5774(10)	N1	C3	1.462(4)
Zn1	S3	2.3645(10)	N2	C5	1.321(5)
Zn1	S4	2.4745(10)	N2	C6	1.475(4)
Zn1	N3	2.132(3)	N2	C7	1.470(4)
S1	C1	1.731(4)	N3	C9	1.336(4)
S2	C1	1.726(4)	N3	C10^1	1.330(4)
S3	C5	1.732(4)	C3	C4	1.515(5)
S4	C5	1.727(4)	C7	C8	1.520(5)
O1	C4	1.426(5)	C9	C10	1.387(5)
O2	C8	1.419(4)	C10	N3^1	1.330(4)
N1	C1	1.334(4)			

6

Cd1	N7	2.401(8)	N2	C23	1.467(13)
Cd1	N1	2.396(8)	N2	C22	1.494(14)
Cd1	S3	2.592(3)	C6	C7	1.405(14)
Cd1	S1	2.612(3)	C13	C51	1.523(19)
Cd1	S4	2.747(3)	C13	C50	1.523(17)
Cd1	S2	2.770(3)	N1	C1	1.347(14)
S2	C11	1.705(10)	C22	C53	1.50(2)
S1	C11	1.718(10)	C22	C54	1.51(2)
S3	C20	1.719(10)	C23	C55	1.51(2)
S4	C20	1.714(10)	C7	C8	1.363(19)
N5	C11	1.358(12)	C10	C9	1.383(18)
N5	C52	1.468(13)	C2	C3	1.332(19)
N5	C13	1.486(13)	C2	C1	1.365(18)
C5	N1	1.330(13)	C9	C8	1.41(2)
C5	C4	1.409(15)	C16	C52	1.498(16)
C5	C6	1.469(15)	C4	C3	1.415(19)
O5	C16	1.406(14)	O2	C55	1.422(15)
N7	C10	1.349(14)	C11	C100	1.785(18)
N7	C6	1.330(13)	C12	C100	1.726(15)
N2	C20	1.332(12)	C13	C100	1.727(16)

7

Cd1	N3	2.3088(17)	N2	C8	1.472(3)
Cd1	S4	2.5447(6)	N2	C11	1.487(3)
Cd1	S1	2.5503(6)	N3	C13	1.479(3)
Cd1	S2	2.6579(8)	N3	C16	1.483(3)
Cd1	S3	2.7461(8)	N4	C14	1.476(3)
S1	C1	1.732(2)	N4	C15	1.473(3)
S2	C1	1.717(2)	C2	C3	1.516(3)

S3	C7	1.717(2)	C4	C5	1.519(3)
S4	C7	1.727(2)	C5	C6	1.524(3)
O1	C3	1.427(3)	C8	C9	1.523(3)
O2	C9	1.425(3)	C10	C11	1.521(3)
N1	C1	1.340(3)	C11	C12	1.522(3)
N1	C2	1.470(3)	C13	C14	1.515(3)
N1	C5	1.489(3)	C15	C16	1.514(3)
N2	C7	1.340(3)			

Table of bond angles for crystals 1-7

Atom	Atom	Atom	Angle/°	Atom	Atom	Atom	Angle/°
1							
S1^{1}	Zn1	S1	102.39(2)	C2	N1	C4	118.17(13)
S1	Zn1	S2	71.346(13)	C7	N2	Zn1	124.04(11)
S1^{1}	Zn1	S2^{1}	71.346(13)	C7	N2	C11	118.66(14)
S1	Zn1	S2^{1}	95.817(14)	C11	N2	Zn1	116.61(10)
S1^{1}	Zn1	S2	95.817(14)	S1	C1	S2	116.40(9)
S2	Zn1	S2^{1}	159.92(2)	N1	C1	S1	121.89(12)
N2^{1}	Zn1	S1	154.11(4)	N1	C1	S2	121.69(12)
N2^{1}	Zn1	S1^{1}	95.37(4)	N1	C2	C3	113.28(14)
N2	Zn1	S1^{1}	154.11(4)	O1	C3	C2	113.86(15)
N2	Zn1	S1	95.37(4)	N1	C4	C5	113.19(13)
N2	Zn1	S2	107.73(4)	N1	C4	C6	109.34(14)
N2^{1}	Zn1	S2^{1}	107.73(4)	C5	C4	C6	112.03(15)
N2^{1}	Zn1	S2	88.38(4)	N2	C7	C8	122.62(16)
N2	Zn1	S2^{1}	88.38(4)	C9	C8	C7	118.65(15)
N2	Zn1	N2^{1}	75.17(7)	C8	C9	C10	119.35(16)
C1	S1	Zn1	86.18(5)	C9	C10	C11	118.77(16)
C1	S2	Zn1	85.48(6)	N2	C11	C10	121.93(15)
C1	N1	C2	120.28(14)	N2	C11	C11^{1}	115.29(9)
C1	N1	C4	120.26(13)	C10	C11	C11^{1}	122.77(10)
2							
S1	Zn1	S1^{1}	161.35(2)	C2	N1	C4	118.84(14)
S1	Zn1	S2	71.342(15)	C6	N2	Zn1	124.69(12)
S1^{1}	Zn1	S2	96.420(16)	C6	N2	C10	118.62(16)
S1^{1}	Zn1	S2^{1}	71.342(15)	C10	N2	Zn1	115.98(12)
S1	Zn1	S2^{1}	96.420(16)	S2	C1	S1	117.53(10)
S2^{1}	Zn1	S2	100.08(2)	N1	C1	S1	120.87(14)
N2^{1}	Zn1	S1	92.60(4)	N1	C1	S2	121.58(14)
N2	Zn1	S1	102.14(4)	N1	C2	C3	114.04(15)
N2^{1}	Zn1	S1^{1}	102.14(4)	O1	C3	C2	109.64(15)
N2	Zn1	S1^{1}	92.60(4)	N1	C4	C5	113.54(15)
N2	Zn1	S2^{1}	159.32(4)	O2	C5	C4	113.94(16)
N2^{1}	Zn1	S2	159.32(4)	N2	C6	C7	122.68(17)
N2	Zn1	S2	94.47(4)	C8	C7	C6	118.17(17)
N2^{1}	Zn1	S2^{1}	94.47(4)	C7	C8	C9	122.45(10)
N2	Zn1	N2^{1}	75.81(8)	C8	C9	C10	115.29(9)
C1	S1	Zn1	85.69(6)	N2	C10	C9	122.71(15)
C1	S2	Zn1	85.20(6)	N2	C10	C10^{1}	115.48(10)
C1	N1	C2	120.15(15)	C9	C10	C10^{1}	121.78(9)
C1	N1	C4	120.92(15)				
3							
S2	Zn1	S1	70.79(3)	C14	N4	Zn1	117.0(2)
S2	Zn1	S3	102.70(3)	C14	N4	C18	118.4(3)
S2	Zn1	S4	94.49(3)	C18	N4	Zn1	124.5(3)
S3	Zn1	S1	95.62(3)	S2	C1	S1	117.3(3)
S4	Zn1	S1	158.10(4)	N1	C1	S1	121.5(3)
S4	Zn1	S3	71.25(3)	N1	C1	S2	121.2(3)
N3	Zn1	S1	92.88(8)	N1	C3	C4	111.5(3)

N3	Zn1	S2	157.85(9)	O1	C4	C3	112.6(3)
N3	Zn1	S3	93.50(9)	S4	C5	S3	117.8(2)
N3	Zn1	S4	105.07(8)	N2	C5	S3	121.8(3)
N3	Zn1	N4	75.28(11)	N2	C5	S4	120.3(3)
N4	Zn1	S1	103.86(8)	N2	C7	C8	111.9(4)
N4	Zn1	S2	93.72(9)	O2	C8	C7	112.2(3)
N4	Zn1	S3	157.84(9)	N3	C9	C10	123.6(4)
N4	Zn1	S4	92.94(8)	C11	C10	C9	118.1(3)
C1	S1	Zn1	84.58(13)	C12	C11	C10	119.0(4)
C1	S2	Zn1	87.09(15)	C11	C12	C13	119.4(4)
C5	S3	Zn1	84.46(13)	N3	C13	C12	122.0(3)
C5	S4	Zn1	85.96(13)	N3	C13	C14	115.1(3)
C1	N1	C2	123.7(3)	C12	C13	C14	122.9(3)
C1	N1	C3	120.8(3)	N4	C14	C13	115.3(3)
C2	N1	C3	115.4(3)	N4	C14	C15	122.4(3)
C5	N2	C6	120.5(3)	C15	C14	C13	122.3(3)
C5	N2	C7	121.8(3)	C14	C15	C16	118.5(4)
C7	N2	C6	117.7(3)	C17	C16	C15	119.3(4)
C9	N3	Zn1	124.9(3)	C18	C17	C16	118.5(3)
C9	N3	C13	117.7(3)	N4	C18	C17	122.9(4)
C13	N3	Zn1	116.9(2)				

4

N1^1	Zn1	N1	68.0(7)	N1	C7	C7^1	121.8(11)
N1^1	Zn1	S2	88.5(4)	N1	C7	C6	115(2)
N1	Zn1	S2	103.5(4)	C7^1	C7	C6	123.1(14)
N1^1	Zn1	S2^1	103.5(4)	N2	C1	S3	122.9(19)
N1	Zn1	S2^1	88.5(4)	N2	C1	S2	117.0(19)
S2	Zn1	S2^1	165.6(3)	S3	C1	S2	119.8(12)
N1^1	Zn1	S3	146.9(4)	N1	C8	C9	126(3)
N1	Zn1	S3	94.9(4)	C1	N2	C2	124(2)
S2	Zn1	S3	67.40(18)	C1	N2	C3	124(2)
S2^1	Zn1	S3	104.2(2)	C2	N2	C3	111.5(19)
N1^1	Zn1	S3^1	94.9(4)	C12	C2	N2	106(4)
N1	Zn1	S3^1	146.9(4)	C4	C3	N2	128(6)
S2	Zn1	S3^1	104.2(2)	C10	C6	C5	119(3)
S2^1	Zn1	S3^1	67.40(18)	C10	C6	C7	123(3)
S3	Zn1	S3^1	112.3(3)	C5	C6	C7	118(2)
C1	S2	Zn1	86.4(7)	C6	C5	C5^1	119.0(15)
C1	S3	Zn1	86.4(8)	C6	C10	C9	121(3)
C8	N1	C7	122(2)	C8	C9	C10	112(3)
C8	N1	Zn1	123.5(16)	C3	C4	O1	100(4)
C7	N1	Zn1	114.1(13)	C2	C12	O2	98(5)

5

S1	Zn1	S2	73.75(3)	C5	N2	C7	123.4(3)
S1	Zn1	S3	148.35(4)	C7	N2	C6	114.4(3)
S1	Zn1	S4	103.64(3)	C9	N3	Zn1	121.8(2)
S3	Zn1	S2	101.68(3)	C10^1	N3	Zn1	120.8(2)
S3	Zn1	S4	74.90(3)	C10^1	N3	C9	117.4(3)

S4	Zn1	S2	169.24(4)	S2	C1	S1	117.8(2)
N3	Zn1	S1	107.30(8)	N1	C1	S1	120.3(3)
N3	Zn1	S2	92.17(8)	N1	C1	S2	121.8(3)
N3	Zn1	S3	104.14(8)	N1	C3	C4	112.1(3)
N3	Zn1	S4	98.55(8)	O1	C4	C3	112.2(3)
C1	S1	Zn1	87.73(12)	S4	C5	S3	116.6(2)
C1	S2	Zn1	80.68(12)	N2	C5	S3	121.0(3)
C5	S3	Zn1	85.85(12)	N2	C5	S4	122.4(3)
C5	S4	Zn1	82.56(12)	N2	C7	C8	112.6(3)
C1	N1	C2	120.7(3)	O2	C8	C7	110.9(3)
C1	N1	C3	121.6(3)	N3	C9	C10	121.0(3)
C3	N1	C2	117.7(3)	N3^{1}	C10	C9	121.6(3)
C5	N2	C6	122.2(3)				
				6			
N7	Cd1	N1	67.3(3)	C20	N2	C22	121.1(8)
N7	Cd1	S3	87.4(2)	C23	N2	C22	117.1(8)
N1	Cd1	S3	117.9(2)	N7	C6	C7	121.3(10)
N7	Cd1	S1	123.7(2)	N7	C6	C5	116.5(8)
N1	Cd1	S1	92.2(2)	C7	C6	C5	122.2(10)
S3	Cd1	S1	144.44(9)	N5	C13	C51	109.5(10)
N7	Cd1	S4	135.7(2)	N5	C13	C50	111.9(10)
N1	Cd1	S4	92.6(2)	C51	C13	C50	113.5(11)
S3	Cd1	S4	67.16(8)	C1	N1	C5	119.4(9)
S1	Cd1	S4	94.78(9)	C1	N1	Cd1	120.7(7)
N7	Cd1	S2	88.6(2)	C5	N1	Cd1	119.8(7)
N1	Cd1	S2	131.8(2)	N2	C22	C53	111.0(11)
S3	Cd1	S2	100.99(9)	N2	C22	C54	111.6(11)
S1	Cd1	S2	66.54(8)	C53	C22	C54	112.7(13)
S4	Cd1	S2	130.12(9)	N2	C23	C55	114.1(11)
C11	S2	Cd1	84.4(3)	N2	C20	S4	120.8(7)
C11	S1	Cd1	89.3(3)	N2	C20	S3	120.3(7)
C20	S3	Cd1	89.4(3)	S4	C20	S3	118.9(5)
C20	S4	Cd1	84.5(3)	C8	C7	C6	119.5(12)
C11	N5	C52	121.2(8)	N7	C10	C9	121.4(12)
C11	N5	C13	120.9(9)	C3	C2	C1	119.4(12)
C52	N5	C13	117.2(8)	N1	C1	C2	122.6(11)
N1	C5	C4	120.9(11)	C8	C9	C10	118.8(12)
N1	C5	C6	116.5(9)	O5	C16	C52	111.2(10)
C4	C5	C6	122.5(10)	C5	C4	C3	117.3(11)
N5	C11	S2	120.7(7)	C2	C3	C4	120.3(12)
N5	C11	S1	119.8(7)	C7	C8	C9	118.8(11)
S2	C11	S1	119.4(5)	N5	C52	C16	114.2(8)
C10	N7	C6	120.0(9)	O2	C55	C23	109.8(12)
C10	N7	Cd1	120.0(8)	C12	C100	C13	113.5(9)
C6	N7	Cd1	119.6(7)	C12	C100	C11	107.9(9)
C20	N2	C23	121.5(8)	C13	C100	C11	109.8(8)
				7			
N3	Cd1	S4	98.26(5)	C16	N3	Cd1	118.42(13)
N3	Cd1	S1	116.47(5)	C14	N4	C15	110.68(17)
S4	Cd1	S1	145.16(2)	N1	C1	S2	120.71(16)
N3	Cd1	S2	104.11(4)	N1	C1	S1	120.07(17)
S4	Cd1	S2	105.98(2)	S2	C1	S1	119.21(12)
S1	Cd1	S2	69.63(2)	N1	C2	C3	115.47(18)

N3	Cd1	S3	99.58(4)	O1	C3	C2	105.02(17)
S4	Cd1	S3	68.30(2)	N1	C5	C4	110.30(19)
S1	Cd1	S3	101.38(2)	N1	C5	C6	111.33(18)
S2	Cd1	S3	156.232(19)	C4	C5	C6	112.31(19)
C1	S1	Cd1	86.81(8)	N2	C7	S3	121.01(16)
C1	S2	Cd1	83.71(7)	N2	C7	S4	119.55(17)
C7	S3	Cd1	82.85(7)	S3	C7	S4	119.43(12)
C7	S4	Cd1	89.07(8)	N2	C8	C9	115.26(17)
C1	N1	C2	120.42(18)	O2	C9	C8	107.93(17)
C1	N1	C5	121.64(18)	N2	C11	C10	110.01(19)
C2	N1	C5	116.74(17)	N2	C11	C12	112.12(18)
C7	N2	C8	120.93(18)	C10	C11	C12	111.79(19)
C7	N2	C11	121.38(18)	N3	C13	C14	109.43(17)
C8	N2	C11	116.26(17)	N4	C14	C13	112.44(18)
C13	N3	C16	110.20(16)	N4	C15	C16	113.44(19)
C13	N3	Cd1	110.93(12)	N3	C16	C15	109.72(18)

Table of hydrogen bond lengths, Å for crystals 1-7

1

D — H···A	D — H, Å	H···A, Å	D···A, Å	D — H···A,º
O(1)--H(1)..S(2)	0.84	2.44	3.2439(16)	159
C(3)--H(3A)..S(1)	0.99	2.80	3.384(2)	119
C(4)--H(4B)..O(1)	0.98	2.53	3.513(2)	176
C(5)--H(5)..S(2)	1.00	2.48	3.0171(19)	113
C(9)--H(9)..S(2)	0.95	2.86	3.550(2)	130

2

D — H···A	D — H, Å	H···A, Å	D···A, Å	D — H···A,º
O(1)--H(1)..O(1W)	0.834(10)	1.883(10)	2.713(2)	174(3)
O(2)--H(2)..O(1)	0.837(10)	1.859(10)	2.696(2)	178(3)
O(1W)--H(11)..O(2^{1})	0.836(10)	1.896(12)	2.717(2)	167(3)
O(1W)--H(12)..S(1^{2})	0.835(10)	2.447(11)	3.2732(15)	170(2)

3

D — H···A	D — H, Å	H···A, Å	D···A, Å	D — H···A,º
O(1)—H(1)..S(4)	0.84	2.49	3.273(3)	155
O(2)—H(2)..S(1)	0.84	2.46	3.301(3)	175
C(2)—H(2A)..S(1)	0.98	2.52	3.060(4)	114
C(3)—H(3B)..S(2)	0.99	2.61	2.996(4)	103
C(7)—H(7B)..S(3)	0.99	2.59	3.017(5)	106
C(9)—H(9)..S(3)	0.95	2.82	3.466(5)	126
C(9)—H(9)..S(4)	0.95	2.72	3.443(4)	133
C(10)—H(10)..O(1)	0.95	2.55	3.499(5)	174
C(18)—H(18)..S(1)	0.95	2.76	3.555(4)	141
C(18)—H(18)..S(2)	0.95	2.85	3.461(5)	123

4

D — H···A	D — H, Å	H···A, Å	D···A, Å	D — H···A,º
O(1)—H(1A)..O(2)	0.82	1.84	2.65(8)	168
O(2)—H(2B)..O(1)	0.82	1.84	2.65(8)	167
C(2))—H(2A)..S(3)	0.97	2.65	3.04(3)	104
C(2))—H(2A)..O(1)	0.97	2.57	3.35(9)	138
C(3))—H(3B)..S(2)	0.97	2.41	3.01(4)	119
C(8))—H(8A)..S(2)	0.93	2.80	3.60(2)	14
C(9))—H(9A)..O(2)	0.93	2.46	3.34(6)	157
C(12))—H(12A)..O(2)	0.97	2.55	3.30(9)	134

5

D — H···A	D — H, Å	H···A, Å	D···A, Å	D — H···A,º
C(1)—H(1C)..S(1)	0.96	2.83	3.649(4)	144
C(2)—H(2B)..S(2)	0.97	2.57	3.063(4)	111
C(6)—H(6A)..S(4)	0.97	2.68	3.017(4)	101

6

D — H···A	D — H, Å	H···A, Å	D···A, Å	D — H···A,º
O(2)—H(2B)..O(5)	0.82	1.88	2.684(14)	167
O(5)—H(5A)..O(2)	0.82	1.87	2.684(14)	170
C(13)—H(13A)..S(1)	0.98	2.46	2.984(12)	113
C(22)—H(22A)..S(3)	0.98	2.40	2.979(12)	117
C(23)—H(23A)..S(4)	0.97	2.64	2.987(12)	101
C(52)—H(52B)..S(2)	0.97	2.61	3.000(11)	104

7

D — H···A	D — H, Å	H···A, Å	D···A, Å	D — H···A,º
O(1)—H(1)..O(2)	0.84	1.89	2.672(2)	155
O(2)—H(2)..N(4)	0.84	1.92	2.750(3)	170
N(3)—H(3)..O(1)	0.88	2.02	2.892(3)	173
C(2)—H(2B)..S(2)	0.99	2.62	2.984(2)	102
C(5)—H(5)..S(1)	1.00	2.46	2.998(2)	113
C(5)—H(5)..S(4)	1.00	2.82	3.640(3)	140
C(8)—H(8B)..S(3)	0.99	2.64	3.006(2)	102

C(11)—H(11)..S(1)	1.00	2.83	3.658(3)	141
C(11)—H(11)..S(4)	1.00	2.45	2.976(2)	112